ROBUST CONTROL DESIGN FOR MECHATRONIC SYSTEMS HAVING NON–SYMMETRIC INPUT GAIN MATRIX

A Dissertation Submitted to
the Graduate School of Engineering and Sciences of
İzmir Institute of Technology
in Partial Fulfillment of the Requirements for the Degree of

DOCTOR OF PHILOSOPHY

in Electronics and Communication Engineering

by
Barış BIDIKLI

August 2016
İZMİR

We approve the thesis of **Barış BIDIKLI**

Examining Committee Members:

Prof. Dr. Aydoğan SAVRAN
Department of Electrical and Electronics Engineering
Ege University

Prof. Dr. Musa ALCI
Department of Electrical and Electronics Engineering
Ege University

Assoc. Prof. Dr. Enver TATLICIOĞLU
Department of Electrical and Electronics Engineering
İzmir Institute of Technology

Asst. Prof. Dr. M. İ. Can DEDE
Department of Mechanical Engineering
Izmir Institute of Technology

Asst. Prof. Dr. Barbaros ÖZDEMİREL
Department of Electrical and Electronics Engineering
Izmir Institute of Technology

15 August 2016

Assoc. Prof. Dr. Enver TATLICIOĞLU
Supervisor
Department of Electrical and Electronics Engineering
İzmir Institute of Technology

Prof. Dr. M. Salih DİNLEYİCİ
Head of the Department of
Electrical and Electronics Engineering

Prof. Dr. Bilge KARAÇALI
Dean of the Graduate School of
Engineering and Sciences

ACKNOWLEDGMENTS

I would like to thank my mom Özlem S. KIRAL, my grandma A. Feral KIRAL for their endless support and encouragement throughout my life.

I would like to thank to Didem CİHAN ŞAHANSOY and Ufuk ŞAHANSOY for their endless support and patience throughout this process.

I would like to thank my friends who are closer than brothers or sisters to me; İlter AKDER, Tufan BAKIRCIGİL, K. Merve DOĞAN, Başak Esin KÖKTÜRK GÜZEL, Burçin GÜZEL, Oktay KARAKUŞ, Meryem DENİZ, B. Orkan OLCAY, Nail AKÇURA, M. Doğan ELBİ and Ferhan KULOĞLU ELBİ.

I would like to thank Bahar CİVAN GEMİCİ and Asst. Prof. Dr. Türkan BAŞYİĞİT for their understanding, confidence and support.

I would like to express my gratitude to Prof. Dr. Serdar İPLİKÇİ for his guidance, leadership and support.

I would like to thank to the supervisor of this dissertation Assoc. Prof. Dr. Enver TATLICIOĞLU for his guidance, support and trust throughout graduate process.

I would like to thank to Prof. Dr. Erkan ZERGEROGLU, Asst. Prof. Dr. Alper BAYRAK and Kamil ÇETİN for their helpful suggestions and comments which improve this dissertation.

I would like to thank to committee members for giving me contribution which helped me a lot for revising this dissertation.

I would like to thank to The Scientific and Technological Research Council of Turkey via grant number 113E147 for providing the experimental setup.

Finally, I would like to thank to TÜBİTAK BİDEB for providing financial support for my works as a sponsor.

ABSTRACT

ROBUST CONTROL DESIGN FOR MECHATRONIC SYSTEMS HAVING NON–SYMMETRIC INPUT GAIN MATRIX

Their highly uncertain and complex structures make the control problem of mechatronic systems a challenging task. This problem becomes more challenging when some special cases that make the input gain matrix of these systems non–symmetric are taken into account. Solving this problem is the main motivation of this dissertation. To realize this purpose, a robust controller that is independent from the structure of the input gain matrix is designed. Since, mechatronic systems are modeled as multi–input multi–output nonlinear systems, this design is realized for a broader class of these type of systems. Asymptotic stability of the designed controller is proven via Lyapunov–based arguments. Since, control gain adjusting process is one of the most restrictive and most important aspects of this design, designed controller is supported by proposing a self–tuning method. After completing the control design process by proposing this self–tuning method, three fundamentally different mechatronic systems are utilized to demonstrate the effectiveness of the designed controller in conjunction with the proposed self–tuning method. Position and orientation control of dynamically positioned surface vessel and unactuated surface vessel manipulated by 6 uni–directional tugboats under the influence of added mass effects, and attitude control of small–scaled unmanned helicopter are ensured by utilizing a lower order version of the designed controller. Each of these mechatronic systems constitutes an example of different cases that make input gain matrix non–symmetric. Performance of the designed controller and proposed self–tuning method are demonstrated via simulations and experiments.

ÖZET

BAKIŞIMLI OLMAYAN GİRİŞ KAZANÇ MATRİSİNE SAHİP MEKATRONİK SİSTEMLER İÇİN GÜRBÜZ DENETLEYİCİ TASARIMI

Yüksek oranda belirsiz ve karmaşık yapıları, mekatronik sistemlerin denetim problemini zor bir iş haline getirmektedir. Bu problem, belirtilen sistemlerin giriş kazanç matrislerini bakışımsız hale getiren bazı özel durumlar hesaba katıldığında daha da zorlayıcı hale gelmektedir. Bu problemi çözmek, bu tezin ana motivasyonudur. Bu amacı gerçekleştirmek için, giriş kazanç matrisinin yapısından bağımsız olan bir gürbüz denetleyici tasarlanmıştır. Mekatronik sistemler çok giriş çok çıkışlı doğrusal olmayan sistemler olarak modellendiğinden, bu tasarım belirtilen tipteki sistemlerin daha geniş bir sınıfı için gerçekleştirilmiştir. Tasarlanan denetleyicinin asimptotik kararlılığı, Lyapunov temelli argümanlar aracılığıyla ispatlanmıştır. Denetim kazançlarının ayarlanma süreci, bu tasarımın en kısıtlayıcı ve en önemli yönlerinden biri olduğundan, tasarlanan denetleyici bir öz ayarlama yöntemi önerilerek desteklenmiştir. Denetleyici tasarımı tamamlandıktan sonra, tasarlanan denetleyicinin öz ayarlama yöntemi ile birlikte verimliliğinin gösterilmesi amacıyla, temelde farklı üç adet mekatronik sistemden faydalanılmıştır. Dinamik olarak konumlandırılmış deniz aracının ve altı adet tek yönlü römork ile yönlendirilen eyleyicisiz deniz aracının eklenmiş kütle etkisi altındaki konum ve yönelim denetimi ve küçük ölçekli insansız helikopterin davranış denetimi, denetleyicinin daha düşük dereceli sürümünden faydalanılarak, sağlanmıştır. Bu mekatronik sistemlerin her biri, giriş kazanç matrisini bakışımsız hale getiren farklı durumlar için örnek oluşturmaktadır. Tasarlanan denetleyicinin ve önerilen öz ayarlama yönteminin başarımı benzetimler ve deneyler aracılığıyla ortaya konulmuştur.

To woman of my life, my mom.

TABLE OF CONTENTS

LIST OF FIGURES

Figure **Page**

LIST OF TABLES

LIST OF SYMBOLS

$h(\cdot)$ ..... An uncertain function.

$g(\cdot)$ ..... An uncertain real valued input gain matrix.

$\tau(t)$, $\delta_{lon}(t)$, $\delta_{lat}(t)$, $\delta_{ped}(t)$ ..... Control inputs.

$X(t)$ ..... Combined state vector.

$S(\cdot)$ ..... Positive definite, symmetric matrix.

D ..... Diagonal matrix.

$U(\cdot)$ ..... Unity upper triangular matrix.

$\varphi(\cdot)$ ..... Auxiliary function.

$M(\cdot)$ ..... Inverse of $S(\cdot)$.

$e_1(t)$ ..... Output tracking error.

$e_i(t)$ for $i = 2, \cdots, n$ ..... Auxiliary error signals.

$r(t)$ ..... Filtered error term.

α ..... Constant, positive–definite, diagonal gain matrix.

$N(\cdot)$ ..... Auxiliary function.

I_m ..... $m \times m$ standard identity matrix.

$\bar{N}(t)$, $\widetilde{N}(t)$ ..... Auxiliary functions.

$X_r(t)$ ..... Combination of the desired trajectory and its time derivatives.

$\Pi(t)$ ..... Auxiliary signal.

β, K ..... Constant, positive definite, diagonal gain matrices.

0_m ..... m dimensional vector of zeros.

Sgn $(\cdot)$ ..... Vector signum function.

sgn $(\cdot)$ ..... Scalar signum function.

k_p, $k_{d,i}$ ..... Constant, positive controller gains.

diag $\{\cdot\}$ ..... Diagonal entries of a matrix.

$\Lambda(t)$, $\Phi(t)$, $\Psi(t)$, $\Theta(t)$ ..... Auxiliary signals.

$\rho_{\widetilde{N}}(\cdot)$, $\rho_{i,j}(\cdot)$ ..... Non–negative, globally invertible, non–decreasing functions of their arguments.

$z(t)$ ..... Combined vector of error terms.

$\zeta_{\bar{N}_i}$, $\zeta_{\bar{U}_{i,j}}$, ζ_{Θ} ..... Positive bounding constants.

$\rho_i(\|z\|)$ ..... Non–negative, globally invertible, non–decreasing functions.

$\lambda_{\min}(\cdot)$ ..... Minimum eigenvalue of $(\cdot)$.

$V_1(\cdot)$ ..... The non–negative function.

$L_1(t)$, $L_2(t)$ ..... Auxiliary functions.
δ,μ, γ_1, γ_2 ..... Positive bounding constants.
ζ_L,$\zeta_{\Omega_{i,j}}$ ..... Positive bounding constant.
$V(\cdot)$ ..... Lyapunov function.
$\theta_1(t)$, $\theta_2(t)$, $\theta_3(t)$ ..... Joint angles.
$q_r(t)$, $x_d(t)$, $\theta_r(t)$, $\eta_r(t)$ ..... Desired trajectories.
M_P ..... Non–symmetric matrix.
γ_p ..... Constant positive value.
$m_{st}(\cdot)$, $f_{st}(\cdot)$ ..... Uncertain nonlinear functions.
$\hat{\beta}(t)$, $k(t)$ ..... Time–varying control gains.
β_2, k_c ..... Constant parts of the time–varying control gains.
χ_1 ..... Positive constant.
$\|\cdot\|_{L_\infty}$ ..... Infinity norm.
ζ_{b_1}, ζ_{b_2} ..... Positive constants.
$P(t)$, $P_1(t)$, $P_2(t)$ ..... Auxiliary functions.
$\hat{\beta}_\infty$, k_∞ ..... Constant values.
$\hat{\beta}_{11}$, $\hat{\beta}_{22}$, k_{11}, k_{22} ..... Diagonal entries of time–varying control gain matrices.
$x_p(t)$, $y_p(t)$ ..... Translational positions of a surface vessel.
$\psi_s(t)$ ..... Yaw angle of the surface vessel.
$M_s(\cdot)$, $M_t(\cdot)$, $M_h(\cdot)$ ..... Inertia matrices.
$C_s(\cdot)$, $C_h(\cdot)$ ..... Centripetal and Coriolis forces.
$D_s(\cdot)$, $D_t(\cdot)$ ..... Hydrodynamic damping terms.
$R(\cdot)$ ..... Rotation matrix.
$M_{RB}(\cdot)$ ..... Positive definite, symmetric rigid body inertia matrix.
$M_A(\cdot)$ ..... Added mass inertia matrix.
S_3 ..... A skew–symmetric matrix.
$G_h(\cdot)$ ..... Vector of conservative forces.
$\tau_h(t)$ ..... Torque input vector.

LIST OF ABBREVIATIONS

SISO . . . . . Single–input single–output.
MIMO . . . . . Multi–input multi–output.
RISE . . . . . Robust integral of sign of error.
UUB . . . . . Uniformly ultimately bounded.
PID . . . . . Proportional integral derivative.
dof . . . . . Degree of freedom.

CHAPTER 1

INTRODUCTION

Mathematical models of several mechatronic systems obtained via Lagrangian have the general form of inertia matrix times the acceleration added to other dynamical effects (such as centripetal and Coriolis, gravitational, frictional effects/terms) and equating to the control input vector. In cases when the control input is not directly applied on the mechatronic system, pre–multiplication with some matrix is essential. Input gain matrix is defined as the pre–multiplication matrix of the vector of control inputs when the highest order term left alone in the equation of motion Zhang et al. (2005).

During the review of the modeling literature on mechatronic systems, some aspects about modeling approaches have been encountered and they can be summarized as:

- They have complex and highly nonlinear structures along with modeling uncertainties.
- They are modeled as second order multi–input multi–output (MIMO) nonlinear systems.
- Non–symmetric structure of the input gain matrix is a critical situation that must be included in the system model for some mechatronic systems.

In the modeling literature of mechatronic systems, cases that make the input gain matrix non–symmetric can be examined under three sub–classes:

- Non–symmetry may appear in the inertia matrix of the system.
- Non–symmetry may be due to the pre–multiplication of the control input with a non–symmetric matrix.
- Non–symmetry may appear as a result of both of the above situations.

The first type of non–symmetry is generally caused from external or internal effects that change the center of mass of the mechatronic system. This change may be seen as a non–symmetric effect on the system and this non–symmetric behavior is reflected to the system model via the inertia matrix. The second type of non–symmetry is caused from

the structure of the system. In some mechatronic systems, control input vector is pre–multiplied with a configuration matrix. This matrix may lose its symmetry as a result of the structure of some mechatronic systems. As a result of either or both of these situations, input gain matrix may become non–symmetric.

One of the most important examples of above mentioned situations can be encountered in unmanned surface vessels. Unmanned surface vessels constitute a good example for the sub–class of general systems considered in this dissertation where non–symmetry appears in the inertia matrix of the system. The effect namely as added mass is encountered during the cruise and it may cause a non–symmetric inertial behavior. Added mass is considered as an effect that is caused from the motion of flow. During the motion, it is considered that this flow is seen as an additional mass that occurs as different vibrations at different parts of the surface vessel. Added mass affects the surface vessel at acceleration level. Since the motion of the surface vessel may be dramatically affected by the flow, effects of the added mass must be taken into account in the modeling phase. In addition to these, this flow vary in different parts of the surface vessel and as a result of this it can be easily said that its effects can also be changed for different parts of these vehicles and this situation shows up as a non–symmetric inertia matrix in the system model Fossen and Strand (1999), Skjetne et al. (2004).

Small–scaled unmanned helicopters constitute a good example for the second sub–class of the general systems considered in this dissertation where the non–symmetry is due to pre–multiplication of the control input with a non–symmetric matrix. For modeling of small–scaled unmanned helicopters, rigid body dynamics and the rotor dynamics are combined by expressing the input torque as a function of actual control inputs namely as elevator servo input, aileron servo input and rudder servo input. To obtain the input torque in terms of actual control inputs, some reasonable simplifications for the rotor model under the hovering flight conditions are utilized. As a result of these simplifications, the input torque is expressed by pre–multiplying control input vector with a non–symmetric matrix Fantoni and Lozano (2002), Liu et al. (2014).

An unactuated surface vessel whose position and orientation are provided via 6 uni–directional tugboats is another mechatronic system that is considered in this dissertation. These systems are unmanned surface vessels and has a similar modeling approach Fossen (1994), Fossen (2002), Skjetne et al. (2004), Arrichiello et al. (2006), Ihle et al. (2006), Fossen (2011). Providing their position and orientation via uni–directional thrust forces of tugboats instead of the control input torque is the main difference between them and dynamically positioned surface vessels. This situation is modeled by the control in-

put of the system model as pre–multiplication of vector of thrust forces provided by the tugboats with a thrust configuration matrix which is a function of the angles and distances between the surface vessel and the tugboats. However, the communication between tugboats appears as an important problem that needs to be addressed. To solve this situation, in the literature, the problem is transformed into positioning of an unactuated surface vessel with 3 bi–directional tugboats by utilizing a specified initial conditioning for the tugboats. As a result of this rearrangement, thrust configuration matrix becomes a 3×3 non–symmetric matrix so these systems constitute another example for the sub–class of the general systems considered in this dissertation where the non–symmetry is due to a pre–multiplication of the control input with a non–symmetric matrix. In addition to these, since these systems are surface vessels, they also constitute an example for the sub–class of general systems considered in this dissertation where non–symmetry appears in inertia matrix of the system due to added mass effect.

Control problem of the mechatronic systems is usually encountered as tracking of a desired/reference trajectory. This problem is a more challenging task when the non–symmetric structure of the input gain matrix is taken into account. Researchers have ignored this non–symmetric behavior and based their designs on the assumption that the input gain matrix being symmetric. From a control theory perspective, the symmetric nature of the inertia matrix is extremely useful as it is utilized in a quadratic term in the Lyapunov function. As a natural result of these, in the control literature, for mechatronic systems, there are several available control designs that assume symmetric input gain matrix. At the same time, these controllers and/or the accompanying stability analysis are strictly dependent to the symmetry of the input gain matrix. Although these control designs are really valuable and applicable to systems that do not have non–symmetry in their dynamics, it is not wrong to say that for some mechatronic systems this effect constitutes a really important problem that needs to be addressed. Solving this problem has become the main motivation of this dissertation. As a result of these, designing a robust controller that is also independent from the structure of the input gain matrix for a broader class of MIMO nonlinear systems was considered as a good starting point.

1.1. Robust Control Design for MIMO Nonlinear Systems

Motivated by the need for a controller for the mechatronic systems having non–symmetric input gain matrix, this dissertation focuses on the tracking control problem for MIMO nonlinear uncertain systems which also include the special class of mechatronic

systems. In the literature, a generalized solution, that covers all nonlinear systems for the aforementioned problem is not available. However, for special cases, there seems to be a great deal of results presented in the literature. To name a few, an adaptive back-stepping method for strict feedback systems was utilized in Krstic et al. (1995) with the assumption that the input gain matrix premultiplying the control input is known. In Kosmatopoulos and Ioannou (2002), a general procedure for the design of switching adaptive controllers including feedback linearizable and parametric–pure feedback systems have been proposed. An adaptive neural network controller for MIMO systems having a block–triangular form was proposed in Gee and Wang (2004).

For nonlinear uncertain systems, especially when the system uncertainties are unstructured, robust type controllers are preferred. However, prior to the introduction of "smooth" robust controllers, most robust controllers were either make use of discontinuous feedback or unnecessarily high controller gains to achieve stability. The first smooth, that is continuous and asymptotically stable, robust controller was designed in Qu and Xu (2002) for a class of single–input single–output (SISO) nonlinear systems. The extensions to MIMO nonlinear systems were then presented in Xian et al. (2003) and Xian et al. (2004). As opposed to the standard sliding mode controllers that utilize sign of the tracking error, this controller formulation makes use of the integral of the sign of the tracking error. Probably due to aforementioned structure, the controller formulations using this type of feedback are also referred as RISE (acronym RISE, which is short for Robust Integral of Sign of Error, was first mentioned in Patre et al. (2008).) feedback and it has been applied to various nonlinear dynamic systems including underwater vehicle control Fischer et al. (2011), aerial vehicle control MacKunis et al. (2010), Shin et al. (2012b), mobile robot control Dierks and Jagannathan (2009), and for control of special classes of nonlinear systems Wang et al. (2010), Sharma et al. (2010), Wang and Behal (2011) since then.

Recently, in Wang et al. (2010), Wang et al. (2011), and Wang and Behal (2011), researchers have proposed robust and adaptive type controller formulations for the MIMO nonlinear systems of the form

$$x^{(n)} = H\left(x, \dot{x}, \cdots, x^{(n-1)}\right) + G\left(x, \dot{x}, \cdots, x^{(n-2)}\right)\tau \tag{1.1}$$

where $x^{(i)}(t) \in \mathbb{R}^m$ $i = 0, \cdots, n$, are the states with $(\cdot)^{(i)}$ denoting the i^{th} derivative with respect to time, $H(\cdot) \in \mathbb{R}^m$ and $G(\cdot) \in \mathbb{R}^{m\times m}$ are uncertain functions with $G(\cdot)$ being an input gain matrix with non–zero leading principal minors, and $\tau(t) \in \mathbb{R}^m$ is the control input. Specifically, in Wang et al. (2010), authors have extended the work of Zhang et al. (2004) by redesigning the controller of Chen et al. (2006) by removing an

algebraic loop and potential singularity in their previous design and obtained a globally uniformly ultimately bounded (UUB) tracking error performance. In Wang et al. (2011), an adaptive controller that ensures asymptotic tracking has been proposed. Recently, a continuous robust controller achieving semi–global asymptotic tracking performance for uncertain MIMO systems of the form (1.1) with two degrees of freedom (dof) was proposed in Wang and Behal (2011).

In this dissertation, the mathematical model of the special mechatronic systems mandates considering a broader class of uncertain MIMO nonlinear systems than that of (1.1) which has the following form

$$x^{(n)} = h\left(x, \dot{x}, \cdots, x^{(n-1)}\right) + g\left(x, \dot{x}, \cdots, x^{(n-1)}\right)\tau \tag{1.2}$$

where $x^{(i)}(t) \in \mathbb{R}^m$ $i = 0, \cdots, n$, are the states, $h(\cdot) \in \mathbb{R}^m$ is an uncertain function, $g(\cdot) \in \mathbb{R}^{m\times m}$ is an uncertain real matrix with non–zero leading principal minors, and $\tau(t) \in \mathbb{R}^m$ is the control input.

It is important to highlight that when compared to (1.1), the dependence of $g(\cdot)$ on $x^{(n-1)}$ complicates the control design, and in the literature, there are only a few works on this model.

In Xu and Ioannou (2003), a robust adaptive control scheme for the class of MIMO nonlinear systems described by (1.2) subject to unknown nonlinearities was presented. The design in the mentioned paper was based on assumptions that $h(\cdot)$ and $g(\cdot)$ are continuous and a sufficient condition for controllability is satisfied. To ensure the adaptive structure of this design, the estimate of $g(\cdot)$ was replaced by the estimate of a scalar function. A new continuous switching function was then used by the adaptive laws to guarantee closed–loop system stability and convergence of the tracking error even in the case where the estimated plant loses controllability. Closed–loop stability and robustness with respect to modeling errors was guaranteed for the MIMO case by utilizing a dead zone technique incorporated in the adaptive law. Semi global stability of the closed–loop system and convergence of the tracking error to a residual set whose size depends on design parameters that can be chosen a priori was guaranteed by the proposed scheme. This control approach provides a procedure for choosing the design parameters to meet the tracking error bound for any given desired upper bound of the steady state value of the tracking error.

In Xian et al. (2004), a full–state feedback tracking controller for a class of uncertain MIMO nonlinear systems was presented. Specifically, tracking control of the class of higher–order MIMO nonlinear systems in (1.2) was examined. A robust controller containing the integral of the signum of the error term was designed. Semi–global asymptotic

tracking was ensured under the assumptions that $h(\cdot)$ and $g(\cdot)$ are second–order differentiable, and $g(\cdot)$ is a positive–definite symmetric matrix. Uncertainties associated with $h(\cdot)$ and $g(\cdot)$ with limited assumptions with regard to the structures of the nonlinearities were compensated by the control approach.

More recently in Chen et al. (2008), a continuous robust tracking controller was developed for the class of higher–order MIMO nonlinear systems given in (1.2). It was considered that the leading principal minors of the input gain matrix are non–zero and their signs are known. The controller was designed by using the availability of these signs and UUB tracking was obtained while unstructured uncertainties in the input gain matrix were compensated.

In this dissertation, under similar restrictions as in Chen et al. (2008), a new continuous robust controller is designed for the class of nonlinear systems described by (1.2). Specifically, by applying a similar formulation to that of Xian et al. (2004), which is a nonlinear proportional integral controller fused with integral of the sign of the error feedback, asymptotic tracking can be achieved as opposed to the UUB tracking result of Chen et al. (2008). From this perspective, it might be said that this work extends the results given in Xian et al. (2004) to a broader class of nonlinear systems. It would like to be highlighted that, due to the nature of the nonlinearities and uncertainties in the system given by (1.2), extending the results given in Xian et al. (2004) is not a straightforward task. Explicitly, Xian et al. (2004) considered the case where the input gain matrix $g(\cdot)$ being positive definite, while it is considered that the case where $g(\cdot)$ has non–zero leading principal minors in this dissertation. The results in Xian et al. (2004) can be considered as special cases of the results presented in this dissertation. The stability analysis is conducted in four steps. Firstly, an initial Lyapunov function is introduced to prove the boundedness of all the signals under the closed–loop operation. Secondly, after utilizing the boundedness of the error signals, an integral inequality is obtained. Thirdly, a novel Lyapunov–like function is constructed and, via the use of the integral inequality, its non–negativeness is proven. Finally, after fusing this Lyapunov–like function with the initial Lyapunov function that was utilized to prove boundedness, asymptotic stability is proven.

1.2. Self–tuning Method for Adjusting Control Gains

Although the designed controller can be seen as a feasible solution for the control problem of mechatronic systems having non–symmetric input gain matrix, the control gain tuning process requires some specific lower bound conditions to be satisfied. These

conditions are utilized for the stability analysis and can be seen as restricting aspects of this approach. Since it directly affects the performance of the system, control gain adjusting process is one of the important tasks for the designed robust controller. Adjusting the control gains via trial–and–error method by considering these specific conditions is a hard and time consuming process. In addition to these, during experimental studies, an inappropriate selection of the control gains may be harmful for the experimental setup. As a result of these, studies were devoted to designing a self–tuning methodology that can be used for the robust controllers. A RISE type control design was utilized to propose a self–tuning methodology that can be used for the control gain adjustment process of the robust controllers.

While utilizing the integral of the sign of the error feedback in the controller formulation removes the need of using discontinuous feedback, similar to the previous variable structure type robust controllers, RISE type controllers still suffer from a high gain condition. The stability analysis presented for RISE type feedback controller dictates that a high controller gain, which needs to be larger than sum of the upper bounds of the overall system uncertainties and their time derivatives, is required to achieve asymptotic stability. Unfortunately, when the upper bounds of the uncertainties are not available, applying unnecessary higher gains usually results in a higher control effort. To reduce the heavy control effort caused by high control gains, some part of the relevant past research was devoted to fusing adaptive Patre et al. (2008) or neural network based Patre et al. (2007), Dierks and Jagannathan (2009) techniques with RISE feedback. While some other past research focused on designing time–varying gains for controllers utilizing RISE feedback. In Yang et al. (2011), a time–varying adaptive uncertainty compensation gain was designed for a neural network based controller utilizing RISE feedback. However, the boundedness of the time–varying adaptive gain was not ensured due to lack of $\mathcal{L}_1$ boundedness of the tracking error. In Zhang et al. (2014), a time–varying Nussbaum gain was proposed for controllers utilizing RISE feedback. However, for the design of the adaptive gain, the proposed methodology makes use of a term that is usually not available.

In this dissertation, the need of prior knowledge of upper bounds of the vector containing the desired system dynamics plus uncertainties (and their derivatives) for the control gain selection of controllers utilizing RISE feedback is removed via the use of an adaptive uncertainty compensation gain formulation. The use of an adaptive uncertainty compensation gain reduces the heavy control effort and therefore eliminates the need of extra feedforward compensation methods. Along with the adaptive uncertainty compensation gain, the proposed methodology also provides a time–varying feedback gain which

eases the overall gain tuning process for robust controllers utilizing RISE feedback. The stability analysis given in this dissertation ensures $\mathcal{L}_1$ boundedness of the tracking error utilized in the design of the time–varying gains which is then utilized to guarantee boundedness and convergence of the time–varying gains. As a result, a fully self tuning RISE feedback formulation has been obtained in this dissertation.

After completing the control design process by proposing this self–tuning method, three fundamentally different mechatronic systems were utilized to demonstrate the effectiveness of the designed controller fused with the proposed self–tuning method.

1.3. Compensating for Added Mass Terms in Dynamically Positioned Surface Vessels

Mostly because of its importance in marine industry, control of marine vehicles, especially control of slowly moving surface vessels, is a popular research topic. Operations such as towing, laying cables to the bottom of the ocean, and most of the operations related to the offshore oil industry usually provide a sufficiently smooth and a slow trajectory to be tracked. Researchers/engineers are required to design controllers/auto–pilots to obtain satisfactory tracking performance.

Several aspects of the above control problem was investigated and can be found in the literature Fossen (1994), Fossen (2002), Fossen (2011). There are linear control designs such as proportional integral derivative (PID) controllers in cascade with a low–pass filter Balchen et al. (1976). Optimal control laws in conjunction with Kalman filtering techniques Grimble et al. (1980), Sørensen et al. (1996) can be considered as other examples of linear control designs. Basically, the aforementioned control formulations linearize the system dynamics about a set of pre–specified yaw angles Fossen and Grøvlen (1998). On the other hand, there are several nonlinear robust and/or adaptive control designs that take the nonlinear ship dynamics into account in order to overcome the problems inherited by linearization Fjellstad and Fossen (1994), Wit et al. (1998), Fossen and Grøvlen (1998), Fang et al. (2004), Skjetne et al. (2004). In Fjellstad and Fossen (1994), a class of nonlinear control laws for position regulation were developed without guaranteeing their robustness against parametric uncertainties, and in Wit et al. (1998), a robust nonlinear control law using singular perturbation theory that takes parametric uncertainties and external disturbances into account was presented. Some other past research has focused on designing output feedback control algorithms Fossen and

Grøvlen (1998), Fang et al. (2004), Wondergem et al. (2011). In Fossen and Grøvlen (1998), a nonlinear output feedback controller utilizing an observer backstepping method was designed. An observer based output feedback tracking controller for fully actuated ships was presented in Wondergem et al. (2011). Review of the relevant literature highlights the fact that while several controllers were designed almost all of the past control designs considered the inertia matrix of the ship to be symmetric and positive definite, and laid their analysis and designs down on this assumption.

As detailed in Fossen (1994), Fossen and Strand (1999), Fossen (2002) and Skjetne et al. (2004), during the cruise, all the flow is effected by the motion of the ship and as a result of this, vibrations with different amplitudes occur on different parts of the flow. This situation results as pressure effects and moments acting on different parts of the ship which causes additional force and has influence on the acceleration of the ship. This effect, referred as added mass, should be represented in the dynamic model. There are different conventions Fossen and Strand (1999), Skjetne et al. (2004) on how to represent the added mass effects in the dynamic model. In Fossen and Strand (1999), after using inertial velocity as the velocity state, the added mass effects are represented via the inertia matrix.

The significance of added mass effects is due to its non–symmetric nature which causes the inertia matrix to lose its symmetry and when not appropriately dealt with, this may cause reduction in performance and even instability. In the literature, there are only a few control designs that considered non–symmetric added mass in the inertia matrix, such as adaptive and robust type controllers designed in Lee et al. (2008a) and Lee et al. (2008b), respectively. The aforementioned controllers were designed based on Lyapunov–type analysis methods, and were able to achieve only the ultimate boundedness of the tracking errors.

In this dissertation, robust control of surface vessels with added mass effect is discussed. The added mass terms are considered to be affecting the system dynamics at the acceleration level (*i.e.*, inertial velocity was chosen as the velocity state). Furthermore, the added mass effects are assumed to be non–symmetric, which results in a non–symmetric inertia matrix in vessel dynamics. In addition, the dynamic model is subject to unstructured uncertainties. In the control design, the mathematical model of the surface vessel is first converted into a compact form where neither symmetry nor positive definiteness of the input gain matrix is known. A matrix decomposition is then applied to the input gain matrix to obtain a symmetric and positive definite matrix that a filtered version of the tracking error is multiplied with. However, this decomposition results in the control

input to be premultiplied first with a known diagonal matrix with entries $+1$ or -1, and next with an uncertain unity upper triangular matrix (a unity upper triangular matrix is an upper triangular matrix with ones on the main diagonal). Then, a lower order form of the robust controller designed in Chapter 2 is proposed. The stability of the closed–loop system and the convergence of the tracking error are demonstrated via Lyapunov–type methods similar to Chapter 2. Numerical simulations are performed to demonstrate the performance of the robust controller.

1.4. Robust Control Design for an Unmanned Helicopter

Helicopters are versatile aerial vehicles that can perform hover and vertical take–off and landing maneuvers. Due to the aforementioned versatility, helicopters are useful for both military and civilian applications. However the corresponding flight dynamics are highly nonlinear and contains uncertainties associated with the dynamical terms. In addition to these, strong coupling effects and natural instability of their system dynamics make the controller design problem a challenging task. In general, the control system of the unmanned helicopters can be divided into two parts; namely as inner–loop level control and outer–loop level control. These parts are related with attitude and position control, respectively. Since position tracking can be ensured via inner–loop control, designing a controller for attitude control of helicopters is considered as the main control objective in this dissertation.

A review of some of the relevant past works on attitude control of helicopter systems is given. In Sakamato et al. (2006), after considering a linearized dynamic models of a helicopter, a PID controller was designed for attitude tracking control where similar approaches were realized with linear quadratic regulator control in Liu et al. (2013), output regulation in Nao et al. (2003) and feedback linearization in Kagawa et al. (2005). H_∞ control Gadewadikar et al. (2008), Kato et al. (2003) and sliding mode control Xian et al. (2015) are other approaches for attitude control of linearized dynamics. In Suzuki et al. (2011), a quartenion based adaptive attitude controller was designed for a small unmanned helicopter by using backstepping technique. In Tee et al. (2008), a robust adaptive neural network controller was presented for helicopters in vertical flight, with dynamics in SISO nonlinear nonaffine form. In Shin et al. (2010), a position tracking controller was developed for a rotorcraft–based unmanned aerial vehicle using RISE feedback in conjunction with neural network feedforward terms. In Liu et al. (2014), a nonlinear robust attitude tracking controller was developed for a small–scaled unmanned helicopter under

input constraints. In addition to these, neural network based control Shin et al. (2012a) and fuzzy control Kadmiry and Driankov (2004) are other approaches that were used for attitude control of helicopters.

In this dissertation, attitude tracking control of a small–scaled unmanned helicopter has been provided by designing a lower order form of the robust controller designed in Chapter 2. This design is based on the actual inputs namely the elevator servo input, the aileron servo input and the rudder servo input. The stability of the closed–loop system and the convergence of the tracking error are demonstrated via Lyapunov–type methods similar to Chapter 2. The performance of the designed controller is then demonstrated via numerical simulations.

1.5. Robust Dynamic Positioning of Surface Vessels via Multiple Uni–directional Tugboats

Position control of large surface vessels like barges, offshore platforms and unactuated ships, throughout a narrow canal or in crowded harbors is an extremely delicate and important application as these large vessels usually are not designed, or not able to generate the necessary control effort to maneuver in these circumstances. Manipulation with multiple tugboats is a feasible solution for maneuvering these type of surface vessels. The motion objective is realized via a group of tugboats that are strategically positioned along the vessel's hull. When this operation is performed manually, due to the radio communication between all involved tugboats, the overall control performance is affected dramatically. Although the communication performance is increased with advanced global positioning systems, control of these type of systems is still challenging due to possible problems that may arise in the communication system during the manipulation. As a result, positioning of unactuated surface vessels has attracted attention of control community.

In the last decade, different types of automatic controller designs have been proposed for these type of applications. Recently, in Vlachos and Papadopoulos (2013), modeling of a novel triangle–shaped floating marine vessel was presented along with the design of a feedback linearization controller. The proposed controller required accurate model knowledge and achieved ultimately bounded position tracking result. In Feemster et al. (2006), orientation tracking control of an unactuated vessel through the utilization of a swarm of vehicles operating in a decentralized fashion was achieved via a robust

control strategy. In this design, the influence of other swarm vehicles was treated as a force disturbance acting on system dynamics. In Smith et al. (2007), an exact model knowledge position and orientation tracking controller was proposed for an unactuated surface vessel. In Feemster and Esposito (2011), a tracking controller subject to control saturation due to the limitations of the tugboats was designed where accurate knowledge of the dynamic model of the unactuated surface vessel was utilized in the control design. In Braganza et al. (2007), an adaptive position control strategy that does not require the location of the tugboats about the vessel hull was proposed. The adaptive controller proposed in Braganza et al. (2007) did not require a communication link between the tugboats as well. Another adaptive control strategy was presented in Bui et al. (2010) that took the uncertainty of system parameters into account. In Esposito et al. (2008), an optimization based force/torque allocation was employed and compared against a commutation based force/torque allocation strategy. In Bui and Kim (2011), position tracking control of ship berthing with assistance of autonomous tugboats was provided by using sliding mode control approach, while, a robust approach was presented in Ji et al. (2013). Recently, in Tran and Im (2012), artificial neural networks were utilized to address the same problem. While several control aspects of the problem were researched, most of the above mentioned works required poses of the tugboats relative to the center of mass of the unactuated surface vessel to remain unchanged (*i.e.*, static positioning was assumed) which is usually not the case due to several disturbances. An attempt to relax the static positioning of the tugboats was discussed in Topp and Feemster (2010) for a simple one dof scenario. Unfortunately, the extension of the result to manipulation of an unactuated surface vessel with multiple tugboats problem was not straightforward.

In this dissertation, a robust controller is proposed for the position tracking control of a large surface vessel manipulated by 6 uni–directional tugboats. For this design, the dynamic model of the surface vessel is considered to be uncertain and it was also considered to be under the influence of added mass effects. The control problem is further complicated by the lack of accurate positions and orientations of the tugboats. First, the dynamic model of a 3 dof unactuated surface vessel manipulated by 6 uni–directional tugboats is given. Upon specification of the initial configurations of the uni–directional tugboats, the control is considered to be performed by 3 bi–directional tugboats where a force decomposition and commutation strategy is employed. Next, the open-loop error system is obtained where an uncertain input gain matrix, which includes uncertain inertia matrix of the surface vessel and uncertain thrust configuration matrix including uncertain possibly time–varying positions and orientations of tugboats, is obtained. A matrix de-

composition is applied to initiate the control design. A lower order form of the robust controller designed in Chapter 2 is then proposed. Stability analysis is presented where asymptotic tracking is ensured. Numerical simulations are performed where the positions and orientations of the tugboats are perturbed with sinusoidal disturbances are presented to illustrate the performance of the proposed method.

The rest of this dissertation is organized in the following manner. Control design is given with its detailed analysis in Chapter 2. Self–tuning method is proposed in Chapter 3. In Chapter 4, mechatronic systems are introduced and the designed controller is adopted for these systems. Efficiency of the proposed methods are demonstrated via numerical results in Chapter 5. Finally, conclusions and possible future works are given in Chapter 6.

The main contributions of this dissertation are:

- **Novel** continuous robust controller for a class of MIMO nonlinear systems that contain unstructured uncertainties in their drift vectors and input matrices was designed. The proposed controller compensates uncertainties in the system dynamics and achieves asymptotic tracking while requiring only the knowledge of the sign of the leading principal minors of the input gain matrix. In assistance of its input gain matrix independent structure, proposed controller became an appropriate design for the mechatronic systems that have non–symmetric input gain matrix.

- A self–tuning method for adjusting the control gains of the designed robust controller is proposed. **It is the first time** that a self–tuning methodology is proposed for these type of controllers.

- Performance of the designed controller in conjunction with the proposed self–tuning method is demonstrated via simulation and experimental results.

- Position tracking control of a dynamically positioned surface vessel is ensured via the proposed controller. Dealing with the non–symmetric effects of added mass appear in the vessel dynamics is the main **novelty** of this design.

- Attitude control of a small–scaled unmanned model helicopter is guaranteed via the proposed controller. Considering a non–symmetric matrix pre–multiplying the control input vector caused from the rotor dynamics of helicopter and dealing with this are the main **novelties** of this design.

- Position tracking control of a large surface vessel manipulated by 6 uni–directional tugboats is addressed. Considering non–symmetric inertial added mass effects in

addition to the non–symmetric and time–varying thrust configuration matrix and dealing with these are the main **novelties** of this design.

The results in this dissertation are presented in the following publications:

- **Bidikli B.**, Tatlicioglu E., Bayrak A. and Zergeroglu E. (2013). A New Robust 'Integral of Sign of Error' Feedback Controller with Adaptive Compensation Gain. In Proc. of IEEE Conference on Decision and Control, Firenze, Italy, pp. 3782–3787.

- **Bidikli B.**, Tatlicioglu E. and Zergeroglu E. (2014). A Self Tuning RISE Controller Formulation. In Proc. of American Control Conference, Portland, OR, USA, pp. 5608–5613.

- **Bidikli B.**, Tatlicioglu E. and Zergeroglu E. (2014). A Robust Tracking Controller for Dynamically Positioned Surface Vessels with Added Mass. In Proc. of IEEE Conference on Decision and Control, Los Angeles, CA, USA, pp. 4385–4390.

- **Bidikli B.**, Tatlicioglu E. and Zergeroglu E. (2015). Robust Control Design for Positioning of an Unactuated Surface Vessels. In Proc. of IEEE International Conference on Intelligent Robots and Systems, Hamburg, Germany, pp. 1071–1076.

- **Bidikli B.**, Tatlicioglu E. and Zergeroglu E. (2016). Robust Dynamic Positioning of Surface Vessels via Multiple Unidirectional Tugboats. Ocean Engineering 113, pp. 237–245.

- **Bidikli B.**, Tatlicioglu E., Zergeroglu E. and Bayrak A. (2016). An Asymptotically Stable Robust Controller Formulation for a Class of MIMO Nonlinear Systems with Uncertain Dynamics. International Journal of Systems Science 47(12), pp. 2913–2924.

- **Bidikli B.**, Tatlicioglu E., Zergeroglu E. and Bayrak A. (2016). A Self Tuning Robust Integral of Sign of Error (RISE) type Feedback Controller Formulation for a Class of Nonlinear Uncertain Systems. IEEE Transactions on Automatic Control, under review.

- **Bidikli B.**, Tatlicioglu E., Zergeroglu E. and Bayrak A. (2016). Compensating of Added Mass Terms in Dynamically Positioned Surface Vehicles: A Continuous Robust Control Approach. Ocean Engineering, under review.

- **Bidikli B.**, Tatlicioglu E. and Zergeroglu E. (2016). Robust Control Design for an Unmanned Helicopter: A Full-state Feedback Approach. In Proc. of The 20th World Congress of the International Federation of Automatic Control, Toulouse, France, under review.

CHAPTER 2

CONTROL DESIGN FOR MIMO NONLINEAR SYSTEMS

In this chapter, the design of a continuous robust controller for a class of MIMO nonlinear systems that contains unstructured uncertainties in their drift vectors and input matrices is presented. The proposed controller compensates uncertainties in the system dynamics and achieves asymptotic tracking while requiring only the knowledge of the sign of the leading principal minors of the input gain matrix. A Lyapunov–based argument backed up with an integral inequality is applied to prove the asymptotic stability of the closed–loop system.

The rest of the chapter is organized as follows. Section 2.1 introduces the error system development while the controller development is presented in Section 2.2. Stability of the closed–loop system under the proposed method is investigated in Section 2.3. Finally, conclusions are given in Section 2.4.

2.1. Open–Loop Error System Development

The uncertain functions $h(\cdot)$ and $g(\cdot)$ of (1.2) are assumed to be at least second–order differentiable (*i.e.*, $h(\cdot), g(\cdot) \in \mathcal{C}^2$). Based on the assumption that $g(\cdot)$ being a real valued matrix with non–zero leading principal minors, the following matrix decomposition is utilized Morse (1993), Costa et al. (2003)

$$g = S(X)DU(X) \tag{2.1}$$

where $X(t) \triangleq \left[\begin{array}{cccc} x^T & \dot{x}^T & \cdots & \left(x^{(n-1)}\right)^T \end{array} \right]^T \in \mathbb{R}^{mn}$ is the combined state vector, $S(X) \in \mathbb{R}^{m\times m}$ is a symmetric, positive definite matrix, $D \in \mathbb{R}^{m\times m}$ is a diagonal matrix with entries being ± 1, and $U(X) \in \mathbb{R}^{m\times m}$ is a unity upper triangular matrix. Similar to Costa et al. (2003) and Chen et al. (2008), it is assumed that D is available for control design. It would like to be noted that since the leading principal minors of $g(X)$ are non–zero, $g^{-1}(X)$ exists and following expression can be obtained by pre–multiplying (1.2) with $g^{-1}(X)$

$$\tau = g^{-1}\left(x^{(n)} - h\right). \tag{2.2}$$

Taking the time derivative of the system model in (1.2) and then substituting into

(2.2) yields

$$x^{(n+1)} = \varphi + SDU\dot{\tau} \tag{2.3}$$

where (2.1) was utilized, and $\varphi\left(X, x^{(n)}\right) \in \mathbb{R}^m$ is an auxiliary function defined to have the following form

$$\varphi \triangleq \dot{h} + \dot{g}g^{-1}\left(x^{(n)} - h\right). \tag{2.4}$$

Multiplying both sides of (2.3) with $S^{-1}(X)$ results in

$$S^{-1}x^{(n+1)} = S^{-1}\varphi + DU\dot{\tau} \tag{2.5}$$

and after defining $M(X) \triangleq S^{-1} \in \mathbb{R}^{m\times m}$ and $f\left(X, x^{(n)}\right) \triangleq S^{-1}\varphi \in \mathbb{R}^m$, it is obtained that

$$Mx^{(n+1)} = f + DU\dot{\tau}. \tag{2.6}$$

It is noted that $M(X)$ satisfies following inequalities

$$\underline{m}\left\|\chi\right\|^2 \leq \chi^T M(X)\chi \leq \bar{m}(X)\left\|\chi\right\|^2 \quad \forall \chi \in \mathbb{R}^m \tag{2.7}$$

with $\underline{m} \in \mathbb{R}$ is a positive bounding constant, and $\bar{m}(X) \in \mathbb{R}$ is a positive, non–decreasing function.

Main control objective is to ensure that the system output $x(t)$ tracks a given smooth desired trajectory while ensuring all signals within the closed–loop system remain bounded. In order to quantify the tracking control objective, the output tracking error denoted by $e_1(t) \in \mathbb{R}^m$, is defined to have the following form

$$e_1 \triangleq x_r - x \tag{2.8}$$

where $x_r(t) \in \mathbb{R}^m$ is the desired trajectory satisfying

$$x_r(t) \in \mathcal{C}^{n+1}, x_r^{(i)}(t) \in \mathcal{L}_\infty, i = 0, 1, \cdots, (n+1). \tag{2.9}$$

In the controller development, a full state feedback approach will be utilized (*i.e.*, the combined state vector $X(t)$ is available).

To facilitate the control design, auxiliary errors, denoted by $e_i(t) \in \mathbb{R}^m$, $i = 2, \cdots, n$, are defined as follows

$$e_2 \triangleq \dot{e}_1 + e_1 \tag{2.10}$$

$$e_3 \triangleq \dot{e}_2 + e_2 + e_1 \tag{2.11}$$

$$\vdots$$

$$e_n \triangleq \dot{e}_{n-1} + e_{n-1} + e_{n-2}. \tag{2.12}$$

A general expression for $e_i(t)$, $i = 2, \cdots, n$, in terms of $e_1(t)$ and its time derivatives can be obtained as

$$e_i = \sum_{j=0}^{i-1} a_{i,j} e_1^{(j)} \tag{2.13}$$

where $a_{i,j} \in \mathbb{R}$ are known positive constants, generated via a Fibonacci number series Xian et al. (2004). Proposed controller development also requires the definition of an auxiliary error term, denoted by $r(t) \in \mathbb{R}^m$, which has the following form

$$r \triangleq \dot{e}_n + \alpha e_n \tag{2.14}$$

where $\alpha \in \mathbb{R}^{m \times m}$ is a constant, positive definite, diagonal gain matrix. It should further be noted that the auxiliary error terms in (2.10)–(2.14) are introduced to obtain a stability analysis where only first order time derivatives are utilized.

After differentiating (2.14) and pre–multiplying the resulting equation with $M(X)$, following expression can be derived

$$M\dot{r} = M\left(x_r^{(n+1)} + \sum_{j=0}^{n-2} a_{n,j} e_1^{(j+2)} + \alpha \dot{e}_n\right) - f - DU\dot{\tau} \tag{2.15}$$

where (2.6), (2.8), (2.13), and the fact that $a_{n,(n-1)} = 1$ were utilized. After defining an auxiliary function, $N\left(X, x^{(n)}, t\right) \in \mathbb{R}^m$, as follows

$$N \triangleq M\left(x_r^{(n+1)} + \sum_{j=0}^{n-2} a_{n,j} e_1^{(j+2)} + \alpha \dot{e}_n\right) - f + e_n + \frac{1}{2}\dot{M}r \tag{2.16}$$

the expression in (2.15) can be reformulated to have the following form

$$M\dot{r} = -\frac{1}{2}\dot{M}r - e_n - DU\dot{\tau} + N. \tag{2.17}$$

Furthermore, the error dynamics in (2.17) can be rearranged as

$$M\dot{r} = -\frac{1}{2}\dot{M}r - e_n - D(U - I_m)\dot{\tau} - D\dot{\tau} + \widetilde{N} + \bar{N} \tag{2.18}$$

where $D\dot{\tau}(t)$ was added and subtracted to the right–hand side, $I_m \in \mathbb{R}^{m \times m}$ is the standard identity matrix, and $\bar{N}(t)$, $\widetilde{N}(t) \in \mathbb{R}^m$ are auxiliary functions defined as follows

$$\bar{N} \triangleq N\big|_{X = X_r, x^{(n)} = x_r^{(n)}} \tag{2.19}$$

$$\widetilde{N} \triangleq N - \bar{N} \tag{2.20}$$

with $X_r(t) \triangleq \left[\begin{array}{cccc} x_r^T & \dot{x}_r^T & \cdots & \left(x_r^{(n-1)}\right)^T \end{array}\right]^T \in \mathbb{R}^{mn}$ being a combination of the desired trajectory and its time derivatives. The main idea behind adding and subtracting $D\dot{\tau}(t)$

term to the right–hand side of (2.18) is to make use of the fact that $U(X)$ is unity upper triangular, and thus $(U - I_m)$ is strictly upper triangular.

Throughout this dissertation, the notation $\bar{(\cdot)}$ is preferred to denote a function that depends on the desired trajectory and its time derivatives, and $\widetilde{(\cdot)}$ denotes a function that can be upper bounded by functions of the error terms.

2.2. Controller Design

Based on the open–loop error system in (2.18) and the subsequent stability analysis, the control input $\tau(t)$ is designed in the following form

$$\tau = DK\left[e_n(t) - e_n(t_0) + \alpha \int_{t_0}^{t} e_n(\sigma)\, d\sigma\right] + D\Pi \tag{2.21}$$

where the auxiliary term $\Pi(t) \in \mathbb{R}^m$ is generated according to the following update rule

$$\dot{\Pi} = \beta \text{Sgn}(e_n) \text{ with } \Pi(t_0) = 0_m. \tag{2.22}$$

In (2.21) and (2.22), $K, \beta \in \mathbb{R}^{m\times m}$ are constant, positive definite, diagonal gain matrices, $0_m \in \mathbb{R}^m$ is a vector of zeros and $\text{Sgn}(\cdot) \in \mathbb{R}^m$ is the vector signum function. Notice that, for $i = n$ in (2.13), $e_n(t)$ and thus $\tau(t)$ depend on $x(t)$, $\dot{x}(t)$, $\cdots$, $x^{(n-1)}(t)$, and not $x^{(n)}(t)$. The control gain is designed as

$$K = I_m + k_p I_m + \text{diag}\left\{k_{d,1}, \cdots, \ k_{d,(m-1)}, 0\right\} \tag{2.23}$$

where k_p, $k_{d,i} \in \mathbb{R}$ are constant, positive, control gains, and $\text{diag}\{\cdot\}$ is used to represent the entries of a diagonal matrix. Finally, after substituting the time derivative of (2.21) into (2.18), the closed–loop error system for $r(t)$ is obtained as

$$M\dot{r} = -\frac{1}{2}\dot{M}r - e_n - Kr + \widetilde{N} + \bar{N} - D(U - I_m)DKr - DUD\beta \text{Sgn}(e_n) \tag{2.24}$$

where the fact that $DD = I_m$ was utilized.

Before proceeding with the stability analysis, last two terms of (2.24) will be investigated separately.

Note that, after utilizing the fact that $(U - I_m)$ being strictly upper triangular, the term $D(U - I_m)DKr$ is rewritten as

$$D(U - I_m)DKr = \begin{bmatrix} \Lambda + \Phi \\ 0 \end{bmatrix} \tag{2.25}$$

where $\Lambda(t)$, $\Phi(t) \in \mathbb{R}^{m-1}$ are auxiliary functions with their entries $\Lambda_i(t)$, $\Phi_i(t) \in \mathbb{R}$, $i = 1, \cdots, (m-1)$, being defined as

$$\Lambda_i \triangleq d_i \sum_{j=i+1}^{m} d_j k_j \widetilde{U}_{i,j} r_j \tag{2.26}$$

$$\Phi_i \triangleq d_i \sum_{j=i+1}^{m} d_j k_j \bar{U}_{i,j} r_j \tag{2.27}$$

with $\bar{U}_{i,j}(X_r)$, $\widetilde{U}_{i,j}(t) \in \mathbb{R}$ are defined as

$$\bar{U}_{i,j} \triangleq U_{i,j}|_{X=X_r} \tag{2.28}$$

$$\widetilde{U}_{i,j} \triangleq U_{i,j} - \bar{U}_{i,j} \tag{2.29}$$

where $U_{i,j}(X) \in \mathbb{R}$ are the entries of $U(X)$. Notice from (2.25) that the last entry of the term $D(U - I_m)DKr$ is equal to 0, and its i^{th} entry depends on the $(i+1)^{\text{th}}$ to m^{th} entries of the control gain matrix K.

The term $DUD\beta\text{Sgn}(e_n)$ is rewritten as

$$DUD\beta\text{Sgn}(e_n) = \begin{bmatrix} \Psi \\ 0 \end{bmatrix} + \Theta \tag{2.30}$$

where $\Psi(t) \in \mathbb{R}^{m-1}$ and $\Theta(t) \in \mathbb{R}^m$ are auxiliary functions defined as

$$\begin{bmatrix} \Psi \\ 0 \end{bmatrix} \triangleq D\left(U - \bar{U}\right) D\beta\text{Sgn}(e_n) \tag{2.31}$$

$$\Theta \triangleq D\bar{U}D\beta\text{Sgn}(e_n) \tag{2.32}$$

where $\bar{U}(X_r) \triangleq U|_{X=X_r} \in \mathbb{R}^{m\times m}$ is a function of desired trajectory and its time derivatives. The terms $\Psi_i(t) \in \mathbb{R}$, $i = 1, \cdots, (m-1)$ and $\Theta_i(t) \in \mathbb{R}$, $i = 1, \cdots, m$, are defined as

$$\Psi_i \triangleq d_i \sum_{j=i+1}^{m} d_j \beta_j \widetilde{U}_{i,j} \text{sgn}(e_{n,j}) \tag{2.33}$$

$$\Theta_i \triangleq d_i \sum_{j=i}^{m} d_j \beta_j \bar{U}_{i,j} \text{sgn}(e_{n,j}). \tag{2.34}$$

The Mean Value Theorem in Khalil (2002) can be utilized to develop the following upper bounds

$$\left\|\widetilde{N}(t)\right\| \leq \rho_{\widetilde{N}}(\|z\|)\|z\| \tag{2.35}$$

$$\left\|\widetilde{U}_{i,j}(t)\right\| \leq \rho_{i,j}(\|z\|)\|z\| \tag{2.36}$$

where $\|\cdot\|$ denotes the standard Euclidean norm, $\rho_{\widetilde{N}}$, $\rho_{i,j} \in \mathbb{R}$ are non–negative, globally invertible, non–decreasing functions of their arguments, and $z(t) \in \mathbb{R}^{(n+1)m}$ is defined by

$$z \triangleq \begin{bmatrix} e_1^T & e_2^T & \cdots & e_n^T & r^T \end{bmatrix}^T. \tag{2.37}$$

It can be seen from (2.9), (2.16), (2.19) that $\bar{N}(t)$ and $\bar{U}_{i,j}(t)$ can be upper bounded in the sense that

$$\left|\bar{N}_i(t)\right| \leq \zeta_{\bar{N}_i} \tag{2.38}$$

$$\left|\bar{U}_{i,j}(t)\right| \leq \zeta_{\bar{U}_{i,j}} \qquad \forall t \tag{2.39}$$

where $\zeta_{\bar{N}_i}$, $\zeta_{\bar{U}_{i,j}} \in \mathbb{R}$ are positive bounding constants. Based on (2.26), (2.27), (2.33) and (2.34), following upper bounds can be obtained

$$|\Lambda_i| \leq \rho_{\Lambda_i}(\|z\|)\|z\| \tag{2.40}$$

$$|\Phi_i| \leq \sum_{j=i+1}^{m} k_j \zeta_{\bar{U}_{i,j}} |r_j| \leq \zeta_{\Phi_i}\|z\| \tag{2.41}$$

$$|\Psi_i| \leq \rho_{\Psi_i}(\|z\|)\|z\| \tag{2.42}$$

$$|\Theta_i| \leq \sum_{j=i}^{m} \beta_j \zeta_{\bar{U}_{i,j}} \leq \zeta_{\Theta_i} \tag{2.43}$$

where (2.35)–(2.39) were utilized. From (2.43), it is easy to see that $\|\Theta(t)\| \leq \zeta_\Theta \ \forall t$ is satisfied for some positive bounding constant $\zeta_\Theta \in \mathbb{R}$, and from (2.40)–(2.42), the following inequality can be obtained

$$|\Lambda_i| + |\Phi_i| + |\Psi_i| \leq \rho_i(\|z\|)\|z\| \tag{2.44}$$

where $\rho_i(\|z\|) \in \mathbb{R}$ $i = 0, 1, \cdots, (m-1)$, are non–negative, globally invertible, non–decreasing functions satisfying

$$\rho_{\Lambda_i} + \rho_{\Psi_i} + \zeta_{\Phi_i} \leq \rho_i. \tag{2.45}$$

As a result of the fact that $\bar{U}(t)$ being unity upper triangular, $\Theta(t)$ in (2.32) can be rewritten as

$$\Theta = (I_m + \Omega)\beta \mathrm{Sgn}(e_n) \tag{2.46}$$

where $\Omega(t) \triangleq D\left(\bar{U} - I_m\right)D \in \mathbb{R}^{m\times m}$ is a strictly upper triangular matrix. Since it is a function of the desired trajectory and its time derivatives, its entries, denoted by $\Omega_{i,j}(t) \in \mathbb{R}$, are bounded in the sense that

$$|\Omega_{i,j}(t)| \leq \zeta_{\Omega_{i,j}} \qquad \forall t \tag{2.47}$$

where $\zeta_{\Omega_{i,j}} \in \mathbb{R}$ are positive bounding constants.

At this point, the stability analysis of the proposed robust controller can be proceeded.

2.3. Stability Analysis

In this section, the stability of the closed–loop system is presented in the following order:

- First, the boundedness of all terms including the error terms will be proven under the closed–loop operation.
- After utilizing the boundedness result, a lemma will be presented with which an upper bound for the integral of the absolute values of the entries of $\dot{e}_n(t)$ will be obtained.
- This upper bound will then be utilized in another lemma to prove the non–negativity of a Lyapunov–like function.
- Then, this Lyapunov–like function will be used in the final analysis to prove asymptotic stability of the tracking error.

Theorem 2.3.1 *For the uncertain MIMO system of* (1.2)*, the controller in* (2.21) *and* (2.22) *guarantees the boundedness of all the closed–loop terms including the error terms in* (2.8)*,* (2.10)–(2.12) *and* (2.14) *provided that the control gains $k_{d,i}$ and k_p are chosen large enough compared to the initial conditions of the system and the following condition is satisfied*

$$\lambda_{\min}(\alpha) \geq \frac{1}{2} \tag{2.48}$$

where the notation $\lambda_{\min}(\alpha)$ denotes the minimum eigenvalue of α.

Proof The non–negative function $V_1(z) \in \mathbb{R}$ is defined as

$$V_1 \triangleq \frac{1}{2}\sum_{i=1}^{n} e_i^T e_i + \frac{1}{2} r^T M r. \tag{2.49}$$

By utilizing (2.7), (2.49) can be bounded in the following manner

$$\frac{1}{2}\min\{1, \underline{m}\}\|z\|^2 \leq V_1(z) \leq \frac{1}{2}\max\{1, \bar{m}(\|z\|)\}\|z\|^2 \tag{2.50}$$

where $z(t)$ was defined in (2.37), and the terms $\underline{m}$, $\bar{m}\left(\|z\|\right)$ were defined in (2.7). Using (2.8) and (2.10)–(2.12) in (2.50), it can be shown that $\|(x, \dot{x}, \cdots, x^{n-1})\| \leq \psi\left(\|z\|\right)$ for some positive function $\psi\left(\cdot\right)$. Thus, $\bar{m}\left(x, \dot{x}, \cdots, x^{n-1}\right) \leq \bar{m}\left(\|z\|\right)$.

Taking the time derivative of (2.49) yields

$$\dot{V}_1 = \sum_{i=1}^{n} e_i^T \dot{e}_i + r^T M \dot{r} + \frac{1}{2} r^T \dot{M} r. \tag{2.51}$$

The first term in the above expression can be written as follows

$$\begin{aligned} \sum_{i=1}^{n} e_i^T \dot{e}_i &= e_1^T \left(e_2 - e_1\right) + e_2^T \left(e_3 - e_2 - e_1\right) + e_3^T \left(e_4 - e_3 - e_2\right) \\ &\quad + ... + e_{n-1}^T \left(e_n - e_{n-1} - e_{n-2}\right) + e_n^T \left(r - \alpha e_n\right) \\ &= -\sum_{i=1}^{n-1} e_i^T e_i + e_{n-1}^T e_n + e_n^T r - e_n^T \alpha e_n \end{aligned} \tag{2.52}$$

where (2.10)–(2.12), (2.14) were utilized. Substituting (2.24)–(2.27), (2.30)–(2.32) and (2.52) into (2.51) results in

$$\begin{aligned} \dot{V}_1 &= -\sum_{i=1}^{n-1} e_i^T e_i + e_{n-1}^T e_n + e_n^T r - e_n^T \alpha e_n + r^T \left(-\frac{1}{2}\dot{M} r - e_n - K r + \widetilde{N} + \bar{N}\right) \\ &\quad - r^T \begin{bmatrix} \Lambda + \Phi \\ 0 \end{bmatrix} - r^T \begin{bmatrix} \Psi \\ 0 \end{bmatrix} - r^T \Theta + \frac{1}{2} r^T \dot{M} r \end{aligned} \tag{2.53}$$

which, after substituting the control gain matrix K, can be rewritten as

$$\begin{aligned} \dot{V}_1 &= -\sum_{i=1}^{n-1} e_i^T e_i + e_{n-1}^T e_n - e_n^T \alpha e_n - r^T r + \left[r^T \widetilde{N} - k_p r^T r\right] \\ &\quad + \left[-\sum_{i=1}^{m-1} r_i \left(\Lambda_i + \Psi_i + \Phi_i\right) - \sum_{i=1}^{m-1} k_{d,i} r_i^2\right] + r^T \bar{N} - r^T \Theta. \end{aligned} \tag{2.54}$$

After completing the squares in bracketed terms, utilizing $\left\|\bar{N}\left(t\right)\right\| \leq \zeta_{\bar{N}}$, $\|\Theta\left(t\right)\| \leq \zeta_{\Theta}$ and $e_{n-1}^T e_n \leq 1/2 \left\|e_{n-1}\right\|^2 + 1/2 \left\|e_n\right\|^2$, the following inequality is obtained

$$\begin{aligned} \dot{V}_1 &\leq -\sum_{i=1}^{n-2} \left\|e_i\right\|^2 - \frac{1}{2}\left\|e_{n-1}\right\|^2 - \left(\lambda_{\min}\left(\alpha\right) - \frac{1}{2}\right)\left\|e_n\right\|^2 - r^T r + \frac{\rho_{\widetilde{N}}^2\left(\|z\|\right)}{4k_p}\|z\|^2 \\ &\quad + \sum_{i=1}^{m-1} \frac{\rho_i^2\left(\|z\|\right)}{4k_{d,i}}\|z\|^2 + \zeta_{\bar{N}}\|r\| + \zeta_{\Theta}\|r\| \end{aligned} \tag{2.55}$$

which can be rearranged as

$$\dot{V}_1 \leq -\left(\lambda_1 - \frac{\rho_{\widetilde{N}}^2\left(\|z\|\right)}{4k_p} - \sum_{i=1}^{m-1} \frac{\rho_i^2\left(\|z\|\right)}{4k_{d,i}}\right)\|z\|^2 + \delta\varepsilon^2 \tag{2.56}$$

where $\lambda_1 \triangleq \min\left\{\frac{1}{2}, \lambda_{\min}(\alpha) - \frac{1}{2}, 1 - \frac{1}{4\delta}\right\}$, $\delta \in \mathbb{R}$ is a positive bounding constant that is constituted by utilizing a definition and an upper bound given as $\varepsilon \triangleq \zeta_{\bar{N}} + \zeta_{\Theta}$ and $\varepsilon \|r\| \leq \frac{1}{4\delta}\|r\|^2 + \delta\varepsilon^2$, respectively. Provided that the controller gains $k_{d,i}$ and k_p are selected sufficiently large (larger than functions of the initial values of the norm of $z(t)$), it can be ensured that the terms in parenthesis on the right hand side of (2.56) remain positive. After utilizing (2.50), the following inequality can then be obtained

$$\dot{V}_1 \leq -\mu_1 V_1 + \delta\varepsilon^2 \tag{2.57}$$

where $\mu_1 \in \mathbb{R}$ is a positive constant. From (2.49) and (2.57), it can be concluded that $V_1(t) \in \mathcal{L}_\infty$, therefore $e_i(t)$, $i = 1, \cdots, n$, and $r(t)$ are uniformly ultimately bounded. Standard signal chasing arguments can then be utilized to prove that all the terms remain bounded under the closed–loop operation.

Lemma 2.3.2 *Provided that $e_n(t)$ and $\dot{e}_n(t)$ are bounded, the following expression for the upper bound of the integral of the absolute value of the i^{th} entry of $\dot{e}_n(t)$, $i = 1, \cdots, m$, can be obtained*

$$\int_{t_0}^{t} |\dot{e}_{n,i}(\sigma)|\, d\sigma \leq \gamma_1 + \gamma_2 \int_{t_0}^{t} |e_{n,i}(\sigma)|\, d\sigma + |e_{n,i}(t)| \tag{2.58}$$

where γ_1, $\gamma_2 \in \mathbb{R}$ are some positive bounding constants.

Proof While the proof is similar to that of the one given in Stepanyan and Kurdila (2009), it is presented for the sake of completeness. First, it should be noted that if $e_{n,i}(t) \equiv 0$ on some interval, then $\dot{e}_{n,i}(t) \equiv 0$ on the same interval, and the inequality (2.58) yields this qualification. Therefore, without loss of generality, it is assumed that $e_{n,i}(t)$ is absolutely greater than zero on the interval of $[t_0, t]$. Let $T \in [t_0, t)$ be the last instant of time when $\dot{e}_{n,i}(t)$ changes sign. Then, on the interval $[T, t]$, $\dot{e}_{n,i}(t)$ has a constant sign, hence

$$\int_{T}^{t} |\dot{e}_{n,i}(\sigma)|\, d\sigma = \left| \int_{T}^{t} \dot{e}_{n,i}(\sigma)\, d\sigma \right| = |e_{n,i}(t) - e_{n,i}(T)|. \tag{2.59}$$

From the boundedness of $\dot{e}_{n,i}(t)$, it follows that there exists a constant $\gamma > 0$ such that $|\dot{e}_{n,i}(t)| \leq \gamma$, therefore

$$\int_{t_0}^{T} |\dot{e}_{n,i}(\sigma)|\, d\sigma \leq \gamma (T - t_0). \tag{2.60}$$

On the other hand, the following equality is obtained after applying the Mean Value Theorem in Khalil (2002)

$$\int_{t_0}^{T} |e_{n,i}(\sigma)|\, d\sigma = e_{n,i_*}(T - t_0) \tag{2.61}$$

where e_{n,i_*} is some constant value of $|e_{n,i}(t)|$ on the interval $[t_0, T]$. By assumption, e_{n,i_*} is bounded away from zero. Therefore, by using inequality (2.60) and equality (2.61), it can be concluded as

$$\int_{t_0}^{T} |\dot{e}_{n,i}(\sigma)|\, d\sigma \leq \gamma_2 \int_{t_0}^{T} |e_{n,i}(\sigma)|\, d\sigma \tag{2.62}$$

where $\gamma_2 \triangleq \gamma / e_{n,i_*}$. Combining the relationships in (2.59) and (2.62), it can be written that

$$\int_{t_0}^{t} |\dot{e}_{n,i}(\sigma)|\, d\sigma \leq |e_{n,i}(T)| + \gamma_2 \int_{t_0}^{T} |e_{n,i}(\sigma)|\, d\sigma + |e_{n,i}(t)| \tag{2.63}$$

which, after defining $\gamma_1 \triangleq \sup |e_{n,i}(T)|$ yields the inequality (2.58). At this point it should be stated that $\sup |\cdot|$ denotes the supremum function.

Lemma 2.3.3 *Consider the term*

$$L \triangleq r^T \left(\bar{N} - (I_m + \Omega)\, \beta \mathit{Sgn}(e_n) \right) \tag{2.64}$$

where $\Omega(t)$ introduced in (2.46) *is a strictly upper triangular matrix that is a function of desired trajectory and its time derivatives. Provided that the entries of the control gain β are chosen to satisfy*

$$\beta_m \geq \zeta_{\bar{N}_m} \left(1 + \frac{\gamma_2}{\alpha_m} \right) \tag{2.65}$$

$$\beta_i \geq \left(\zeta_{\bar{N}_i} + \sum_{j=i+1}^{m} \zeta_{\Omega_{i,j}} \beta_j \right) \left(1 + \frac{\gamma_2}{\alpha_i} \right), i = (m-1), \cdots, 1 \tag{2.66}$$

then it can be concluded that

$$\int_{t_0}^{t} L(\sigma)\, d\sigma \leq \zeta_L \tag{2.67}$$

where $\zeta_L \in \mathbb{R}$ is a positive bounding constant defined as

$$\zeta_L \triangleq \gamma_1 \sum_{i=1}^{m-1} \sum_{j=i+1}^{m} \zeta_{\Omega_{i,j}} \beta_j + \gamma_1 \sum_{i=1}^{m} \zeta_{\bar{N}_i} + \sum_{i=1}^{m} \beta_i |e_{n,i}(t_0)|. \tag{2.68}$$

Proof Analysis is started by integrating (2.64) in time from t_0 to t

$$\begin{aligned}\int_{t_0}^{t} L(\sigma)\, d\sigma &= \int_{t_0}^{t} e_n^T(\sigma)\,\alpha^T\left(\bar{N}(\sigma) - \beta \mathrm{Sgn}(e_n(\sigma))\right) d\sigma \\ &\quad - \int_{t_0}^{t} e_n^T(\sigma)\,\alpha^T \Omega(\sigma)\,\beta \mathrm{Sgn}(e_n(\sigma))\, d\sigma \\ &\quad + \int_{t_0}^{t} \dot{e}_n^T(\sigma)\,\bar{N}(\sigma)\, d\sigma \\ &\quad - \int_{t_0}^{t} \dot{e}_n^T(\sigma)\,\Omega(\sigma)\,\beta \mathrm{Sgn}(e_n(\sigma))\, d\sigma \\ &\quad - \int_{t_0}^{t} \dot{e}_n^T(\sigma)\,\beta \mathrm{Sgn}(e_n(\sigma))\, d\sigma \end{aligned} \tag{2.69}$$

where (2.14) was utilized. To ease the presentation, each term on the right–hand side of (2.69) will upper bounded separately. The first term:

$$\begin{aligned}&\int_{t_0}^{t} e_n^T(\sigma)\,\alpha^T\left(\bar{N}(\sigma) - \beta \mathrm{Sgn}(e_n(\sigma))\right) d\sigma \\ =\ &\int_{t_0}^{t} \sum_{i=1}^{m} \alpha_i e_{n,i}(\sigma)\left(\bar{N}_i(\sigma) - \beta_i \mathrm{sgn}(e_{n,i}(\sigma))\right) d\sigma \\ \leq\ &\sum_{i=1}^{m} \alpha_i \left(\zeta_{\bar{N}_i} - \beta_i\right) \int_{t_0}^{t} |e_{n,i}(\sigma)|\, d\sigma. \end{aligned} \tag{2.70}$$

The second term:

$$\begin{aligned}&-\int_{t_0}^{t} e_n^T(\sigma)\,\alpha^T \Omega(\sigma)\,\beta \mathrm{Sgn}(e_n(\sigma))\, d\sigma \\ =\ &-\int_{t_0}^{t} \sum_{i=1}^{m-1} \alpha_i e_{n,i}(\sigma) \sum_{j=i+1}^{m} \beta_j \Omega_{i,j}(\sigma)\,\mathrm{sgn}(e_{n,j}(\sigma))\, d\sigma \\ \leq\ &\sum_{i=1}^{m-1}\sum_{j=i+1}^{m} \alpha_i \beta_j \zeta_{\Omega_{i,j}} \int_{t_0}^{t} |e_{n,i}(\sigma)|\, d\sigma. \end{aligned} \tag{2.71}$$

The third term:

$$\begin{aligned}\int_{t_0}^{t} \dot{e}_n^T(\sigma)\,\bar{N}(\sigma)\,d\sigma &= \int_{t_0}^{t} \sum_{i=1}^{m} \dot{e}_{n,i}^T(\sigma)\,\bar{N}_i(\sigma)\,d\sigma \\ &\leq \sum_{i=1}^{m} \zeta_{\bar{N}_i} \int_{t_0}^{t} |\dot{e}_{n,i}(\sigma)|\,d\sigma \\ &\leq \sum_{i=1}^{m} \zeta_{\bar{N}_i} \left(\gamma_1 + \gamma_2 \int_{t_0}^{t} |e_{n,i}(\sigma)|\,d\sigma + |e_{n,i}(t)| \right). \end{aligned} \tag{2.72}$$

The fourth term:

$$\begin{aligned} & -\int_{t_0}^{t} \dot{e}_n^T(\sigma)\,\Omega(\sigma)\,\beta \mathrm{Sgn}(e_n(\sigma))\,d\sigma \\ = & -\int_{t_0}^{t} \sum_{i=1}^{m-1} \dot{e}_{n,i}(\sigma) \sum_{j=i+1}^{m} \beta_j \Omega_{i,j}(\sigma)\,\mathrm{sgn}(e_{n,j}(\sigma))\,d\sigma \\ \leq & \sum_{i=1}^{m-1} \sum_{j=i+1}^{m} \beta_j \zeta_{\Omega_{i,j}} \int_{t_0}^{t} |\dot{e}_{n,i}(\sigma)|\,d\sigma \\ \leq & \sum_{i=1}^{m-1} \sum_{j=i+1}^{m} \beta_j \zeta_{\Omega_{i,j}} \left(\gamma_1 + \gamma_2 \int_{t_0}^{t} |e_{n,i}(\sigma)|\,d\sigma + |e_{n,i}(t)| \right). \end{aligned} \tag{2.73}$$

The fifth term:

$$\begin{aligned} -\int_{t_0}^{t} \dot{e}_n^T(\sigma)\,\beta \mathrm{Sgn}(e_n(\sigma))\,d\sigma &= -\int_{t_0}^{t} \sum_{i=1}^{m} \beta_i \dot{e}_{n,i}(\sigma)\,\mathrm{sgn}(e_{n,i}(\sigma))\,d\sigma \\ &= -\sum_{i=1}^{m} \beta_i \int_{t_0}^{t} \mathrm{sgn}(e_{n,i}(\sigma))\,d(e_{n,i}) \\ &= -\sum_{i=1}^{m} \beta_i \int_{t_0}^{t} d(|e_{n,i}|) \\ &= -\sum_{i=1}^{m} \beta_i |e_{n,i}(t)| + \sum_{i=1}^{m} \beta_i |e_{n,i}(t_0)|. \end{aligned} \tag{2.74}$$

It is noted that, the result of Lemma 2.3.2 was utilized to obtain the last lines of (2.72)

and (2.73). After combining the upper bounds in (2.70)–(2.74), it is obtained that

$$\begin{aligned}\int_{t_0}^{t} L(\sigma)\, d\sigma \;\leq\; & \sum_{i=1}^{m-1} \alpha_i \left[\left(1+\frac{\gamma_2}{\alpha_i}\right) \left(\zeta_{\bar{N}_i} + \sum_{j=i+1}^{m} \zeta_{\Omega_{i,j}} \beta_j \right) - \beta_i \right] \int_{t_0}^{t} |e_{n,i}(\sigma)|\, d\sigma \\ & + \alpha_m \left[\left(1+\frac{\gamma_2}{\alpha_m}\right) \zeta_{\bar{N}_m} - \beta_m \right] \int_{t_0}^{t} |e_{n,m}(\sigma)|\, d\sigma \\ & + \left(\zeta_{\bar{N}_m} - \beta_m\right) |e_{n,m}(t)| \\ & + \sum_{i=1}^{m-1} \left(\zeta_{\bar{N}_i} + \sum_{j=i+1}^{m} \zeta_{\Omega_{i,j}} \beta_j - \beta_i \right) |e_{n,i}(t)| \\ & + \gamma_1 \sum_{i=1}^{m-1} \sum_{j=i+1}^{m} \zeta_{\Omega_{i,j}} \beta_j + \gamma_1 \sum_{i=1}^{m} \zeta_{\bar{N}_i} + \sum_{i=1}^{m} \beta_i |e_{n,i}(t_0)| . \end{aligned} \tag{2.75}$$

Based on (2.75), β_m is firstly chosen to satisfy (2.65) to make second and third lines on the right–hand side negative, and then β_i is selected by starting from $(m-1)$ with a decreasing order to satisfy (2.66), and finally, the definition of ζ_L in (2.68) was utilized to obtain (2.67), thus completing the proof of Lemma 2.3.3.

Theorem 2.3.4 *Given the uncertain MIMO nonlinear system of the form* (1.2)*, the controller of* (2.21) *and* (2.22) *ensures that the tracking error and its time derivatives converge to zero asymptotically in the sense that*

$$\left\| e_1^{(i)}(t) \right\| \to 0 \text{ as } t \to +\infty\,,\ \forall i = 0, \cdots, n$$

provided that α is chosen to satisfy (2.48)*, the entries of β are chosen to satisfy* (2.65) *and* (2.66)*, and $k_{d,i}$ and k_p are chosen large enough compared to the initial conditions of the system.*

Proof Let the auxiliary function $P(t) \in \mathbb{R}$ be defined as follows

$$P \triangleq \zeta_L - \int_{t_0}^{t} L(\sigma)\, d\sigma \tag{2.76}$$

where the terms $L(t)$ and ζ_L were defined in (2.64) and (2.68), respectively. Provided that the entries of the control gain matrix β are chosen to satisfy (2.65), from the proof of Lemma 2.3.3, it can be concluded that $P(t)$ is non–negative.

Consider the Lyapunov function, denoted by $V(s,t) \in \mathbb{R}$, defined as follows

$$V \triangleq V_1 + P \tag{2.77}$$

where $s(t) \in \mathbb{R}^{(n+1)m+1}$ is defined as

$$s \triangleq \begin{bmatrix} z^T & \sqrt{P} \end{bmatrix}^T \tag{2.78}$$

and $V_1(t) \in \mathbb{R}$ was defined in (2.49). By utilizing (2.7), (2.77) can be upper and lower bounded in the following form

$$W_1(s) \leq V(s,t) \leq W_2(s) \tag{2.79}$$

where $W_1(s)$, $W_2(s) \in \mathbb{R}$ are defined as

$$W_1 \triangleq \lambda_2 \|s\|^2, W_2 \triangleq \lambda_3(\|s\|)\|s\|^2 \tag{2.80}$$

with $\lambda_2 \triangleq \frac{1}{2}\min\{1, \underline{m}\}$ and $\lambda_3 \triangleq \max\left\{1, \frac{1}{2}\bar{m}(\|z\|)\right\}$.

Taking the time derivative of $V(t)$, utilizing the time derivative of (2.67), canceling common terms and following similar steps to that of proof of Theorem 2.3.1 yields

$$\begin{aligned}\dot{V} = & -\sum_{i=1}^{n-1} e_i^T e_i + e_{n-1}^T e_n - e_n^T \alpha e_n - r^T r + \left[r^T \widetilde{N} - k_p r^T r\right] \\ & + \left[-\sum_{i=1}^{m-1} r_i(\Lambda_i + \Psi_i + \Phi_i) - \sum_{i=1}^{m-1} k_{d,i} r_i^2\right]\end{aligned} \tag{2.81}$$

which can be rearranged to have the following form

$$\begin{aligned}\dot{V} \leq & -\sum_{i=1}^{n-2}\|e_i\|^2 - \frac{1}{2}\|e_{n-1}\|^2 - \left(\lambda_{\min}(\alpha) - \frac{1}{2}\right)\|e_n\|^2 - r^T r + \frac{\rho_{\widetilde{N}}^2(\|z\|)}{4k_p}\|z\|^2 \\ & + \sum_{i=1}^{m-1}\frac{\rho_i^2(\|z\|)}{4k_{d,i}}\|z\|^2 \\ \leq & -\left(\lambda_4 - \frac{\rho_{\widetilde{N}}^2(\|z\|)}{4k_p} - \sum_{i=1}^{m-1}\frac{\rho_i^2(\|z\|)}{4k_{d,i}}\right)\|z\|^2\end{aligned} \tag{2.82}$$

where $\lambda_4 \triangleq \min\left\{\frac{1}{2}, \lambda_{\min}(\alpha) - \frac{1}{2}\right\}$. When the controller gains k_p and $k_{d,i}$ for $i = 1, \cdots, (m-1)$ are selected large enough such that the regions defined by $\mathcal{D}_z \triangleq \{z : \|z\| \leq \mathcal{R}\}$ and $\mathcal{D}_s \triangleq \{s : \|s\| \leq \mathcal{R}\}$ with $\mathcal{R}$ defined as

$$\mathcal{R} = \min\left\{\rho_{\widetilde{N}}^{-1}\left(2\sqrt{k_p\frac{1-\mu}{m}}\right), \rho_1^{-1}\left(2\sqrt{k_{d,1}\frac{1-\mu}{m}}\right), \cdots, \rho_{m-1}^{-1}\left(2\sqrt{k_{d,2}\frac{1-\mu}{m}}\right)\right\} \tag{2.83}$$

are non–empty, from (2.82) and the definition of s, one can restate

$$\dot{V} \leq -\mu\|z\|^2 = -W(s), \forall s \in \mathcal{D}_s \tag{2.84}$$

where $\mu \in \mathbb{R}$ is a positive constant that satisfies $0 \leq \mu < 1$.

From (2.77) and (2.84), it is obvious that $V(t) \in \mathcal{L}_\infty$, and from the proof of Theorem 2.3.1, it was concluded that all terms in the closed–loop error system are bounded

and furthermore, from the boundedness of $\dot{W}(s)$, it can be stated $W(s)$ is uniformly continuous.

Based on the definition of $\mathcal{D}_s$, another region, $\mathcal{S}$, can be defined in the following form

$$\begin{aligned}
\mathcal{S} \triangleq & \left\{ s \in \mathcal{D}_s : W_2(s) < \lambda_3 \left(\rho_{\widetilde{N}}^{-1} \left(2\sqrt{k_p \frac{1-\mu}{m}} \right) \right)^2 \right\} \\
\cap & \left\{ s \in \mathcal{D}_s : W_2(s) < \lambda_3 \left(\rho_1^{-1} \left(2\sqrt{k_{d,1} \frac{1-\mu}{m}} \right) \right)^2 \right\} \\
\cap & \quad \vdots \\
\cap & \left\{ s \in \mathcal{D}_s : W_2(s) < \lambda_3 \left(\rho_{(m-1)}^{-1} \left(2\sqrt{k_{d,(m-1)} \frac{1-\mu}{m}} \right) \right)^2 \right\}.
\end{aligned} \tag{2.85}$$

A direct application of Theorem 8.4 in Khalil (2002) can be used to prove that $\|z(t)\| \to 0$ as $t \to +\infty \; \forall s(t_0) \in \mathcal{S}$. Based on the definition of $z(t)$, it is easy to show that $\|e_i(t)\|, \|r(t)\| \to 0$ as $t \to +\infty \; \forall s(t_0) \in \mathcal{S}$, $i = 1, \cdots, n$. From (2.14), it is clear that $\|\dot{e}_n(t)\| \to 0$ as $t \to +\infty \; \forall s(t_0) \in \mathcal{S}$. By utilizing (2.13) recursively, it can be proven that $\left\| e_1^{(i)}(t) \right\| \to 0$ as $t \to +\infty$, $i = 1, \cdots, n \; \forall s(t_0) \in \mathcal{S}$. Note that the region of attraction can be made arbitrarily large to include any initial conditions by choosing the controller gains k_p and $k_{d,i}$, $i = 1, \cdots, (m-1)$. This fact implies that the stability result obtained by the proposed method is semi–global.

2.4. Conclusions

In this chapter, the design of a continuous nonlinear robust controller for a class of uncertain MIMO nonlinear systems was presented. The designed controller required only the knowledge of the sign of leading principal minors of the input gain matrix and did not require accurate knowledge of the system dynamics. As a result, different from the existing results in the literature, neither symmetry nor positive definiteness of the input gain matrix was imposed on the system dynamics. The asymptotic stability of the closed–loop system was investigated via a four step stability analysis based on Lyapunov–type arguments.

The proposed controller in this chapter is now compared with some of the closest robust control works in the literature. After considering the same class of uncertain MIMO

nonlinear systems and imposing the same assumptions on the system model, the results in Chen et al. (2008) were extended to asymptotic as opposed to their UUB result. At this point, the differences of the Lyapunov function used in Theorem 2.3.4 and the one given in equation (22) of Chen et al. (2008) are highlighted. While the structure of both are similar and the summation of the norm squares of the error signals $e_i(t)$, $i = 1, \cdots, n$, are same, the second terms are fundamentally different (*i.e.*, see (2.14) in this dissertation and (8) in Chen et al. (2008)). Similarly, in Xian et al. (2004), the same system model was considered. The results in Xian et al. (2004) were also extended by relaxing the positive definiteness of the input gain matrix requirement. After this, the results in Xian et al. (2004) can now be considered as a special case of the controller presented in this chapter (*i.e.*, when $DU(X)$ is an identity matrix).

CHAPTER 3

SELF–TUNING METHOD FOR ADJUSTING CONTROL GAINS

Controller formulations utilizing RISE type feedback have been successfully applied to a variety of nonlinear systems over the past decade. The main drawbacks of RISE type feedback controllers are the need of prior knowledge of the upper bounds of the system uncertainties and the absence of a proper gain tuning methodology. This drawback is also valid for the controller proposed in Chapter 2. Specifically, the entries of the gain matrix β should be greater than the absolute value of the entries of uncertain matrices and vectors according to (2.65) and (2.66). Since these modeling matrices and vectors are uncertain usually a trial and error method is preferred. However, in real world applications, it is not easy to adjust the control gains. To tackle the aforementioned weaknesses, in this chapter, a fully self tuning RISE type feedback controller formulation has been presented. The proposed controller formulation makes use of a time–varying compensation gain to cope for the need of upper bound of the system uncertainties and a time–varying feedback control gain to achieve self gain adjustment. Lyapunov based arguments are utilized to ensure asymptotic stability and convergence of the time–varying gains to constant final values.

3.1. System Model and Error System Development

In this section, the system model and the error system are presented. To ease the presentation, a SISO system model is considered. However, extension to MIMO systems is straightforward where numerical simulations and experimental studies are conducted to demonstrate the performance of application to second order MIMO systems. Also, since the proposed work aims to extend the previous findings in Xian et al. (2004), the notation in Xian et al. (2004) is borrowed for a better comparison.

Following SISO nonlinear system is considered in Xian et al. (2004)

$$m_{st}\left(x, \dot{x}, \cdots, x^{(n-1)}\right) x^{(n)} + f_{st}\left(x, \dot{x}, \cdots, x^{(n-1)}\right) = \tau \tag{3.1}$$

where $x^{(i)}(t) \in \mathbb{R}\ i = 0, ..., n$ are system states, $m_{st}(\cdot)$, $f_{st}(\cdot) \in \mathbb{R}$ are uncertain nonlin-

ear functions, and $\tau(t) \in \mathbb{R}$ is the control input. The standard assumption that the sign of the uncertain function m_{st} being known is made and without loss of generality, it is considered to be positive (*i.e.*, $m_{st} > 0$) with the following bounds being satisfied

$$\underline{m} \leq m_{st}(x) \leq \overline{m} \tag{3.2}$$

where $\underline{m}$, $\overline{m}\left(|x|, |\dot{x}|, \cdots, \left|x^{(n-1)}\right|\right) \in \mathbb{R}$ are a positive bounding constant and a positive non–decreasing function of its arguments, respectively. The uncertain functions m_{st} and f_{st} are assumed to be continuously differentiable up to their second order time derivatives.

The output tracking error, denoted by $e_1(t) \in \mathbb{R}$, is defined as

$$e_1 \triangleq x_r - x \tag{3.3}$$

where $x_r(t) \in \mathbb{R}$ is the bounded desired trajectory with bounded continuous time derivatives (*i.e.*, $x_r^{(i)}(t) \in \mathcal{L}_\infty$ for $i = 0, \cdots, (n+2)$). The main control objective is to ensure that $e_1(t) \to 0$ via the design of a continuous robust control law under full–state feedback (*i.e.*, $x^{(i)}$, $i = 0, \cdots, (n-1)$ are available). The other objective is to design time–varying control gains that are functions of error terms and converge to constant final values during the control process (*i.e.*, self–tuning control gains).

To facilitate the control design, auxiliary errors, denoted by $e_i(t) \in \mathbb{R}$, $i = 2, \cdots, n$, are defined in the following manner

$$e_2 \triangleq \dot{e}_1 + e_1 \tag{3.4}$$

$$\vdots$$

$$e_n \triangleq \dot{e}_{n-1} + e_{n-1} + e_{n-2} \tag{3.5}$$

where all of which can alternatively be obtained in terms of output tracking error $e_1(t)$ and its time derivatives as

$$e_i = \sum_{j=0}^{i-1} a_{i,j} e_1^{(j)} \tag{3.6}$$

where $a_{i,j} \in \mathbb{R}$ are known positive constant coefficients with $a_{n,(n-1)} = 1$. Another auxiliary error, denoted by $r(t) \in \mathbb{R}$, is defined as

$$r \triangleq \dot{e}_n + \alpha e_n \tag{3.7}$$

with $\alpha \in \mathbb{R}$ being a positive constant gain.

To obtain the open–loop dynamics for $r(t)$, the time derivative of (3.7) is multiplied with m_{st}, the second time derivative of (3.6) for $i = n$, and the time derivative of (3.1) are then substituted

$$m_{st}\dot{r} = -\frac{1}{2}\dot{m}_{st} r - e_n - \dot{\tau} + N \tag{3.8}$$

where $N\left(x,\cdots,x^{(n)},e_1,\cdots,e_n,r,x_r^{(n+1)}\right)\in\mathbb{R}$ is an auxiliary function defined as

$$N \triangleq m_{st}\left[x_r^{(n+1)}+\sum_{j=0}^{n-2}a_{n,j}e_1^{(j+2)}+\alpha\dot{e}_n\right]+\dot{m}_{st}\left(\frac{1}{2}r+x^{(n)}\right)+\dot{f}_{st}+e_n. \tag{3.9}$$

The above auxiliary function is segregated as sum of two auxiliary terms which are denoted by $\bar{N}\left(x_r,\cdots,x_r^{(n)}\right)$, $\tilde{N}\left(x,\cdots,x^{(n)},e_1,\cdots,e_n,r,x_r^{(n+1)}\right)\in\mathbb{R}$ and are defined as

$$\bar{N} \triangleq N\big|_{x=x_r,\cdots,x^{(n)}=x_r^{(n)}} \tag{3.10}$$

$$\tilde{N} \triangleq N-\bar{N}. \tag{3.11}$$

It should be noted that since both $\bar{N}(t)$ and $\dot{\bar{N}}(t)$ are functions of the desired trajectory and its time derivatives, they are bounded functions of time (*i.e.*, $\bar{N}(t)$, $\dot{\bar{N}}(t)\in\mathcal{L}_\infty$). On the other hand, since the auxiliary term N defined in (3.9) is continuously differentiable, Mean Value Theorem in Khalil (2002) can be utilized to demonstrate that $\tilde{N}$ can be upper bounded as

$$\left|\tilde{N}\right|\leq\rho\left(\|z\|\right)\|z\| \tag{3.12}$$

where $\rho\in\mathbb{R}$ is some globally invertible, non–decreasing function of its argument and $z(t)\in\mathbb{R}^{n+1}$ is the combined error defined as

$$z \triangleq \left[e_1,\cdots,e_n,r\right]^T. \tag{3.13}$$

Based on the subsequent stability analysis, the following continuous robust controller is proposed

$$\tau(t)=k(t)\,e_n(t)-k(t_0)\,e_n(t_0)+\alpha\int_{t_0}^{t}k(\sigma)\,e_n(\sigma)\,d\sigma+\int_{t_0}^{t}\hat{\beta}(\sigma)\,\mathrm{sgn}\left(e_n(\sigma)\right)d\sigma \tag{3.14}$$

where $\hat{\beta}(t)\in\mathbb{R}$ is a subsequently designed time–varying (uncertainty compensation) control gain, $\mathrm{sgn}(\cdot)$ is the standard signum function, and $k(t)\in\mathbb{R}$ is a time–varying control gain updated according to

$$k(t)=1+k_c+\frac{1}{2}e_n^2(t)+\alpha\int_{t_0}^{t}e_n^2(\sigma)\,d\sigma \tag{3.15}$$

with $k_c\in\mathbb{R}$ being its positive constant part. The constant term $k(t_0)\,e_n(t_0)$ is utilized in the construction of the controller to ensure $\tau(t_0)=0$. The time–varying control gain $\hat{\beta}(t)$ has the following structure

$$\hat{\beta}(t)=\hat{\beta}_1(t)+\beta_2 \tag{3.16}$$

where $\hat{\beta}_1(t) \in \mathbb{R}$ is its time–varying part and $\beta_2 \in \mathbb{R}$ is its positive constant part (*i.e.*, $\beta_2 > 0$). The time–varying part of the control gain is updated according to

$$\hat{\beta}_1(t) = |e_n(t)| - |e_n(t_0)| + \alpha \int_{t_0}^{t} |e_n(\sigma)| \, d\sigma \tag{3.17}$$

where $\hat{\beta}_1(t_0) = 0$.

Substituting the time derivative of the control input in (3.14) into the open–loop error system in (3.8) yields the below closed–loop error system for $r(t)$

$$m_{st}\dot{r} = -\frac{1}{2}\dot{m}_{st}r - e_n - kr - \dot{k}e_n - \left(\hat{\beta}_1 + \beta_2\right) \text{sgn}(e_n) + \bar{N} + \tilde{N}. \tag{3.18}$$

A comparison of the development thus far and the corresponding part of Xian et al. (2004) is now given. While the error system development and the open–loop error dynamics are similar, the controller in (3.14) is fundamentally different than that of the controller in Xian et al. (2004). Specifically, the controller formulation in Xian et al. (2004) has the form

$$\tau(t) = K\left[e_n(t) - e_n(t_0) + \alpha \int_{t_0}^{t} e_n(\sigma) \, d\sigma\right] + \beta \int_{t_0}^{t} \text{sgn}(e_n(\sigma)) \, d\sigma$$

where K and β are constant control gains. It is clear that, the main difference between these two controllers is that the controller gains in the design presented in this dissertation are time–varying where they were constant in Xian et al. (2004). This is a **novel** departure from the existing controllers utilizing RISE feedback.

3.2. Stability Analysis

In this section, the stability of the tracking error and its time derivatives and the convergence of the time–varying control gains are investigated. Firstly, two lemmas are stated where both of which will later be utilized in the proof of the first theorem.

Lemma 3.2.1 *The auxiliary function, denoted by $L_1(t) \in \mathbb{R}$, is defined as*

$$L_1 \triangleq r\left(\bar{N} - \chi_1 sgn(e_n)\right) \tag{3.19}$$

where $\chi_1 \in \mathbb{R}$ is a positive constant. Provided that χ_1 satisfy

$$\chi_1 \geq \left\|\bar{N}(t)\right\|_{\mathcal{L}_\infty} + \frac{1}{\alpha}\left\|\dot{\bar{N}}(t)\right\|_{\mathcal{L}_\infty} \tag{3.20}$$

where $\|\cdot\|_{\mathcal{L}_\infty}$ denotes infinity norm, then

$$\int_{t_0}^{t} L_1(\sigma) \, d\sigma \leq \zeta_{b_1} \tag{3.21}$$

where $\zeta_{b_1} \in \mathbb{R}$ is a positive constant.

Proof After substituting (3.7) into (3.19) and then integrating in time, the following expression is obtained

$$\begin{aligned}\int_{t_0}^{t} L_1(\sigma)\,d\sigma &= \alpha\int_{t_0}^{t} e_n(\sigma)\left[\bar{N}(\sigma)-\chi_1\text{sgn}(e_n(\sigma))\right]d\sigma \\ &\quad+\int_{t_0}^{t}\frac{de_n(\sigma)}{d\sigma}\bar{N}(\sigma)\,d\sigma-\chi_1\int_{t_0}^{t}\frac{de_n(\sigma)}{d\sigma}\text{sgn}(e_n(\sigma))\,d\sigma. \quad (3.22)\end{aligned}$$

After integrating the second integral on the right–hand side by parts and evaluating the third integral Krstic (2009), following expression is obtained

$$\begin{aligned}\int_{t_0}^{t} L_1(\sigma)\,d\sigma &= \alpha\int_{t_0}^{t} e_n(\sigma)\left[\bar{N}(\sigma)-\chi_1\text{sgn}(e_n(\sigma))\right]d\sigma \\ &\quad+e_n(\sigma)\bar{N}(\sigma)|_{t_0}^{t}-\int_{t_0}^{t} e_n(\sigma)\frac{d\bar{N}(\sigma)}{d\sigma}-\chi_1|e_n(\sigma)|\,|_{t_0}^{t} \\ &= \alpha\int_{t_0}^{t} e_n(\sigma)\left[\bar{N}(\sigma)-\frac{1}{\alpha}\frac{d\bar{N}(\sigma)}{d\sigma}-\chi_1\text{sgn}(e_n(\sigma))\right]d\sigma \\ &\quad+e_n(t)\bar{N}(t)-e_n(t_0)\bar{N}(t_0)-\chi_1|e_n(t)|+\chi_1|e_n(t_0)|. \quad (3.23)\end{aligned}$$

The right–hand side of (3.23) can be upper bounded as

$$\begin{aligned}\int_{t_0}^{t} L_1(\sigma)\,d\sigma &\le \alpha\int_{t_0}^{t}|e_n(\sigma)|\left(\left|\bar{N}(\sigma)\right|+\frac{1}{\alpha}\left|\frac{d\bar{N}(\sigma)}{d\sigma}\right|-\chi_1\right)d\sigma \\ &\quad+|e_n(t)|\left(\left|\bar{N}(t)\right|-\chi_1\right)+\chi_1|e_n(t_0)|-e_n(t_0)\bar{N}(t_0). \quad (3.24)\end{aligned}$$

From (3.24), it is easy to see that if χ_1 satisfies (3.20), then (3.21) holds with

$$\zeta_{b1} \triangleq \chi_1|e_n(t_0)|-e_n(t_0)\bar{N}(t_0). \quad (3.25)$$

In Lemma 3.2.1, a constant parameter, namely χ_1, is introduced. This constant parameter is required to satisfy the condition in (3.20) but it is not utilized in the controller in (3.14). On the other hand, in Xian et al. (2004), a similar constant parameter was utilized in the controller design. This difference is an important **novelty** of this work when compared to Xian et al. (2004) which is removing the need for the knowledge of the upper bounds of the uncertain function and its time derivative.

Lemma 3.2.2 *The auxiliary function, denoted by $L_2(t) \in \mathbb{R}$, is defined as*

$$L_2 \triangleq -\chi_2\dot{e}_n sgn(e_n). \quad (3.26)$$

Provided that $\chi_2 > 0$ then

$$\int_{t_0}^{t} L_2(\sigma)\,d\sigma \le \zeta_{b_2} \quad (3.27)$$

where $\zeta_{b_2} \in \mathbb{R}$ is a positive constant.

Proof After integrating (3.26) in time, following steps can be obtained Krstic (2009)

$$\begin{aligned}\int_{t_0}^{t} L_2(\sigma)\, d\sigma &= -\chi_2 \int_{t_0}^{t} \dot{e}_n(\sigma)\, \text{sgn}(e_n(\sigma))\, d\sigma \\ &= -\chi_2 \int_{t_0}^{t} \text{sgn}(e_n)\, d(e_n) \\ &= -\chi_2 \int_{t_0}^{t} d(|e_n|) \\ &= -\chi_2 (|e_n(t)| - |e_n(t_0)|) \\ &\leq \chi_2 |e_n(t_0)|. \end{aligned} \tag{3.28}$$

From (3.28), it is easy to see that if χ_2 is chosen as positive, then (3.27) holds with

$$\zeta_{b2} \triangleq \beta_2 |e_n(t_0)|. \tag{3.29}$$

In this study, different from the stability analysis in Xian et al. (2004), a **new** lemma (*i.e.*, Lemma 3.2.2) is presented. In the proof of Lemma 3.2.2, the constant β_2 is only required to be positive and no additional constraints are imposed. While β_2 is in the controller in (3.14) (via being the positive constant part of the time–varying control gain $\hat{\beta}(t)$ as introduced in (3.16)), it being positive suffices.

The tracking result will now be proven via the following theorem.

Theorem 3.2.3 *The controller in* (3.14) *with the time–varying gains in* (3.16) *and* (3.17) *ensures semi–global asymptotic convergence of the tracking error and its time derivatives in the sense that* $\left|e_1^{(i)}(t)\right| \to 0$ *as* $t \to \infty$ *provided that* α *is selected to satisfy* $\alpha > \frac{1}{2}$*, and* β_2 *is chosen to be positive.*

Proof Following Lyapunov function, denoted by $V(y,t) \in \mathbb{R}$, is defined

$$V \triangleq \frac{1}{2}\sum_{j=1}^{n} e_j^2 + \frac{1}{2}mr^2 + \frac{1}{2}\tilde{\beta}_1^2 + P_1 + P_2 \tag{3.30}$$

where $P_1(t)$, $P_2(t) \in \mathbb{R}$ are defined as

$$P_1 \triangleq \zeta_{b_1} - \int_{t_0}^{t} L_1(\sigma)\, d\sigma \tag{3.31}$$

$$P_2 \triangleq \zeta_{b_2} - \int_{t_0}^{t} L_2(\sigma)\, d\sigma \tag{3.32}$$

and $\tilde{\beta}_1(t) \in \mathbb{R}$ is defined as

$$\tilde{\beta}_1 \triangleq \chi_1 - \hat{\beta}_1 \tag{3.33}$$

and $y(t) \in \mathbb{R}^{n+4}$ is defined as

$$y \triangleq \left[z^T, \tilde{\beta}_1, \sqrt{P_1}, \sqrt{P_2}\right]^T \tag{3.34}$$

where $z(t)$ was defined in (3.13).

From the proofs of Lemmas 3.2.1 and 3.2.2, it is clear that $P_1(t)$ and $P_2(t)$ are non–negative and thus $V(y,t)$ is also non–negative. The Lyapunov function in (3.30) can be bounded as

$$\frac{1}{2}\min\{1,\underline{m}\}\|y\|^2 \leq V \leq \max\left\{\frac{1}{2}\overline{m}(\|y\|),1\right\}\|y\|^2 \tag{3.35}$$

where (3.2) was utilized.

When compared with the Lyapunov function in (33) of Xian et al. (2004), (3.30) includes two additional terms (*i.e.*, $\frac{1}{2}\tilde{\beta}_1^2(t)$ and $P_2(t)$). The first new term is added as a direct consequence of the time–varying nature of the uncertainty compensation gain $\hat{\beta}(t)$. On the other hand, the $P_2(t)$ term is introduced to prove $\mathcal{L}_1$ boundedness of $e_n(t)$ (as will be demonstrated subsequently). This is required to prove the boundedness and the convergence of the time–varying gains $\hat{\beta}(t)$ and $k(t)$ to constant final values. While proving the boundedness of $\hat{\beta}(t)$ is a significant improvement over the similar results in Yang et al. (2011) where boundedness was not ensured, a **novel** approach will be utilized to achieve convergence of the time–varying gains.

After taking the time derivative of (3.30) and substituting (3.5), (3.7) and (3.18), following expression can be obtained

$$\dot{V} = -\sum_{j=1}^{n-1} e_j^2 - \alpha e_n^2 + e_{n-1}e_n - r^2 - kr^2 + r\tilde{N} - \alpha\beta_2|e_n| - \dot{k}re_n \tag{3.36}$$

where (3.19) and (3.26) were also utilized. By using the fact that $e_{n-1}e_n \leq \frac{1}{2}\left(e_{n-1}^2 + e_n^2\right)$, an upper bound on (3.36) can be obtained as

$$\dot{V} \leq -\min\left\{\frac{1}{2}, \alpha - \frac{1}{2}\right\}\|z\|^2 + \frac{\rho^2(\|z\|)}{4k_c}\|z\|^2 - \alpha\beta_2|e_n| - \dot{k}re_n \tag{3.37}$$

where (3.12) was utilized. Provided that α is selected to satisfy $\alpha > \frac{1}{2}$, from (3.37), following expression is stated

$$\dot{V} \leq -\gamma\|z\|^2 - \alpha\beta_2|e_n| - r^2e_n^2 \leq -\gamma\|z\|^2 - \alpha\beta_2|e_n| \tag{3.38}$$

where the time derivative of (3.15) is substituted and $\gamma \in \mathbb{R}$ is some positive constant. From (3.30), (3.35) and (3.38), it is clear that $V(y,t) \in \mathcal{L}_\infty$ and thus $e_1(t), \cdots, e_n(t)$, $r(t)$, $\tilde{\beta}_1(t)$, $P_1(t)$, $P_2(t) \in \mathcal{L}_\infty$. Boundedness of $e_n(t)$ and $r(t)$ can be utilized along with (3.7) to show that $\dot{e}_n(t) \in \mathcal{L}_\infty$. These boundedness statements can be utilized along with (3.4)–(3.6) to prove that $\dot{e}_1(t), \cdots, \dot{e}_{n-1}(t) \in \mathcal{L}_\infty$. From the time derivative of (3.14), it can easily be concluded that $\dot{\tau}(t) \in \mathcal{L}_\infty$. The boundedness of the auxiliary errors

and their time derivatives can be utilized along with (3.6) to conclude that $e_1^{(i)}(t) \in \mathcal{L}_\infty$ $i = 1, \cdots, n$, which can then be utilized along with (3.3) and its time derivatives to prove that $x^{(i)}(t) \in \mathcal{L}_\infty$ $i = 1, \cdots, n$. The above boundedness statements can be utilized along with $m(\cdot)$, $f_{st}(\cdot) \in \mathcal{C}_2$, to prove that $m_{st}(\cdot)$, $f_{st}(\cdot)$, $\dot{m}_{st}(\cdot)$, $\dot{f}_{st}(\cdot) \in \mathcal{L}_\infty$. From (3.18), it is concluded that $\dot{r}(t) \in \mathcal{L}_\infty$.

After integrating (3.38) in time from initial time to infinity, following expression can be obtained

$$\gamma \int_{t_0}^{\infty} \|z(\sigma)\|^2 d\sigma + \alpha\beta_2 \int_{t_0}^{\infty} |e_n(\sigma)| d\sigma \leq V(t_0) - V(\infty) \tag{3.39}$$

and since $V(\infty) \geq 0$ following expressions are valid

$$\int_{t_0}^{\infty} \|z(\sigma)\|^2 d\sigma \leq \frac{V(t_0)}{\gamma} \text{ and } \int_{t_0}^{\infty} |e_n(\sigma)| d\sigma \leq \frac{V(t_0)}{\alpha\beta_2}. \tag{3.40}$$

From (3.40), it is clear that $z(t) \in \mathcal{L}_2$ and $e_n(t) \in \mathcal{L}_1$. Since $e_n(t) \in \mathcal{L}_1 \cap \mathcal{L}_\infty$, from (3.17), it is concluded that $\hat{\beta}_1(t) \in \mathcal{L}_\infty$, and since $r(t) \in \mathcal{L}_\infty$, then from the time derivative of (3.17), it is clear that $\dot{\hat{\beta}}_1(t) \in \mathcal{L}_\infty$. Since $e_n(t) \in \mathcal{L}_2 \cap \mathcal{L}_\infty$, from (3.15), it is clear that $k(t) \in \mathcal{L}_\infty$. Standard signal chasing arguments can be utilized to prove that all the remaining signals remain bounded under the closed–loop operation. Since $z(t) \in \mathcal{L}_2 \cap \mathcal{L}_\infty$ and $\dot{z}(t) \in \mathcal{L}_\infty$, Barbalat's Lemma in Krstic et al. (1995) can be utilized to prove that $\|z(t)\| \to 0$ as $t \to \infty$, and from its definition in (3.13), it is clear that the tracking error and its time derivatives asymptotically converge to zero.

One concern of the controllers with time–varying gains (including dynamic adaptive update rules) is their convergence. The following theorem investigates the convergence analysis of the time–varying gains.

Theorem 3.2.4 *There exist constants $\hat{\beta}_\infty$ and $k_\infty \in \mathbb{R}$ such that*

$$\hat{\beta}(t) \to \hat{\beta}_\infty \text{ and } k(t) \to k_\infty \text{ as } t \to +\infty. \tag{3.41}$$

Proof Applying the limit operation to (3.17) yields

$$\lim_{t\to\infty} \hat{\beta}_1(t) = -|e_n(t_0)| + \alpha \lim_{t\to\infty} \left[\int_{t_0}^{t} |e_n(\sigma)| d\sigma\right] \tag{3.42}$$

where $e_n(t) \to 0$ was utilized. Since, from the proof of Theorem 3.2.3, $e_n(t) \in \mathcal{L}_1$, the existence of $\lim_{t\to\infty} \left[\int_{t_0}^{t} |e_n(\sigma)| d\sigma\right]$ is ensured via Theorem 3.1 of Krstic (1996). In view of this, from (3.42), it is easy to see that (3.41) is obtained.

Similarly, taking the limit of (3.15) results in

$$\lim_{t\to\infty} k(t) = k_c + \alpha \lim_{t\to\infty} \left[\int_{t_0}^{t} e_n^2(\theta) d\theta\right] \tag{3.43}$$

where $e_n(t) \to 0$ was utilized. Since $e_n(t) \in \mathcal{L}_2$, from Theorem 3.1 in Krstic (1996), the existence of $\lim_{t\to\infty}\left[\int_{t_0}^{t} e_n^2(\sigma)\, d\sigma\right]$ is ensured from which the result in (3.41) follows.

3.3. Conclusions

In this chapter, the need of prior knowledge of the upper bounds of the system uncertainties and the absence of a proper gain tuning methodology weaknesses of controllers utilizing RISE type feedback were tackled by proposing a self–tuning method to adjust their control gains. To realize this objective, a self-tuning RISE feedback controller formulation with a time–varying feedback gain and an adaptive uncertainty compensation gain were utilized. Semi–global tracking was ensured via Lyapunov–type analysis and the convergence of the time–varying gains to constant final values was also proven.

The result presented in this chapter is **the only design that addresses the self–tuning of the gains for controllers utilizing RISE feedback**. The time–varying controller gains designed in this chapter can be utilized in conjunction with the robust controller designed in Chapter 2.

CHAPTER 4

CONTROL DESIGN FOR MECHATRONIC SYSTEMS

Main purposes of this chapter can be summarized as:

- A tracking controller formulation is provided for dynamically positioned surface vessels subject to non–symmetric added mass terms effecting the system dynamics at the acceleration level.
- The robust attitude tracking control problem for small–scaled unmanned helicopters is focused by considering the rotor dynamics. These dynamics are reflected to the dynamic model by premultiplying the vector that contains actual system inputs, namely the elevator servo input, the aileron servo input and the rudder servo input, with a non–symmetric matrix.
- Problem of accurate positioning of an unactuated surface vessel by using multiple uni–directional tugboats is investigated.

The control design process is divided into two parts. Initially, the problems are transformed into second order systems with an uncertain non–symmetric input gain matrix. Then, novel robust controllers are proposed by utilizing the general control design in Chapter 2. Since these mechatronic systems are second order nonlinear systems with 3 inputs and 3 outputs, control design given in this chapter is a special case of the general control design given in Chapter 2 for $n = 2$ and $m = 3$. As a result of these, design steps are similar to Chapter 2. However, all steps of synthesis and analysis are provided for the sake of completeness.

The rest of this chapter is organized as follows. A brief information about dynamic models and model properties of dynamically positioned surface vessel, small–scaled unmanned helicopter and unactuated surface vessel manipulated by multiple uni–directional tugboats are presented in Sections 4.1, 4.2 and 4.3, respectively. Then, control design to these systems is presented in Section 4.4.

4.1. System Model and Properties of Dynamically Positioned Surface Vessel

The mathematical model for a dynamically positioned fully actuated 3 dof surface vessel is commonly represented by Fossen (1994), Fossen (2002), Skjetne et al. (2004), Ihle et al. (2006), Fossen (2011)

$$M_s\dot{v} + C_s v + D_s v = \tau \tag{4.1}$$

$$\dot{x} = Rv \tag{4.2}$$

where $x(t) \triangleq [x_p,\, y_p,\, \psi_s]^T \in \mathbb{R}^3$ is the position vector that contains translational positions $x_p\,(t)$, $y_p\,(t) \in \mathbb{R}$ in X– and Y– directions, respectively, and the yaw angle of a surface vessel $\psi_s\,(t) \in \mathbb{R}$, $v(t) = \left[u, v, \dot{\psi_s}\right]^T \in \mathbb{R}^3$ includes body–fixed linear and angular velocities. Also in (4.1), $M_s\,(\psi_s)$, $C_s(v, v_r)$, $D_s(v, v_r) \in \mathbb{R}^{3\times3}$ represent inertia matrix, centripetal and Coriolis forces, hydrodynamic damping terms, respectively, $v_r(t) \in \mathbb{R}^3$ is the relative velocity between the fluids and the vessel, and the control input torque vector is represented by $\tau(t) \in \mathbb{R}^3$. It is noted that, in 6 dof modeling approach for dynamically positioned surface vessels, there are 3 translational positions in X–, Y– and Z– directions as well as yaw, pitch and roll angles of the vessel. On the other hand, while obtaining a 3 dof model, translational position in Z– direction and pitch and roll angles are not taken into account. Although they are in different frames, translational positions in X– and Y– directions and the yaw angle are commonly expressed in 3 dof modeling approach by utilizing rotation matrix denoted by $R(\psi_s) \in SO(3)$ Fossen (1994), Fossen (2002), Fossen (2011). The rotation matrix has the form

$$R\,(\psi_s) = \begin{bmatrix} \cos\,(\psi_s) & -\sin\,(\psi_s) & 0 \\ \sin\,(\psi_s) & \cos\,(\psi_s) & 0 \\ 0 & 0 & 1 \end{bmatrix}. \tag{4.3}$$

While the mathematical model in (4.1) and (4.2) is utilized in almost all past works, as detailed in Fossen (1994), Fossen and Strand (1999), Fossen (2002) and Skjetne et al. (2004), during the cruise, the motion of the surface vessel effects all the flow, resulting in vibrations with different amplitudes to occur on various parts of the flow. It is important to note that motion in one direction causes forces not only in the same direction but also in other directions Newman (1977), Lewis (1989). This situation results as pressure effects and moments acting on different parts of the surface vessel which causes additional force and thus has an influence on the acceleration of the surface vessel. For

precise control design, this effect, referred as the added mass, is required to be represented in the dynamic model. There are different conventions in the literature on how to represent the added mass effects in the dynamic model Fossen and Strand (1999), Skjetne et al. (2004). In Fossen and Strand (1999), after using inertial velocity as the velocity state, the added mass effects are represented as part of the inertia matrix of the surface vessel. Following the convention given in Fossen and Strand (1999), in this work, the added mass terms are considered to be affecting the dynamics of the surface vessel at the acceleration level (*i.e.*, inertial velocity is chosen as the velocity state). As a result, the inertia matrix of the surface vessel in (4.1) is obtained as Fossen (1994)

$$M_s = M_{RB} + M_A \tag{4.4}$$

where $M_{RB}(\psi_s) \in \mathbb{R}^{3\times3}$ represents the positive definite, symmetric rigid body inertia matrix and $M_A(\psi_s) \in \mathbb{R}^{3\times3}$ represents the added mass inertia matrix. The entries of added mass inertia matrix represented by $M_{A_{ij}}$ denote the mass associated with a force on the body in the i^{th} direction due to a unit acceleration in the j^{th} direction Techet (2015).

As noted in Fossen (1994), the inertia matrix due to added mass is not necessarily symmetric. It is also considered that the added mass term does not lead to a rank deficiency in M_s (*i.e.*, M_s is full rank). After summed the inertia matrix due to added mass with the symmetric $M_{RB}(\psi_s)$, the overall inertia matrix $M_s(\psi_s)$ of the system loses its symmetry. The non–symmetric inertia matrix, when not appropriately dealt with, may result in degradation of the controller performance, and even instability. Therefore, the main problem caused by added mass effects are due to its non–symmetric nature. From a control design perspective, the symmetric nature of the inertia matrix is extremely useful especially when constructing quadratic terms in the Lyapunov function.

In an attempt to obtain a compact representation of the mathematical model of the surface vessel in (4.1) and (4.2), the time derivative of (4.2) is taken

$$\ddot{x} = \dot{R}v + R\dot{v} \tag{4.5}$$

which includes the time derivative of the rotation matrix that can be obtained as

$$\dot{R} = RS_3 \tag{4.6}$$

with $S_3\left(\dot{\psi}_s\right) \in \mathbb{R}^{3\times3}$ being a skew–symmetric matrix defined as

$$S_3 \triangleq \dot{\psi}_s \begin{bmatrix} 0 & -1 & 0 \\ 1 & 0 & 0 \\ 0 & 0 & 0 \end{bmatrix}. \tag{4.7}$$

After substituting (4.1) and (4.6) into (4.5), it is easy to obtain

$$\ddot{x} = RM_s^{-1}\tau - R\left[M_s^{-1}\left(C_s + D_s\right) - S_3\right]R^T\dot{x}. \tag{4.8}$$

In order to ease the presentation of the subsequent development, the right–hand side of (4.8) can be rewritten as

$$\ddot{x} = h + g\tau \tag{4.9}$$

where $h\left(x, \dot{x}\right) \in \mathbb{R}^3$ and $g\left(x, \dot{x}\right) \in \mathbb{R}^{3\times 3}$ are defined as

$$h \triangleq -R\left[M_s^{-1}\left(C_s + D_s\right) - S_3\right]R^T\dot{x} \tag{4.10}$$

$$g \triangleq RM_s^{-1}. \tag{4.11}$$

Since $M_s\left(\psi_s\right)$ is full rank then $g\left(x, \dot{x}\right)$ is a real matrix with non–zero leading principle minors.

4.2. System Model and Properties of Small–scaled Unmanned Helicopter

The dynamic model of a small–scaled unmanned helicopter is expressed as Fantoni and Lozano (2002)

$$M_h\ddot{x} + C_h\dot{x} + G_h = \tau_h \tag{4.12}$$

where $x\left(t\right)$, $\dot{x}\left(t\right)$ and $\ddot{x}\left(t\right) \in \mathbb{R}^3$ position, velocity and the acceleration vector while the three Euler angles are contained by the position vector that is expressed as $x = \begin{bmatrix} \phi & \theta & \psi \end{bmatrix}^T$. From these Euler angles, $\phi\left(t\right) \in \mathbb{R}$ is the yaw angle, $\theta\left(t\right) \in \mathbb{R}$ is the roll angle, and $\psi\left(t\right)$ is the pitch angle. The inertia matrix, the centripetal and Coriolis forces matrix and vector of conservative forces are denoted by $M_h\left(x\right)$, $C_h\left(x, \dot{x}\right) \in \mathbb{R}^{3\times 3}$ and $G_h\left(x\right) \in \mathbb{R}^3$, respectively, while the torque input vector is represented by $\tau_h\left(t\right) \in \mathbb{R}^3$.

The torque input $\tau_h\left(t\right)$ is expressed as Mettler (2003), Cai et al. (2011)

$$\tau_h = S_h^{-T}\left(Av_c + B\right) \tag{4.13}$$

where $S_h\left(t\right) \in \mathbb{R}^{3\times 3}$ denotes the velocity transformation matrix from the body frame to the inertia frame and defined as

$$S_h \triangleq \begin{bmatrix} 1 & \dfrac{\sin\left(\phi\right)\sin\left(\theta\right)}{\cos\left(\theta\right)} & \dfrac{\cos\left(\phi\right)\sin\left(\theta\right)}{\cos\left(\theta\right)} \\ 0 & \cos\left(\phi\right) & -\sin\left(\phi\right) \\ 0 & \dfrac{\sin\left(\phi\right)}{\cos\left(\theta\right)} & \dfrac{\cos\left(\phi\right)}{\cos\left(\theta\right)} \end{bmatrix}. \tag{4.14}$$

At this point, it should be noted that $\cos(\theta)$ term appearing in the denominator of some terms of velocity transformation matrix does not cause indefiniteness of these terms because of the feasible interval of θ. More detailed explanations about the feasible intervals of yaw, roll and pitch angles along with the dynamic model parameters can be found in modeling studies Fantoni and Lozano (2002), Mettler (2003), and Cai et al. (2011). In (4.13), $\upsilon_c(t) \in \mathbb{R}^3$ is a vector that is expressed as $\upsilon_c = \begin{bmatrix} a & b & T_T \end{bmatrix}^T$ where $a(t)$, $b(t) \in \mathbb{R}$ are the flapping angles and $T_T(t) \in \mathbb{R}$ is the tail rotor thrust. In addition to these, $A \in \mathbb{R}^{3\times3}$ and $B \in \mathbb{R}^3$ are a constant invertible matrix and a constant vector, respectively. A simplified model for flapping angles and the tail rotor thrust at hovering flight condition can be expressed as Mettler (2003)

$$\begin{aligned} a &= A_b b - A_{lon}\delta_{lon} \\ b &= -B_a a + B_{lat}\delta_{lat} \\ T_T &= K_{ped0}\delta_{ped} \end{aligned} \tag{4.15}$$

where A_b, A_{lon}, B_a, B_{lat} and $K_{ped0} \in \mathbb{R}$ are constant parameters that are related with the helicopter dynamics. As a result, a simplified rotor model can be expressed as

$$\tau_h = S_h^{-T}\left(AC_\delta\tau + B\right) \tag{4.16}$$

where the matrix $C_\delta \in \mathbb{R}^{3\times3}$ is defined as

$$C_\delta \triangleq \begin{bmatrix} -\dfrac{A_{lon}}{A_bB_a+1} & \dfrac{A_bB_{lat}}{A_bB_a+1} & 0 \\ \dfrac{B_{lat}}{A_bB_a+1} & \dfrac{B_aA_{lon}}{A_bB_a+1} & 0 \\ 0 & 0 & K_{ped0} \end{bmatrix} \tag{4.17}$$

and $\tau = \begin{bmatrix} \delta_{lon} & \delta_{lat} & \delta_{ped} \end{bmatrix}^T$ denotes the actual control input that contains the elevator servo input $\delta_{lon}(t) \in \mathbb{R}$, the aileron servo input $\delta_{lat}(t) \in \mathbb{R}$, and the rudder servo input $\delta_{ped}(t) \in \mathbb{R}$. In view of (4.16), the dynamic model given in (4.12) can be re–arranged in the form given in (4.9) where $h(x, \dot{x}) \in \mathbb{R}^3$ and $g(x) \in \mathbb{R}^{3\times3}$ are defined as

$$h \triangleq M_h^{-1}\left(S_h^{-T}B - C_h\dot{x} - G_h\right) \tag{4.18}$$

$$g \triangleq M_h^{-1}S_h^{-T}AC_\delta. \tag{4.19}$$

4.3. System Model and Properties of an Unactuated Surface Vessel Manipulated by 6 Uni–directional Tugboats

The dynamic model of a 3 dof unactuated surface vessel manipulated by 6 uni–directional tugboats can be written as Fossen (1994), Fossen (2002), Skjetne et al. (2004), Arrichiello et al. (2006), Ihle et al. (2006), Fossen (2011)

$$M_t\dot{\nu} + D_t\nu = F \tag{4.20}$$

$$\dot{x} = R\nu \tag{4.21}$$

where $F = [F_x, F_y, M_z]^{\mathrm{T}} \in \mathbb{R}^3$ represents the total forces and moments applied to and acting on the center of mass of the vessel provided by the tugboats. The inertia matrix, denoted by $M_t(\nu) \in \mathbb{R}^{3\times3}$, is given as Fossen (1994)

$$M_t = M_{RB} + M_A \tag{4.22}$$

where $M_{RB}(\nu) \in \mathbb{R}^{3\times3}$ denotes the positive definite, symmetric rigid body part of the inertia matrix while the effects due to added mass are represented by $M_A(\nu) \in \mathbb{R}^{3\times3}$. It should be noted that M_A is not necessarily symmetric, resulting in a possibly non–symmetric M_t Fossen (1994). It is considered that the added mass term does not lead to a rank deficiency in M_t (*i.e.*, M_t is full rank). The matrix $D_t(\nu) \in \mathbb{R}^{3\times3}$ denotes the hydrodynamic damping terms while $x(t) = [x_p, y_p, \psi]^{\mathrm{T}} \in \mathbb{R}^3$ represents the composite inertial position $x_p(t)$, $y_p(t)$, and heading $\psi(t)$ of the vessel while body fixed linear and angular velocity signals are represented by $\nu(t) = \left[u(t), v(t), \dot{\psi}(t)\right]^{\mathrm{T}} \in \mathbb{R}^3$. The rotation matrix is denoted by $R(\psi) \in SO(3)$ and has the following form

$$R(\psi) = \begin{bmatrix} \cos(\psi) & -\sin(\psi) & 0 \\ \sin(\psi) & \cos(\psi) & 0 \\ 0 & 0 & 1 \end{bmatrix}. \tag{4.23}$$

4.3.1. Force Decomposition and Commutation Strategy

The unactuated vessel is moved via thrust inputs provided from 6 uni–directional tugboats in contact with the vessel's hull as illustrated in Figure 4.1. Accordingly, F in (4.20) is a result of the combined efforts provided from 6 uni–directional tugboats and is expressed as

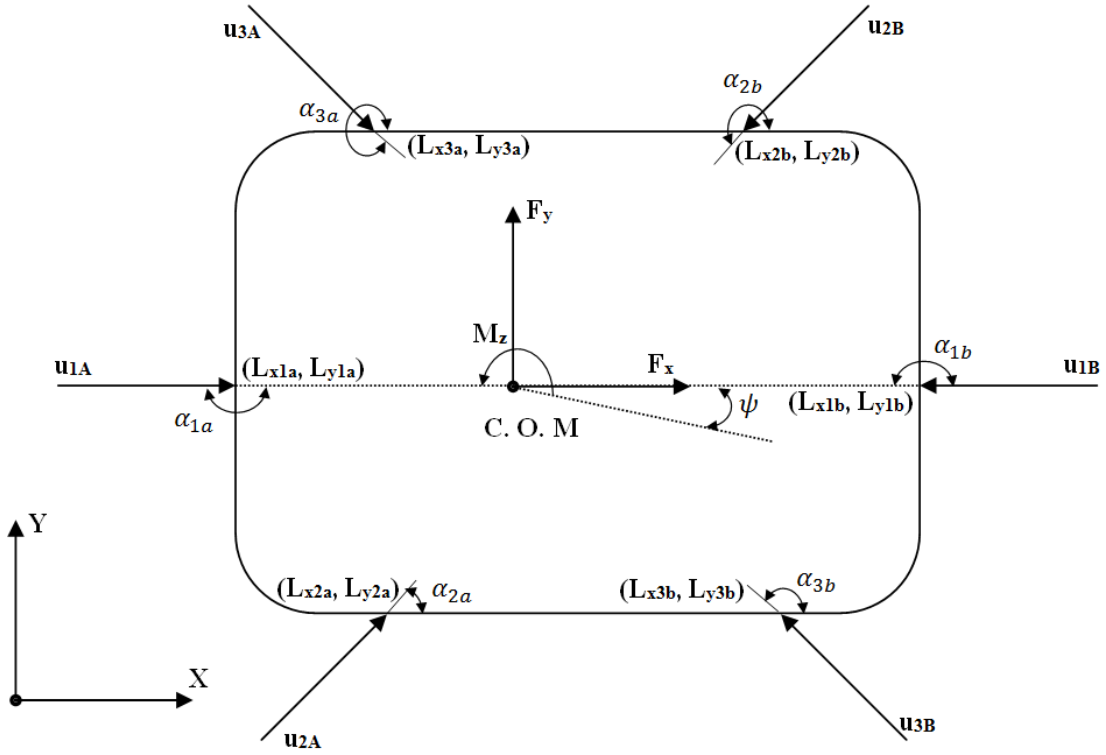

Figure 4.1. System description showing the vessel frames

$$F = B_1 \tau_1 \tag{4.24}$$

where $\tau_1(t) = [u_{1a}, u_{1b}, u_{2a}, u_{2b}, u_{3a}, u_{3b}]^{\mathrm{T}} \in \mathbb{R}^6$ denotes a thrust input vector from 6 uni–directional tugboats while the thrust configuration matrix is shown by $B_1 \in \mathbb{R}^{3\times 6}$ and has the following structure

$$B_1 = \begin{bmatrix} \cos(\alpha_{1a}) & \sin(\alpha_{1a}) & L_{y1a}\cos(\alpha_{1a}) - L_{x1a}\sin(\alpha_{1a}) \\ \cos(\alpha_{1b}) & \sin(\alpha_{1b}) & L_{y1b}\cos(\alpha_{1b}) - L_{x1b}\sin(\alpha_{1b}) \\ \cos(\alpha_{2a}) & \sin(\alpha_{2a}) & L_{y2a}\cos(\alpha_{2a}) - L_{x2a}\sin(\alpha_{2a}) \\ \cos(\alpha_{2b}) & \sin(\alpha_{2b}) & L_{y2b}\cos(\alpha_{2b}) - L_{x2b}\sin(\alpha_{2b}) \\ cos(\alpha_{3a}) & sin(\alpha_{3a}) & -L_{y3a}\cos(\alpha_{3a}) + L_{x3a}\sin(\alpha_{3a}) \\ \cos(\alpha_{3b}) & \sin(\alpha_{3b}) & -L_{y3b}\cos(\alpha_{3b}) + L_{x3b}\sin(\alpha_{3b}) \end{bmatrix}^{\mathrm{T}}. \tag{4.25}$$

The opposite tugboats can then be placed as

$$\begin{aligned} \alpha_{1b} &= \alpha_{1a} + \pi \quad L_{x1b} = L_{x1a} \quad L_{y1b} = L_{y1a} \\ \alpha_{2b} &= \alpha_{2a} + \pi \quad L_{x2b} = L_{x2a} \quad L_{y2b} = L_{y2a} \\ \alpha_{3b} &= \alpha_{3a} - \pi \quad L_{x3b} = L_{x3a} \quad L_{y3b} = L_{y3a} \end{aligned} \tag{4.26}$$

which allows the force equation in (4.24) to be rewritten as

$$F = B\tau \tag{4.27}$$

where $\tau(t) = [u_1, u_2, u_3]^{\mathrm{T}} \in \mathbb{R}^3$ is the combined bi–directional control efforts from the opposing uni–directional tugboats with $u_i = u_{ia} - u_{ib}$, $\forall i = 1, 2, 3$ and $B \in \mathbb{R}^{3\times 3}$ is the thrust configuration matrix obtained as

$$B = \begin{bmatrix} \cos(\alpha_{1a}) & \sin(\alpha_{1a}) & L_{y1a}\cos(\alpha_{1a}) - L_{x1a}\sin(\alpha_{1a}) \\ \cos(\alpha_{2a}) & \sin(\alpha_{2a}) & L_{y2a}\cos(\alpha_{2a}) - L_{x2a}\sin(\alpha_{2a}) \\ \cos(\alpha_{3a}) & \sin(\alpha_{3a}) & -L_{y3a}\cos(\alpha_{3a}) + L_{x3a}\sin(\alpha_{3a}) \end{bmatrix}^T. \tag{4.28}$$

It is remarked that, similar to Braganza et al. (2007), the tugboats are considered to be placed according to the configurations in (4.26). In this dissertation, unlike Braganza et al. (2007), it is considered that the configurations in (4.26) are the initial configurations and they may vary after the motion starts. This relaxes the static positioning assumption in the literature including Braganza et al. (2007) and is an important **novel** departure from the existing literature.

In the subsequent sections, the control input $\tau(t)$ will be designed to obtain satisfactory tracking performance. The following commutation strategy can then be applied to $\tau(t)$ to specify uni–directional thrust effects to be provided by the bi–directional tugboats de Queiroz and Dawson (1996)

$$u_{ia} = \frac{1}{2}\left(u_i + \sqrt{u_i^2 + \epsilon_0^2}\right) \tag{4.29}$$

$$u_{ib} = \frac{1}{2}\left(-u_i + \sqrt{u_i^2 + \epsilon_0^2}\right) \tag{4.30}$$

for $i = 1, 2, 3$ and where ϵ_0 denotes a positive controller parameter selected to obtain non–zero $u_{ia}(t)$ and $u_{ib}(t)$ to prevent the tugboats from losing contact with the vessel.

The time derivative of (4.21) is taken to obtain

$$\ddot{x} = \dot{R}\nu + R\dot{\nu} \tag{4.31}$$

which contains the time derivative of $R(\psi)$ that can be obtained as a result of the special orthogonal structure of the rotation matrix in the following manner

$$\dot{R} = RS_3 \tag{4.32}$$

where $S_3\left(\dot{\psi}\right) \in \mathbb{R}^{3\times 3}$ is a skew–symmetric matrix defined as

$$S_3 \triangleq \dot{\psi}\begin{bmatrix} 0 & -1 & 0 \\ 1 & 0 & 0 \\ 0 & 0 & 0 \end{bmatrix}. \tag{4.33}$$

After substituting (4.32) into (4.31), the right–hand side of (4.31) can be re–arranged as

$$\ddot{x} = -R\left(M_t^{-1}D_t - S_3R^T\dot{x}\right) + RM_t^{-1}B\tau \tag{4.34}$$

where (4.20) and (4.27) were utilized. A more compact form of the above model is obtained as given in (4.9) with the functions $h\left(x,\dot{x}\right) \in \mathbb{R}^3$ and $g\left(x,\dot{x}\right) \in \mathbb{R}^{3\times 3}$ defined in the following form

$$\begin{aligned} h &\triangleq -R\left(M_t^{-1}D_t - S_3R^T\dot{x}\right) \\ g &\triangleq RM_t^{-1}B. \end{aligned} \tag{4.35}$$

At this point, it should be stated that, the subsequent control design will utilize only the knowledge of a constant diagonal matrix that is obtained from the decomposition of g which can be an identity matrix for some mechatronic systems. The remaining terms are considered as uncertain for all three mechatronic systems.

4.4. Control Design for Mechatronic Systems

Since all three mechatronic systems are rearranged in a form that is compatible with (1.2) where all of them are second order MIMO nonlinear systems with three inputs and three outputs, steps of the control design and stability analysis are similar. These steps are examined for the sake of completeness and are presented in the following subsections of this chapter.

4.4.1. Open–Loop Error System Development

At this point, it should be noted that since g is a real matrix with non–zero leading principal minors, the following matrix decomposition is possible Morse (1993), Costa et al. (2003)

$$g = SDU \tag{4.36}$$

where $S\left(x,\dot{x}\right) \in \mathbb{R}^{3\times 3}$ represents a symmetric, positive definite matrix, $D \in \mathbb{R}^{3\times 3}$ is a diagonal matrix with entries being ± 1 and $U\left(x,\dot{x}\right) \in \mathbb{R}^{3\times 3}$ unity upper triangular matrix. While the entries of D are constant, uncertain terms are injected in S and U, thus these matrices are not precisely known. As a result of applying the above matrix decomposition to the models that are available in the literature, D came out to be an identity matrix.

Despite this, the derivations given in this study will be presented for the general case where it is assumed that D is available for control design (see Costa et al. (2003) and Chen et al. (2008) for the precedence of this type assumption).

After taking the time derivative of (4.9), following expression is obtained

$$\dddot{x} = \varphi + SDU\dot{\tau} \tag{4.37}$$

where (4.9) and (4.36) were utilized, and $\varphi\left(x, \dot{x}, \ddot{x}\right) \in \mathbb{R}^3$ is an auxiliary term defined as

$$\varphi \triangleq \dot{h} + \dot{g}g^{-1}\left(\ddot{x} - h\right). \tag{4.38}$$

At this point, the inverse of S is designed as $M\left(x, \dot{x}\right) \in \mathbb{R}^{3\times 3}$. It is remarked that M is symmetric and positive definite because of symmetry and positive definiteness of S. In addition to this, the following bounds are valid for $M\left(x, \dot{x}\right)$

$$\underline{m}\left\|\chi\right\|^2 \leq \chi^T M\left(x, \dot{x}\right)\chi \leq \bar{m}\left\|\chi\right\|^2 \quad \forall \chi \in \mathbb{R}^3 \tag{4.39}$$

where $\underline{m} \in \mathbb{R}$ and $\bar{m}\left(x, \dot{x}\right) \in \mathbb{R}$ denote a positive bounding constant and a positive non–decreasing bounding function, respectively.

Following expression can be obtained after multiplying both sides of (4.37) with M

$$M\dddot{x} = f + DU\dot{\tau} \tag{4.40}$$

where $f\left(x, \dot{x}, \ddot{x}\right) \triangleq M\varphi \in \mathbb{R}^3$.

Ensuring a good tracking performance for the mechatronic systems and guaranteeing boundedness of all the terms under the closed–loop operation constitute main control objectives. The subsequent control design is based on the availability of $x\left(t\right)$ and $\dot{x}\left(t\right)$ (*i.e.*, full–state feedback).

To quantify the tracking control objective, the output tracking error, denoted by $e_1\left(t\right) \in \mathbb{R}^3$, is defined as

$$e_1 \triangleq x_d - x \tag{4.41}$$

where $x_d\left(t\right) \in \mathbb{R}^3$ is a smooth desired trajectory that is chosen in the sense that

$$x_d\left(t\right) \in \mathcal{C}^3 \text{ and } x_d^{(i)}\left(t\right) \in \mathcal{L}_\infty, i = 0, 1, 2, 3. \tag{4.42}$$

In order to eliminate the higher order time derivatives from the subsequent Lyapunov–based stability analysis, auxiliary errors, denoted by $e_2\left(t\right) \in \mathbb{R}^3$ and $r\left(t\right) \in \mathbb{R}^3$, are defined as follows

$$e_2 \triangleq \dot{e}_1 + e_1 \tag{4.43}$$

$$r \triangleq \dot{e}_2 + \alpha e_2 \tag{4.44}$$

where $\alpha \in \mathbb{R}^{3\times 3}$ denotes a constant, positive–definite, diagonal gain matrix. The following expression is obtained by taking the time derivative of (4.44) and premultiplying the resulting expression with M

$$M\dot{r} = M\left(\dddot{x}_d + \ddot{e}_1 + \alpha\dot{e}_2\right) - \dot{f} - DU\dot{\tau} \tag{4.45}$$

where (4.40), and the time derivatives of (4.41) and (4.43) were utilized. The right–hand side of (4.45) can be re–arranged as

$$M\dot{r} = -\frac{1}{2}\dot{M}r - e_2 - DU\dot{\tau} + N \tag{4.46}$$

where $N\left(x, \dot{x}, \ddot{x}, x_d, \dot{x}_d, \ddot{x}_d, \dddot{x}_d, t\right) \in \mathbb{R}^3$ is an auxiliary term defined as

$$N \triangleq M\left(\dddot{x}_d + \ddot{e}_1 + \alpha\dot{e}_2\right) - \dot{f} + e_2 + \frac{1}{2}\dot{M}r. \tag{4.47}$$

The auxiliary function N can be partitioned as sum of two auxiliary terms denoted by $\bar{N}\left(t\right), \widetilde{N}\left(t\right) \in \mathbb{R}^3$. These auxiliary terms are defined as

$$\bar{N} \triangleq N|_{x=x_d, \dot{x}=\dot{x}_d, \ddot{x}=\ddot{x}_d} \tag{4.48}$$

$$\widetilde{N} \triangleq N - \bar{N}. \tag{4.49}$$

After substituting the above definitions, the final form of open–loop error system can be obtained as follows

$$M\dot{r} = -\frac{1}{2}\dot{M}r - e_2 - DU\dot{\tau} + \widetilde{N} + \bar{N}. \tag{4.50}$$

4.5. Controller Formulation

Motivated by the subsequent stability analysis and based on the open–loop error system in (4.50), the control input $\tau\left(t\right)$ is designed as

$$\tau = DK\left[e_2\left(t\right) - e_2\left(t_0\right) + \alpha\int_{t_0}^{t} e_2\left(\sigma\right)d\sigma\right] + D\Pi \tag{4.51}$$

where the auxiliary term $\Pi\left(t\right) \in \mathbb{R}^3$ is generated according to the update law

$$\dot{\Pi}\left(t\right) = \beta\text{Sgn}\left(e_2\left(t\right)\right) \text{ with } \Pi\left(t_0\right) = 0_3. \tag{4.52}$$

In (4.51) and (4.52), K, $\beta \in \mathbb{R}^{3\times 3}$ denote constant, positive definite, diagonal gain matrices while a vector of zeros is represented by $0_3 \in \mathbb{R}^3$ and $\text{Sgn}(\cdot) \in \mathbb{R}^3$ is the vector sign function. The control gain is chosen as $K = I_3 + k_p I_3 + \text{diag}\left\{k_{d,1}, k_{d,2}, 0\right\}$ where

k_p, $k_{d,1}$, $k_{d,2} \in \mathbb{R}$ are constant, positive controller gains, the notation diag $\{\cdot\}$ represents a diagonal matrix, and $I_3 \in \mathbb{R}^{3\times 3}$ is the standard identity matrix. Before continuing with the closed–loop error system, the required measurements from the system are clarified by examining all terms of the proposed controller in (4.51) closely. The control design requires the measurements of the auxiliary error e_2. From its definition in (4.43) and the definition of tracking error in (4.41), it is clear that measurements of the position and the velocity of the mechatronic systems are required. Since the control design is based on the full–state feedback assumption these measurements are available.

The following closed–loop error system is obtained by substituting the time derivative of (4.51) into (4.50) and then adding and subtracting $DKr(t)$

$$M\dot{r} = -\frac{1}{2}\dot{M}r - e_2 - Kr + \widetilde{N} + \bar{N}D(U - I_3)DKr - DUD\beta\text{Sgn}(e_2) \tag{4.53}$$

where (4.52) and the fact that $DD = I_3$ were utilized.

Before presenting the accompanying stability analysis, a more detailed examination of the last two terms of (4.53) are given. The $D(U - I_3)DKr$ term can be rewritten as

$$D(U - I_3)DKr = \begin{bmatrix} \Lambda_1 \\ \Lambda_2 \\ 0 \end{bmatrix} + \begin{bmatrix} \Phi_1 \\ \Phi_2 \\ 0 \end{bmatrix} \tag{4.54}$$

where the auxiliary terms $\Lambda_1(t)$, $\Lambda_2(t)$, $\Phi_1(t)$, $\Phi_2(t) \in \mathbb{R}$ are defined as

$$\Lambda_1 \triangleq d_1 d_2 k_2 \widetilde{U}_{1,2} r_2 + d_1 d_3 k_3 \widetilde{U}_{1,3} r_3 \tag{4.55}$$

$$\Lambda_2 \triangleq d_2 d_3 k_3 \widetilde{U}_{2,3} r_3 \tag{4.56}$$

$$\Phi_1 \triangleq d_1 d_2 k_2 \bar{U}_{1,2} r_2 + d_1 d_3 k_3 \bar{U}_{1,3} r_3 \tag{4.57}$$

$$\Phi_2 \triangleq d_2 d_3 k_3 \bar{U}_{2,3} r_3 \tag{4.58}$$

with the following definitions of $\bar{U}_{1,2}(t)$, $\bar{U}_{1,3}(t)$, $\bar{U}_{2,3}(t)$, $\widetilde{U}_{1,2}(t)$, $\widetilde{U}_{1,3}(t)$, $\widetilde{U}_{2,3}(t) \in \mathbb{R}$ as

$$\bar{U}_{i,j} \triangleq U_{i,j}|_{x=x_d, \dot{x}=\dot{x}_d} \tag{4.59}$$

$$\widetilde{U}_{i,j} \triangleq U_{i,j} - \bar{U}_{i,j} \tag{4.60}$$

where $U_{i,j}(x, \dot{x}) \in \mathbb{R}$ represents the (i,j)–th entry of $U(x, \dot{x})$. From (4.56), it can be seen that $\Lambda_2(t)$ depends on k_3, and from (4.55), it is clear that, $\Lambda_1(t)$ depends on k_3 and k_2. From (4.57) and (4.58), it can also seen that $\Phi_1(t)$ depends on k_3 and k_2 while $\Phi_2(t)$ depends on k_3.

On the other hand, the following decomposition can be applied to $DUD\beta\text{Sgn}(e_2)$ term

$$DUD\beta\text{Sgn}(e_2) = \left[\Psi^T, 0\right]^T + \Theta \tag{4.61}$$

where two auxiliary terms, denoted by $\Psi(t) \in \mathbb{R}^2$ and $\Theta(t) \in \mathbb{R}^3$, have the following forms

$$\begin{bmatrix} \Psi \\ 0 \end{bmatrix} \triangleq D\left(U - \bar{U}\right) D\beta\text{Sgn}(e_2) \tag{4.62}$$

$$\Theta \triangleq D\bar{U}D\beta\text{Sgn}(e_2) \tag{4.63}$$

where $\bar{U}(x_d, \dot{x}_d) \triangleq U|_{x=x_d, \dot{x}=\dot{x}_d} \in \mathbb{R}^{3\times 3}$ is a function of desired trajectory and its time derivative, and $\Psi_i(t) \in \mathbb{R}$, $i = 1, 2$ and $\Theta_i(t) \in \mathbb{R}$, $i = 1, 2, 3$, are defined as

$$\Psi_i \triangleq d_i \sum_{j=i+1}^{3} d_j C_j \widetilde{U}_{i,j} \text{sgn}(e_{2,j}) \tag{4.64}$$

$$\Theta_i \triangleq d_i \sum_{j=i}^{3} d_j C_j \bar{U}_{i,j} \text{sgn}(e_{2,j}). \tag{4.65}$$

The following upper bounds can be developed by utilizing the Mean Value Theorem in Khalil (2002)

$$\left\|\widetilde{N}\right\| \leq \rho_{\widetilde{N}}(\|z\|)\|z\| \tag{4.66}$$

$$\left\|\widetilde{U}_{i,j}\right\| \leq \rho_{i,j}(\|z\|)\|z\| \tag{4.67}$$

where $\rho_{\widetilde{N}}$, $\rho_{i,j} \in \mathbb{R}$ are non–negative, globally invertible, non–decreasing functions of their arguments, and $z(t) \in \mathbb{R}^9$ is defined as

$$z \triangleq \begin{bmatrix} e_1^T & e_2^T & r^T \end{bmatrix}^T. \tag{4.68}$$

It can be seen from (4.48) and (4.59) that the entries of $\bar{N}(t)$ and $\bar{U}_{i,j}(t)$ can be upper bounded as

$$\left|\bar{N}_i(t)\right| \leq \zeta_{\bar{N}_i} \tag{4.69}$$

$$\left|\bar{U}_{i,j}(t)\right| \leq \zeta_{\bar{U}_{u_{i,j}}} \tag{4.70}$$

where $\zeta_{\bar{N}_i}$, $\zeta_{\bar{U}_{u_{i,j}}} \in \mathbb{R}$ are positive bounding constants. Based on (4.55)–(4.58), (4.64), (4.65), following upper bounds can be obtained

$$|\Lambda_i| \leq \rho_{\Lambda_i}(\|z\|)\|z\| \tag{4.71}$$

$$|\Phi_i| \leq \zeta_{\Phi_i}\|z\| \tag{4.72}$$

$$|\Psi_i| \leq \rho_{\Psi_i}(\|z\|)\|z\| \tag{4.73}$$

for $i = 1, 2$ and the following upper bound can also be obtained

$$|\Theta_i| \leq \zeta_{\Theta_i} \tag{4.74}$$

for $i = 1, 2, 3$ where (4.66)–(4.70) were utilized. From (4.74), it is clear that $\|\Theta\| \leq \zeta_\Theta$ is provided for some positive bounding constant $\zeta_\Theta \in \mathbb{R}$, and from (4.71)–(4.73), the following expression is obtained

$$|\Lambda_i| + |\Phi_i| + |\Psi_i| \leq \rho_i \left(\|z\|\right) \|z\| \tag{4.75}$$

where $\rho_i \left(\|z\|\right) \in \mathbb{R}$ $i = 1, 2$, are non–negative, globally invertible, non–decreasing functions satisfying

$$\rho_{\Lambda_i} + \rho_{\Psi_i} + \zeta_{\Phi_i} \leq \rho_i. \tag{4.76}$$

After this point, boundedness and convergence analysis of the closed–loop systems can be proceeded.

4.6. Stability Analysis

Proving the boundedness of the errors under the closed–loop operation is the first purpose of this section. Then, by making use of the boundedness result a lemma will be presented to obtain an upper bound for the integral of the absolute values of the entries of the time derivative of $e_2(t)$. This upper bound will be utilized in another lemma to prove the non–negativity of a Lyapunov–like function. Finally, asymptotic stability of the overall closed–loop system will be proven by using the results of this lemma.

Theorem 4.6.1 *The controller in* (4.51) *and* (4.52) *guarantees the boundedness of the closed–loop system including the errors in* (4.41)*,* (4.43)*,* (4.44) *provided that the controller gains $k_{d,1}$, $k_{d,2}$ and k_p are chosen large enough compared to the initial conditions of the system and the following condition is satisfied*

$$\lambda_{\min}(\alpha) \geq \frac{1}{2} \tag{4.77}$$

where $\lambda_{\min}(\alpha)$ is the minimum eigenvalue of the gain matrix α.

Proof The non–negative function $V_1(z) \in \mathbb{R}$ is defined as

$$V_1 \triangleq \frac{1}{2} e_1^T e_1 + \frac{1}{2} e_2^T e_2 + \frac{1}{2} r^T M r. \tag{4.78}$$

The Lyapunov function in (4.78) can be lower and upper bounded as follows by utilizing (4.39)

$$\lambda_1 \|z\|^2 \leq V_1(z) \leq \lambda_2 \|z\|^2 \tag{4.79}$$

with $\lambda_1 \triangleq \frac{1}{2}\min\{1, \underline{m}\}$ and $\lambda_2 \triangleq \max\left\{1, \frac{1}{2}\bar{m}(\|z\|)\right\}$ and the terms $\underline{m}$, $\bar{m}(\|z\|)$ were defined in (4.39) and $z(t)$ was defined in (4.68). The following inequality is obtained by taking the time derivative of (4.78), making necessary substitutions, and then performing straightforward mathematical manipulations and grouping

$$\dot{V}_1 \leq -\mu_1 V_1 + \delta_1 \tag{4.80}$$

where μ_1, $\delta_1 \in \mathbb{R}$ denote positive constants. The boundedness of $V_1(t)$ can be obtained from (4.78) and (4.80) (*i.e.*, $V_1(t) \in \mathcal{L}_\infty$), therefore $e_1(t)$, $e_2(t)$ and $r(t)$ are UUB. Making use of standard signal chasing arguments allows that to prove the boundedness of all remaining terms under the closed–loop operation.

Lemma 4.6.2 *Provided that $e_2(t)$ and $\dot{e}_2(t)$ are bounded, the following expression for the upper bound of the integral of the absolute value of the i^{th} entry of $\dot{e}_2(t)$ $i = 1, 2, 3$ can be obtained*

$$\int_{t_0}^{t} |\dot{e}_{2,i}(\sigma)|\, d\sigma \leq \gamma_1 + \gamma_2 \int_{t_0}^{t} |e_{2,i}(\sigma)|\, d\sigma + |e_{2,i}(t)| \tag{4.81}$$

where γ_1, $\gamma_2 \in \mathbb{R}$ are some positive bounding constants.

Proof First, it is noted that if $e_{2,i}(t) \equiv 0$ on some interval, then $\dot{e}_{2,i}(t) \equiv 0$ on the same interval, and the inequality (4.81) yields this qualification. Therefore, without loss of generality, it is assumed that $e_{2,i}(t)$ is absolutely greater than zero on the interval of $[t_0, t]$. Let $T \in [t_0, t)$ be the last instant of time when $\dot{e}_{2,i}(t)$ changes sign. Then, on the interval $[T, t]$, $\dot{e}_{2,i}(t)$ has a constant sign, hence

$$\int_{T}^{t} |\dot{e}_{2,i}(\sigma)|\, d\sigma = \left| \int_{T}^{t} \dot{e}_{2,i}(\sigma)\, d\sigma \right| = |e_{2,i}(t) - e_{2,i}(T)|. \tag{4.82}$$

From the boundedness of $\dot{e}_{2,i}(t)$, it follows that there exist a constant $\kappa > 0$ such that $|\dot{e}_{2,i}(t)| \leq \kappa$, therefore

$$\int_{t_0}^{T} |\dot{e}_{2,i}(\sigma)|\, d\sigma \leq \gamma (T - t_0). \tag{4.83}$$

On the other hand, the following equality is obtained from the application of the Mean Value Theorem in Khalil (2002)

$$\int_{t_0}^{T} |e_{2,i}(\sigma)|\, d\sigma = e_{2,i_*}(T - t_0) \tag{4.84}$$

where e_{2,i_*} is some constant intermediate value of $|e_{2,i}(t)|$ on the interval $[t_0, T]$. By assumption, e_{2,i_*} is bounded away from zero. Therefore, by using inequality (4.83) and equality (4.84), it can be concluded as follows

$$\int_{t_0}^{T} |\dot{e}_{2,i}(\sigma)|\, d\sigma \leq \gamma_2 \int_{t_0}^{T} |e_{2,i}(\sigma)|\, d\sigma \tag{4.85}$$

where $\gamma_2 \triangleq \gamma / e_{2,i_*}$. Combining the relationships in (4.82) and (4.85), it can be written

$$\int_{t_0}^{t} |\dot{e}_{2,i}(\sigma)|\, d\sigma \leq |e_{2,i}(T)| + \gamma_2 \int_{t_0}^{T} |e_{2,i}(\sigma)|\, d\sigma + |e_{2,i}(t)| \tag{4.86}$$

which after defining $\gamma_1 \triangleq \sup |e_{2,i}(T)|$ yields (4.81). At this point it should be stated that $\sup|\cdot|$ denotes the supremum function.

Following decomposition is essential for the proof of Lemma 4.6.3.

Notice that, as a result of the fact that $\bar{U}(t)$ being unity upper triangular, $\Theta(t)$ in (4.63) can be rewritten as

$$\Theta = (I_3 + \Omega)\, \beta \text{Sgn}(e_2) \tag{4.87}$$

where $\Omega(t) \triangleq D\left(\bar{U} - I_3\right) D \in \mathbb{R}^{3\times 3}$ is a strictly upper triangular matrix. Since it is a function of the desired trajectory and its time derivatives, its entries, denoted by $\Omega_{i,j}(t) \in \mathbb{R}$, are bounded in the sense that

$$|\Omega_{i,j}| \leq \zeta_{\Omega_{i,j}} \tag{4.88}$$

where $\zeta_{\Omega_{i,j}} \in \mathbb{R}$ are positive bounding constants.

Lemma 4.6.3 *Consider the term*

$$L \triangleq r^T \left[\bar{N} - (I_3 + \Omega)\, \beta \textit{Sgn}(e_2)\right]. \tag{4.89}$$

Provided that the entries of the control gain matrix β are chosen to satisfy the following in an orderly fashion

$$\beta_3 \geq \zeta_{\bar{N}_3}\left(1 + \frac{\gamma_2}{\alpha_3}\right) \tag{4.90}$$

$$\beta_2 \geq \left(\zeta_{\bar{N}_2} + \zeta_{\Omega_{2,3}}\beta_3\right)\left(1 + \frac{\gamma_2}{\alpha_2}\right) \tag{4.91}$$

$$\beta_1 \geq \left(\zeta_{\bar{N}_1} + \zeta_{\Omega_{1,2}}\beta_2 + \zeta_{\Omega_{1,3}}\beta_3\right)\left(1 + \frac{\gamma_2}{\alpha_1}\right) \tag{4.92}$$

where α_i for $i = 1, 2, 3$ denotes the i^{th} diagonal entry of α, then it can be concluded that

$$\int_{t_0}^{t} L(\sigma)\, d\sigma \leq \zeta_L \tag{4.93}$$

where $\zeta_L \in \mathbb{R}$ is a positive bounding constant defined as

$$\zeta_L \triangleq \gamma_1 \sum_{i=1}^{2} \sum_{j=i+1}^{3} \zeta_{\Omega_{i,j}} \beta_j + \gamma_1 \sum_{i=1}^{3} \zeta_{\bar{N}_i} + \sum_{i=1}^{3} \beta_i \left| e_{2,i}\left(t_0\right)\right|. \tag{4.94}$$

Proof The analysis is started by integrating (4.89) in time from t_0 to t

$$\begin{aligned}
\int_{t_0}^{t} L\left(\sigma\right) d\sigma &= \int_{t_0}^{t} e_2^T\left(\sigma\right) \alpha^T \left(\bar{N}\left(\sigma\right) - \beta \text{Sgn}\left(e_2\left(\sigma\right)\right)\right) d\sigma \\
&\quad - \int_{t_0}^{t} e_2^T\left(\sigma\right) \alpha^T \Omega\left(\sigma\right) \beta \text{Sgn}\left(e_2\left(\sigma\right)\right) d\sigma \\
&\quad + \int_{t_0}^{t} \dot{e}_2^T\left(\sigma\right) \bar{N}\left(\sigma\right) d\sigma \\
&\quad - \int_{t_0}^{t} \dot{e}_2^T\left(\sigma\right) \Omega\left(\sigma\right) \beta \text{Sgn}\left(e_2\left(\sigma\right)\right) d\sigma \\
&\quad - \int_{t_0}^{t} \dot{e}_2^T\left(\sigma\right) \beta \text{Sgn}\left(e_2\left(\sigma\right)\right) d\sigma
\end{aligned} \tag{4.95}$$

where (4.44) was utilized. To ease the presentation, each term on the right–hand side of (4.95) will be considered separately. The first term:

$$\begin{aligned}
&\int_{t_0}^{t} e_2^T\left(\sigma\right) \alpha^T \left(\bar{N}\left(\sigma\right) - \beta \text{Sgn}\left(e_2\left(\sigma\right)\right)\right) d\sigma \\
= &\int_{t_0}^{t} \sum_{i=1}^{3} \alpha_i e_{2,i}\left(\sigma\right) \left(\bar{N}_i\left(\sigma\right) - \beta_i \text{sgn}\left(e_{2,i}\left(\sigma\right)\right)\right) d\sigma \\
\leq &\sum_{i=1}^{3} \alpha_i \left(\zeta_{\bar{N}_i} - \beta_i\right) \int_{t_0}^{t} \left|e_{2,i}\left(\sigma\right)\right| d\sigma.
\end{aligned} \tag{4.96}$$

The second term:

$$\begin{aligned}
&- \int_{t_0}^{t} e_2^T\left(\sigma\right) \alpha^T \Omega\left(\sigma\right) \beta \text{Sgn}\left(e_2\left(\sigma\right)\right) d\sigma \\
= &- \int_{t_0}^{t} \sum_{i=1}^{2} \alpha_i e_{2,i}\left(\sigma\right) \sum_{j=i+1}^{3} \beta_j \Omega_{i,j}\left(\sigma\right) \text{sgn}\left(e_{2,j}\left(\sigma\right)\right) d\sigma \\
\leq &\sum_{i=1}^{2} \sum_{j=i+1}^{3} \alpha_i \beta_j \zeta_{\Omega_{i,j}} \int_{t_0}^{t} \left|e_{2,i}\left(\sigma\right)\right| d\sigma.
\end{aligned} \tag{4.97}$$

The third term:

$$\begin{aligned}\int_{t_0}^{t} \dot{e}_2^T(\sigma)\,\bar{N}(\sigma)\,d\sigma &= \sum_{i=1}^{3}\int_{t_0}^{t} \dot{e}_{2,i}^T(\sigma)\,\bar{N}_i(\sigma)\,d\sigma \\ &\leq \sum_{i=1}^{3}\zeta_{\bar{N}_i}\int_{t_0}^{t}\left|\dot{e}_{2,i}(\sigma)\right|d\sigma \\ &\leq \sum_{i=1}^{3}\zeta_{\bar{N}_i}\left(\gamma_1+\gamma_2\int_{t_0}^{t}\left|e_{2,i}(\sigma)\right|d\sigma+\left|e_{2,i}(t)\right|\right). \quad (4.98)\end{aligned}$$

The fourth term:

$$\begin{aligned}&-\int_{t_0}^{t}\dot{e}_2^T(\sigma)\,\Omega(\sigma)\,\beta\mathrm{Sgn}\left(e_2(\sigma)\right)d\sigma \\ =\ &-\int_{t_0}^{t}\sum_{i=1}^{2}\dot{e}_{2,i}(\sigma)\sum_{j=i+1}^{3}\beta_j\Omega_{i,j}(\sigma)\,\mathrm{sgn}\left(e_{2,j}(\sigma)\right)d\sigma \\ \leq\ &\sum_{i=1}^{2}\sum_{j=i+1}^{3}\beta_j\zeta_{\Omega_{i,j}}\int_{t_0}^{t}\left|\dot{e}_{2,i}(\sigma)\right|d\sigma \\ \leq\ &\sum_{i=1}^{2}\sum_{j=i+1}^{3}\beta_j\zeta_{\Omega_{i,j}}\left(\gamma_1+\gamma_2\int_{t_0}^{t}\left|e_{2,i}(\sigma)\right|d\sigma+\left|e_{2,i}(t)\right|\right). \quad (4.99)\end{aligned}$$

The fifth term:

$$\begin{aligned}-\int_{t_0}^{t}\dot{e}_2^T(\sigma)\,\beta\mathrm{Sgn}\left(e_2(\sigma)\right)d\sigma &= -\sum_{i=1}^{3}\int_{t_0}^{t}\beta_i\dot{e}_{2,i}(\sigma)\,\mathrm{sgn}\left(e_{2,i}(\sigma)\right)d\sigma \\ &= -\sum_{i=1}^{3}\beta_i\int_{t_0}^{t}\mathrm{sgn}\left(e_{2,i}(\sigma)\right)d\left(e_{2,i}\right) \\ &= -\sum_{i=1}^{3}\beta_i\int_{t_0}^{t}d\left(\left|e_{2,i}\right|\right) \\ &= -\sum_{i=1}^{3}\beta_i\left|e_{2,i}(t)\right|+\sum_{i=1}^{3}\beta_i\left|e_{2,i}(t_0)\right|. \quad (4.100)\end{aligned}$$

It is noted that, the result of Lemma 4.6.2 was utilized to obtain the last lines of (4.98) and (4.99). After combining the upper bounds in (4.96)–(4.100), the following expression is

obtained

$$\begin{aligned}\int_{t_0}^{t} L(\sigma)\, d\sigma \;\leq\; & \sum_{i=1}^{2} \gamma_i \left[\left(1+\frac{\gamma_2}{\alpha_i}\right) \left(\zeta_{\bar{N}_i} + \sum_{j=i+1}^{3} \zeta_{\Omega_{i,j}} \beta_j \right) - \beta_i \right] \int_{t_0}^{t} |e_{2,i}(\sigma)|\, d\sigma \\ & + \alpha_3 \left[\left(1+\frac{\gamma_2}{\alpha_3}\right) \zeta_{\bar{N}_3} - \beta_3 \right] \int_{t_0}^{t} |e_{2,3}(\sigma)|\, d\sigma \\ & + (\zeta_{\bar{N}_3} - \beta_3)\, |e_{2,3}(t)| \\ & + \sum_{i=1}^{2} \left(\zeta_{\bar{N}_i} + \sum_{j=i+1}^{3} \zeta_{\Omega_{i,j}} \beta_j - \beta_i \right) |e_{2,i}(t)| \\ & + \gamma_1 \sum_{i=1}^{2} \sum_{j=i+1}^{3} \zeta_{\Omega_{i,j}} \beta_j + \gamma_1 \sum_{i=1}^{3} \zeta_{\bar{N}_i} + \sum_{i=1}^{3} \beta_i\, |e_{2,i}(t_0)| \,. \end{aligned} \tag{4.101}$$

Based on (4.101), β_3 is firstly chosen to satisfy (4.90) to make second and third lines on the right–hand side negative, next β_2 and β_1 are chosen according to (4.91) and (4.92), respectively to satisfy (4.90) to make first and fourth lines on the right–hand side negative, and finally, the definition of ζ_L in (4.94) is utilized to obtain (4.93), thus completing the proof of Lemma 4.6.3.

Theorem 4.6.4 *The controller of* (4.51) *and* (4.52) *ensures the convergence of the tracking error* $e_1(t)$ *asymptotically to the origin in the sense that*

$$\|e_1(t)\| \to 0 \text{ as } t \to +\infty \tag{4.102}$$

provided that α *is chosen to satisfy* (4.77)*, the entries of* β *are chosen to satisfy* (4.90)–(4.92)*, and* k_p*,* $k_{d,1}$*,* $k_{d,2}$ *are chosen large enough.*

Proof The auxiliary function $P(t) \in \mathbb{R}$ is defined as

$$P \triangleq \zeta_L - \int_{t_0}^{t} L(\sigma)\, d\sigma. \tag{4.103}$$

where the terms ζ_L and $L(t)$ were defined in (4.89) and (4.94), respectively. When the entries of the control gain matrix β are chosen to satisfy (4.90)–(4.92), from the proof of Lemma 4.6.3, it can be concluded that $P(t)$ is non–negative.

At this stage, consider the Lyapunov function $V_2(z,t) \in \mathbb{R}$ defined as

$$V_2 \triangleq V_1 + P \tag{4.104}$$

where $V_1(z) \in \mathbb{R}$ was defined in (4.78) and $s(t) \in \mathbb{R}^{10}$ is defined as

$$s \triangleq \begin{bmatrix} z^T & \sqrt{P} \end{bmatrix}^T. \tag{4.105}$$

After utilizing (4.39), the Lyapunov function in (4.104) can be lower and upper bounded as follows

$$W_1(s) \leq V_2(s,t) \leq W_2(s) \tag{4.106}$$

where $W_1(s)$, $W_2(s) \in \mathbb{R}$ are defined as

$$W_1 \triangleq \lambda_1 \|s\|^2, W_2 \triangleq \lambda_2(\|z\|)\|s\|^2. \tag{4.107}$$

Taking the time derivative of V_2, utilizing the time derivative of (4.93), canceling common terms yields

$$\begin{aligned} \dot{V}_2 = & - e_1^T e_1 + e_1^T e_2 - e_2^T \alpha e_2 - r^T r + \left[r^T \widetilde{N} - k_p r^T r \right] \\ & + \left[-\sum_{i=1}^{2} r_i (\Lambda_i + \Psi_i + \Phi_i) - \sum_{i=1}^{2} k_{d,i} r_i^2 \right] \end{aligned} \tag{4.108}$$

which can be rearranged to have the following form

$$\begin{aligned} \dot{V}_2 \leq & -\frac{1}{2}\|e_1\|^2 - \left(\lambda_{\min}(\alpha) - \frac{1}{2}\right)\|e_2\|^2 - r^T r + \frac{\rho_{\widetilde{N}}^2(\|z\|)}{4k_p}\|z\|^2 \\ & + \sum_{i=1}^{2} \frac{\rho_i^2(\|z\|)}{4k_{d,i}}\|z\|^2 \\ \leq & -\left(\lambda_3 - \frac{\rho_{\widetilde{N}}^2(\|z\|)}{4k_p} - \sum_{i=1}^{2} \frac{\rho_i^2(\|z\|)}{4k_{d,i}}\right)\|z\|^2 \end{aligned} \tag{4.109}$$

where $\lambda_3 \triangleq \min\left\{\frac{1}{2}, \lambda_{\min}(\alpha) - \frac{1}{2}\right\}$. When the controller gains k_p, $k_{d,1}$, $k_{d,2}$ are selected large enough such that the regions defined by $\mathcal{D}_z \triangleq \{z : \|z\| \leq \mathcal{R}\}$ and $\mathcal{D}_s \triangleq \{s : \|s\| \leq \mathcal{R}\}$ with $\mathcal{R}$ being defined as

$$\mathcal{R} = \min\left\{\rho_{\widetilde{N}}^{-1}\left(2\sqrt{k_p\frac{1-\mu}{3}}\right), \rho_1^{-1}\left(2\sqrt{k_{d,1}\frac{1-\mu}{3}}\right), \rho_2^{-1}\left(2\sqrt{k_{d,2}\frac{1-\mu}{3}}\right)\right\} \tag{4.110}$$

are non–empty. From (4.109), (4.110) and the definition of s, one can then restate

$$\dot{V}_2 \leq -\mu\|z\|^2 \triangleq W(s) \forall s \in \mathcal{D}_s \tag{4.111}$$

where $\mu \in \mathbb{R}$ is a positive constant that satisfies $0 < \mu \leq 1$. From (4.104) and (4.111), it is obvious that $V_2(t) \in \mathcal{L}_\infty$, and from the proof of Theorem 4.6.1, it can be concluded that all terms in the closed–loop error system are bounded and furthermore, from the boundedness of $\dot{W}(s)$, it can be stated that $W(s)$ is uniformly continuous.

Based on the definition of $\mathcal{D}_s$, another region, $\mathcal{S}$, can be defined in the following form

$$\begin{aligned}\mathcal{S} \triangleq & \left\{ s \in \mathcal{D}_s : W_2(s) < \lambda_2 \left(\rho_{\widetilde{N}}^{-1} \left(2\sqrt{k_p \frac{1-\mu}{m}} \right) \right)^2 \right\} \\ \cap & \left\{ s \in \mathcal{D}_s : W_2(s) < \lambda_2 \left(\rho_1^{-1} \left(2\sqrt{k_{d,1} \frac{1-\mu}{3}} \right) \right)^2 \right\} \\ \cap & \left\{ s \in \mathcal{D}_s : W_2(s) < \lambda_2 \left(\rho_2^{-1} \left(2\sqrt{k_{d,2} \frac{1-\mu}{3}} \right) \right)^2 \right\}.\end{aligned} \tag{4.112}$$

A direct application of Theorem 8.4 in Khalil (2002) can be used to prove that $\|z(t)\| \rightarrow 0$ as $t \rightarrow +\infty \ \forall s(t_0) \in \mathcal{S}$. Based on the definition of $z(t)$, it is easy to show that $\|e_1(t)\|, \|e_2(t)\|, \|r(t)\| \rightarrow 0$ as $t \rightarrow +\infty \ \forall s(t_0) \in \mathcal{S}$. Note that the region of attraction can be made arbitrarily large to include any initial conditions by choosing the controller gains k_p, $k_{d,1}$ and $k_{d,2}$. This fact implies that the stability result obtained by the proposed method is semi–global.

4.7. Conclusions

At the beginning of this chapter, system models and model properties of dynamically positioned surface vessel, small–scaled unmanned helicopter and unactuated surface vessel manipulated by 6 uni–directional tugboats were introduced.

Then, novel robust controllers were proposed by utilizing the general control design in Chapter 2 to ensure the position and orientation control of dynamically positioned surface vessel and unactuated surface vessel manipulated by 6 uni–directional tugboat under the influence of added mass effects, and the attitude control of small–scaled unmanned helicopter after transforming the dynamic models of these mechatronic systems into second order systems with an uncertain non–symmetric input gain matrix.

CHAPTER 5

NUMERICAL RESULTS

In this chapter, effectiveness of the designed robust controllers are demonstrated via simulation and experimental studies. During these studies, the proposed self–tuning method was utilized to adjust the control gains. Before presenting the numerical results some important aspects of these studies are stated as:

- Simulation studies were performed to examine the performance of the designed controller in Chapter 2 and the self–tuning method Chapter 3. In Section 5.1.1, a modified version of a model of a two–link robot manipulator with coupling between the two links was utilized. Obtaining a model that is compatible with the general system model that was utilized for the control design is the main purpose of this modification.

- Simulations were performed for three different scenarios:

  - In section 5.1.1.1, the performance of the designed controller in Chapter 2 was examined for desired trajectories that were selected as sinusoidal trajectories with frequency values of 0.1, 0.5 and 1 rad/sec. The convergence performance, effects of selection of different constant parts of the time–varying control gains, and the final values of the time–varying gains were examined.
  - Next, in Section 5.1.1.2 the performance of the designed controller in Chapter 2 was examined for sinusoidal desired trajectories with frequency values higher than 5 rad/sec. Since trajectories with frequency values higher than 5 rad/sec are fast varying, they are harder to follow and this is a more challenging task.
  - Finally, in Section 5.1.1.3 adaptation performance of the proposed self–tuning method were examined for two different scenarios. First, the desired trajectory was selected as a sinusoidal desired trajectory that contains different frequency components and then it was selected as a combination of sinusoidal and step desired trajectories. In addition to these, an additive sinusoidal disturbance with the amplitude value of 0.025 and frequency value of 10 rad/sec was applied to the outputs for these simulations to see the robustness of the designed controller against an additive disturbance.

- Experiments were also performed to demonstrate the performance of the designed controller in Chapter 2. These results are presented in Section 5.1.2 in a detailed manner.

- Integral of the square of the norm of the tracking error $\int_{t_0}^{t} \|e_1(\sigma)\|^2 d\sigma$ and the control input $\int_{t_0}^{t} \|\tau(\sigma)\|^2 d\sigma$ were observed and recorded as performance measures. These values are demonstrated in the related tables.

- Simulations of mechatronic systems are presented in the following sections of this chapter. Simulations were performed for dynamically positioned surface vessel, small–scaled unmanned helicopter and unactuated surface vessel manipulated by 6 uni–directional tugboats in Sections 5.2, 5.3 and 5.4, respectively. In these sections, first the system models are introduced which are followed by numerical results.

- For all simulation and experimental studies, figures of actual and desired trajectories and the tracking errors are given to clarify the tracking results. Required control efforts are clarified via figures of control inputs.

- In the cases that the proposed self–tuning method is utilized for adjusting the control gains, figures of the diagonal entries of the time–varying gain matrices denoted by $\hat{\beta}_{11}$ and $\hat{\beta}_{22}$ for $\hat{\beta}(t)$ and k_{11} and k_{22} for $K(t)$ are given to show their change and constant final values.

5.1. Robotic Systems

In this section, the performances of the designed controller in Chapter 2 and proposed self–tuning method in Chapter 3 are tested on modified robotic systems in simulation and experimental studies. For simulation studies, modified model of a robot manipulator is utilized. Experimental studies are realized by using a robot manipulator that is under the influence of a multiplicative input disturbance. Obtaining a structure that is compatible with (1.2) is the main purpose of these modifications and they are explained in Sections 5.1.1 and 5.1.2. In these studies, different scenarios are considered to examine the performance of the designed controller in Chapter 2 and the self–tuning method in Chapter 3 in a more detailed manner.

5.1.1. Simulation Studies

Similar to Chen et al. (2008), the performance of the proposed controller has been tested on a modified version of the model of a two–link robot manipulator with coupling between the two links Slotine and Li (1991). The equations of motion are given as Chen et al. (2008)

$$\begin{bmatrix} \ddot{q}_1 \\ \ddot{q}_2 \end{bmatrix} = \begin{bmatrix} M_{11} & M_{12} \\ M_{12} & M_{22} \end{bmatrix}^{-1} \begin{bmatrix} -b\dot{q}_2 & -b\left(\dot{q}_1 + \dot{q}_2\right) \\ -b\dot{q}_1 & 0 \end{bmatrix} \begin{bmatrix} \dot{q}_1 \\ \dot{q}_2 \end{bmatrix} + \begin{bmatrix} M_{11} & M_{12} \\ M_{12} & M_{22} \end{bmatrix}^{-1} \begin{bmatrix} 1 & 1 \\ 0 & 1 \end{bmatrix} \begin{bmatrix} \tau_1 \\ \tau_2 \end{bmatrix} \tag{5.1}$$

where $q_1(t)$, $q_2(t) \in \mathbb{R}$ denote the positions, $\tau_1(t)$ and $\tau_2(t)$ are the control inputs and M_{11}, M_{12}, M_{22} and b are explicitly defined as

$$M_{11} = a_1 + 2a_3 \cos q_2 + 2a_4 \sin q_2 + a_5\left(\cos \dot{q}_2 + \sin \dot{q}_2\right) + a_6\left(\cos q_1 + \sin q_1\right) \tag{5.2}$$

$$M_{12} = a_2 + a_3 \cos q_2 + a_4 \sin q_2 \tag{5.3}$$

$$M_{22} = a_2 + a_7\left(\cos \dot{q}_1 + \sin \dot{q}_1\right) \tag{5.4}$$

$$b = a_3 \sin q_2 - a_4 \sin q_2. \tag{5.5}$$

where $a_1 = 4.42kgm^2$, $a_2 = 0.97kgm^2$, $a_3 = 1.04kgm^2$, $a_4 = 0.6kgm^2$, $a_5 = 0.25kgm^2$, $a_6 = 0.2kgm^2$ and $a_7 = 0.5kgm^2$.

The tracking control objective is to make $q_1(t)$ and $q_2(t)$ follow a desired trajectory chosen as

$$q_r(t) = \left(1 - \exp(-0.3t^3)\right) \begin{bmatrix} \frac{\pi}{6} \sin\left(\omega_r t\right) \\ \frac{\pi}{4} \sin\left(\omega_r t\right) \end{bmatrix} \text{(rad)} \tag{5.6}$$

where $\omega_r \in \mathbb{R}$ denotes the frequency of the desired trajectory. During all simulation studies, the constant gain α was chosen as $\alpha = I_2$ for a better comparison.

5.1.1.1. Tracking Results for Sinusoidal Desired Trajectories with Frequency Values of 0.1, 0.5 and 1 rad/sec

For this part of the simulation studies, ω_r was selected as 0.1, 0.5 and 1 rad/sec. Control performances were examined for different values of constant parts of control gains (*i.e.*, k_c in (3.15) and β_2 in (3.16)).

Simulation results for $\omega_r = 0.1$ rad/sec can be seen in Figures 5.1–5.5. For the results given in these figures, the constant parts of the control gains were selected as $\beta_2 = k_c = 10^{-6} I_2$. For these selections, actual and desired positions are shown in Figure 5.1, while the tracking errors are given in Figure 5.2. From these figures, it is seen that the tracking control objective was met. Control inputs are shown in Figure 5.3. In addition to these, entries of the time–varying gain matrices $\hat{\beta}(t)$ and $K(t)$ are shown in Figures 5.4 and 5.5, respectively. From these figures, it can be seen that time–varying control gains converged to the constant final values that were obtained as $K_\infty = \text{diag}\{1.018, 1.005\}$ and $\hat{\beta}_\infty = \text{diag}\{0.2415, 0.0373\}$.

Numerical simulations were then performed by selecting the constant parts of the control gains as $\beta_2 = k_c = 10^{-3} I_2$. In these simulations, while meeting the tracking control objective, it was observed that control gains converged approximately to same constant final values. Then, simulation was performed without using self–tuning method where constant final values of the control gains were utilized and the tracking control objective was also met.

Finally, simulation studies were performed by selecting the constant parts of the time–varying gain matrices as $k_c = 0.1 I_2$ and $\beta_2 = \text{diag}\{0.75, 0.5\}$. In these simulations, while the tracking control objective was met control gains converged to higher constant final values as a result of increasing their constant parts.

All of these results are summarized in Tables 5.1, 5.2 and 5.3. In the first and second columns of Table 5.1, constant parts of the time–varying gains are given while the constant final values they converged to are given in the third and fourth columns. Integral of the square of the norm of the tracking error and the control input measures are shown in the third and fourth columns of Table 5.2. Performance measures that were obtained by using constant control gains are given in Table 5.3.

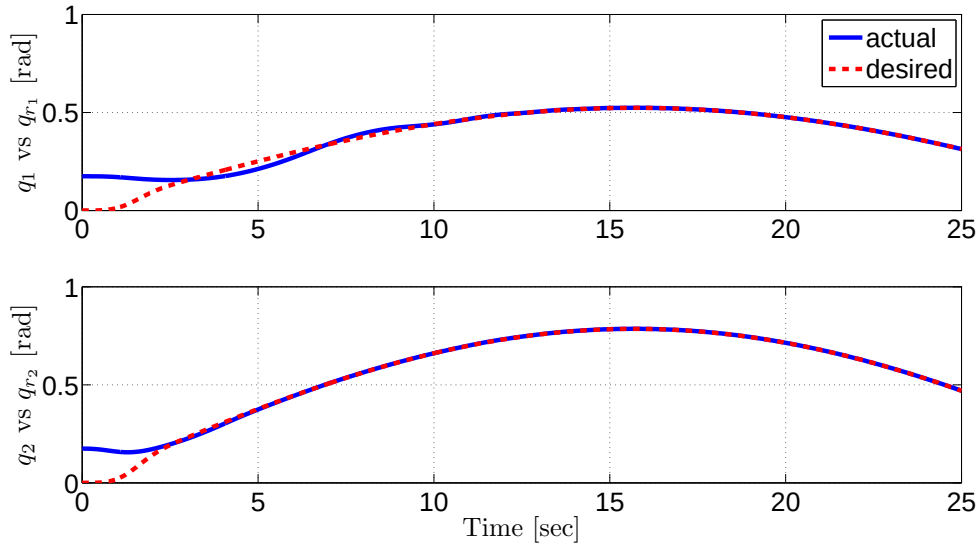

Figure 5.1. Positions for $\omega_r = 0.1$ rad/sec and for $\beta_2 = k_c = 10^{-6} I_2$

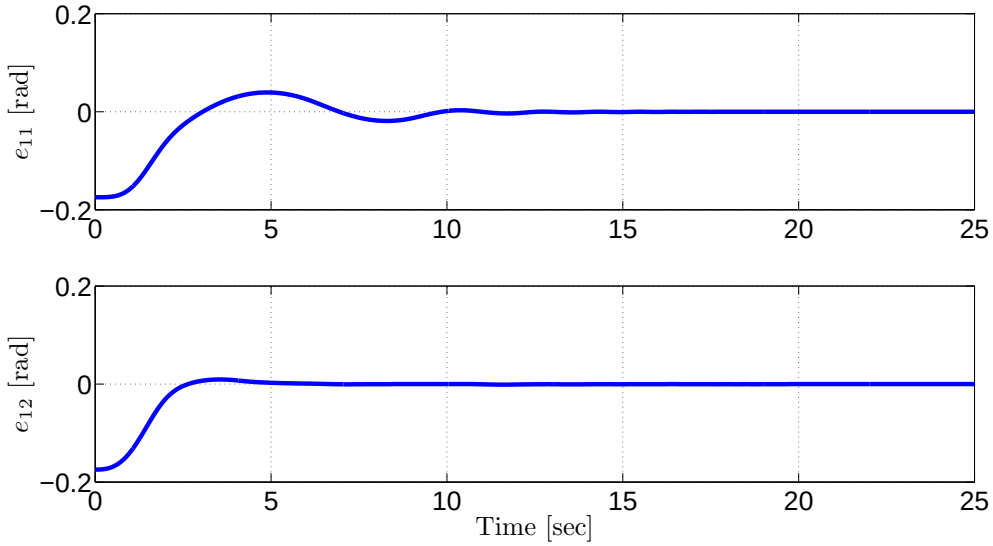

Figure 5.2. Tracking errors for $\omega_r = 0.1$ rad/sec and for $\beta_2 = k_c = 10^{-6} I_2$

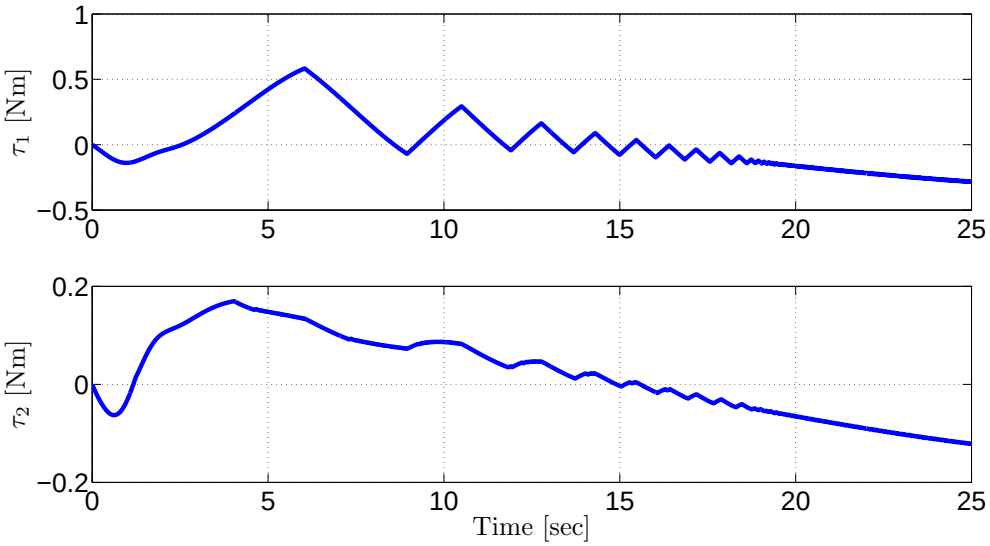

Figure 5.3. Control inputs for $\omega_r = 0.1$ rad/sec and for $\beta_2 = k_c = 10^{-6} I_2$

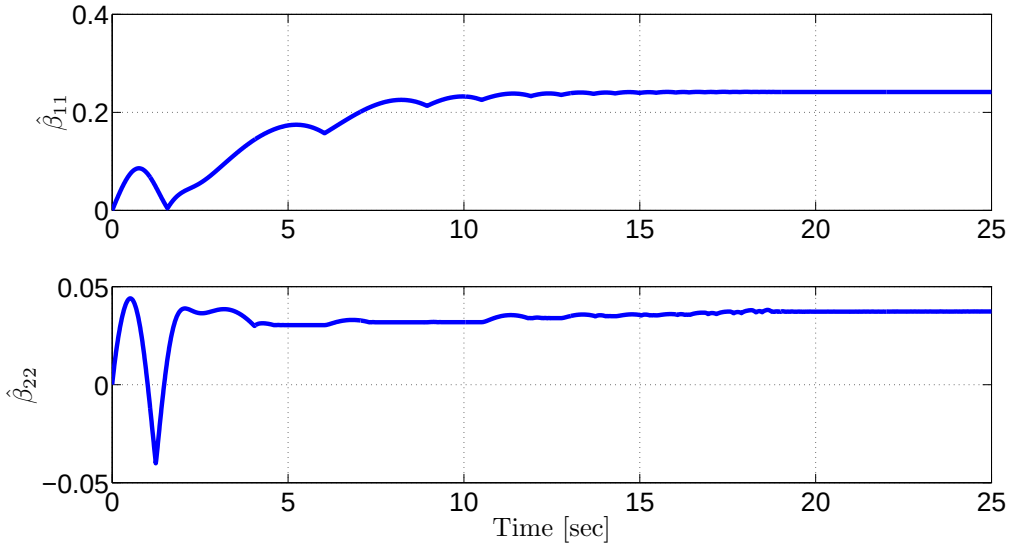

Figure 5.4. Entries of the time–varying gain matrix $\hat{\beta}(t)$ for $\omega_r = 0.1$ rad/sec and for $\beta_2 = k_c = 10^{-6} I_2$

Table 5.1. Constant parts of time–varying control gains (1^{st} and 2^{nd} columns) and final values of control gains (3^{rd} and 4^{th} columns) for $\omega_r = 0.1$ rad/sec

k_c	β_2	K_∞	$\hat{\beta}_\infty$
$10^{-6}I_2$	$10^{-6}I_2$	diag $\{1.018, 1.005\}$	diag $\{0.2415, 0.0373\}$
$10^{-3}I_2$	$10^{-3}I_2$	diag $\{1.018, 1.005\}$	diag $\{0.2415, 0.0373\}$
$0.1I_2$	diag $\{0.75, 0.5\}$	diag $\{1.121, 1.097\}$	diag $\{0.9670, 0.4520\}$

Table 5.2. Performance measures for $\omega_r = 0.1$ rad/sec with time–varying gains

k_c	β_2	$\int_{t_0}^{t} \|e_1(\sigma)\|^2 d\sigma$	$\int_{t_0}^{t} \|\tau(\sigma)\|^2 d\sigma$
$10^{-6}I_2$	$10^{-6}I_2$	0.083	1.315
$10^{-3}I_2$	$10^{-3}I_2$	0.083	1.315
$0.1I_2$	diag $\{0.75, 0.5\}$	0.063	2.598

Table 5.3. Performance measures for $\omega_r = 0.1$ rad/sec with constant gains (*i.e.*, without using self–tuning method)

K	β	$\int_{t_0}^{t} \|e_1(\sigma)\|^2 d\sigma$	$\int_{t_0}^{t} \|\tau(\sigma)\|^2 d\sigma$
diag $\{1.018, 1.005\}$	diag $\{0.2415, 0.0373\}$	0.103	1.312

Simulation results for $\omega_r = 0.5$ rad/sec can be seen in Figures 5.6–5.10. For the results given in these figures, the constant parts of the control gains were selected as $\beta_2 = k_c = 10^{-3}I_2$. For these selections, actual and desired positions are shown in Figure 5.6, while the tracking errors are given in Figure 5.7. From these figures, it is seen that the tracking control objective was met. Control inputs are shown in Figure 5.8. In addition to these, entries of the time–varying gain matrices $\hat{\beta}(t)$ and $K(t)$ are shown in Figures 5.9 and 5.10, respectively. From these figures, it can be seen that, time–varying control gains converged to the constant final values that were obtained as $K_\infty = \text{diag}\{1.63, 1.21\}$ and $\hat{\beta}_\infty = \text{diag}\{2.13, 0.585\}$.

Numerical simulations were then performed by selecting the constant parts of the control gains as $\beta_2 = k_c = 0.1I_2$. In these simulations, while meeting the tracking control objective, it was observed that control gains converged approximately to same constant final values. Then, simulation was performed without using self–tuning method where

constant final values of the control gains were utilized and the tracking control objective was met.

Finally, simulation studies were performed by selecting the constant parts of the time–varying gain matrices as $k_c = \text{diag}\{1.2, 0.5\}$ and $\beta_2 = \text{diag}\{3.25, 1.25\}$. In these simulations, while the tracking control objective was met control gains converged to higher constant final values as a result of increasing their constant parts.

All of these results are summarized in Tables 5.4, 5.5 and 5.6. In the first and second columns of Table 5.4, constant parts of the time–varying gains are given while the constant final values they converged to are given in the third and fourth columns. Integral of the square of the norm of the tracking error and the control input measures are shown in the third and fourth columns of Table 5.5. Performance measures that were obtained by using constant control gains are given in Table 5.6.

Table 5.4. Constant parts of time–varying control gains (1^{st} and 2^{nd} columns) and final values of control gains (3^{rd} and 4^{th} columns) for $\omega_r = 0.5$ rad/sec

k_c	β_2	K_∞	$\hat{\beta}_\infty$
$10^{-3} I_2$	$10^{-3} I_2$	diag $\{1.589, 1.129\}$	diag $\{2.190, 0.555\}$
$0.1 I_2$	$0.1 I_2$	diag $\{1.630, 1.210\}$	diag $\{2.130, 0.585\}$
diag $\{1.2, 0.5\}$	diag $\{3.25, 1.25\}$	diag $\{2.472, 1.525\}$	diag $\{4.204, 1.391\}$

Table 5.5. Performance measures for $\omega_r = 0.5$ rad/sec with time–varying gains

k_c	β_2	$\int_{t_0}^{t} \|e_1(\sigma)\|^2 d\sigma$	$\int_{t_0}^{t} \|\tau(\sigma)\|^2 d\sigma$
$10^{-3} I_2$	$10^{-3} I_2$	0.388	81.09
$0.1 I_2$	$0.1 I_2$	0.340	79.16
diag $\{1.2, 0.5\}$	diag $\{3.25, 1.25\}$	0.111	83.06

Simulation results for $\omega_r = 1$ rad/sec can be seen in Figures 5.11–5.15. For the results given in these figures, the constant parts of the control gains were selected as $\beta_2 = k_c = 0.1 I_2$. For these selections, actual and desired positions are shown in Figure 5.11, while the tracking errors are given in Figure 5.12. From these figures, it

Table 5.6. Performance measures for $\omega_r = 0.5$ rad/sec with constant gains (*i.e.*, without using self–tuning method)

K	β	$\int_{t_0}^{t} \|e_1(\sigma)\|^2 d\sigma$	$\int_{t_0}^{t} \|\tau(\sigma)\|^2 d\sigma$
diag $\{1.63, 1.21\}$	diag $\{2.13, 0.585\}$	0.252	79.62

is seen that the tracking control objective was met. Control inputs are shown in Figure 5.13. In addition to these, entries of the time–varying gain matrices $\hat{\beta}(t)$ and $K(t)$ are shown in Figures 5.14 and 5.15, respectively. From these figures, it can be seen that, time–varying control gains converged to the constant final values that were obtained as $K_\infty = \text{diag}\{4.868, 1.672\}$ and $\hat{\beta}_\infty = \text{diag}\{6.535, 1.876\}$.

Numerical simulations were then performed by selecting the constant parts of the control gains as $\beta_2 = k_c = 0.5 I_2$. In these simulations, while meeting the tracking control objective, it was observed that control gains converged approximately to same constant final values. Then, simulation was performed without using self–tuning method where constant final values of the control gains were utilized and the control objective was met.

Finally, simulation studies were performed by selecting the constant parts of the time–varying gain matrices as $k_c = \text{diag}\{4.881, 1.873\}$ and $\beta_2 = \text{diag}\{6.512, 1.855\}$. In these simulations, while the tracking control objective was met control gains converged to higher constant final values as a result of increasing their constant parts.

All of these results are summarized in Tables 5.7, 5.8 and 5.9. In the first and second columns of Table 5.7, constant parts of the time–varying gains are given while the constant final values they converged to are given in the third and fourth columns. Integral of the square of the norm of the tracking error and the control input measures are shown in the third and fourth columns of Table 5.8. Performance measures that were obtained by using constant control gains are given in Table 5.9.

Results can be summarized as:

- For the selections of the constant parts of time–varying control gains $k_c < 1$ and $\beta_2 < 1$, time–varying gains converged approximately to same constant values. The final constant values of time–varying control gains increase when their constant parts increase. This situation may yield to an increased control effort.

- For $\omega_r \leq 1$, control objective was met by using constant final values of the con-

Table 5.7. Constant parts of time–varying control gains (1st and 2nd columns) and final values of control gains (3rd and 4th columns) for $\omega_r = 1$ rad/sec

k_c	β_2	K_∞	$\hat{\beta}_\infty$
$0.1I_2$	$0.1I_2$	diag $\{4.868, 1.672\}$	diag $\{6.535, 1.876\}$
$0.5I_2$	$0.5I_2$	diag $\{4.881, 1.873\}$	diag $\{6.512, 1.855\}$
diag $\{6.5, 1.5\}$	diag $\{10, 5\}$	diag $\{7.816, 2.489\}$	diag $\{10.87, 4.897\}$

Table 5.8. Performance measures for $\omega_r = 1$ rad/sec with time–varying gains

k_c	β_2	$\int_{t_0}^{t} \|e_1(\sigma)\|^2 d\sigma$	$\int_{t_0}^{t} \|\tau(\sigma)\|^2 d\sigma$
$0.1I_2$	$0.1I_2$	1.763	552.4
$0.5I_2$	$0.5I_2$	1.524	556.8
diag $\{6.5, 1.5\}$	diag $\{10, 5\}$	0.128	433.0

trol gains as constant control gains (*i.e.*, not utilizing the self–tuning method). This situation can be considered as the demonstration of switch off and switch on mechanism of the proposed self–tuning method. It means that, the self–tuning method can be switched off when the control objective is met. Then, if the desired trajectory or other conditions change during the control process it can be switched on again to self tune the control gains. This situation may be useful for experimental studies to avoid unnecessarily high control gains.

- Since the tracking error converges to zero faster, tracking performance improves while the constant parts of the time–varying gains are increased. However, high control gains may cause high control performances that can not be provided by the actuators.

Table 5.9. Performance measures for $\omega_r = 1$ rad/sec with constant gains (*i.e.*, without using self–tuning method)

K	β	$\int_{t_0}^{t} \|e_1(\sigma)\|^2 d\sigma$	$\int_{t_0}^{t} \|\tau(\sigma)\|^2 d\sigma$
diag $\{4.881, 1.873\}$	diag $\{6.512, 1.855\}$	0.548	502.2

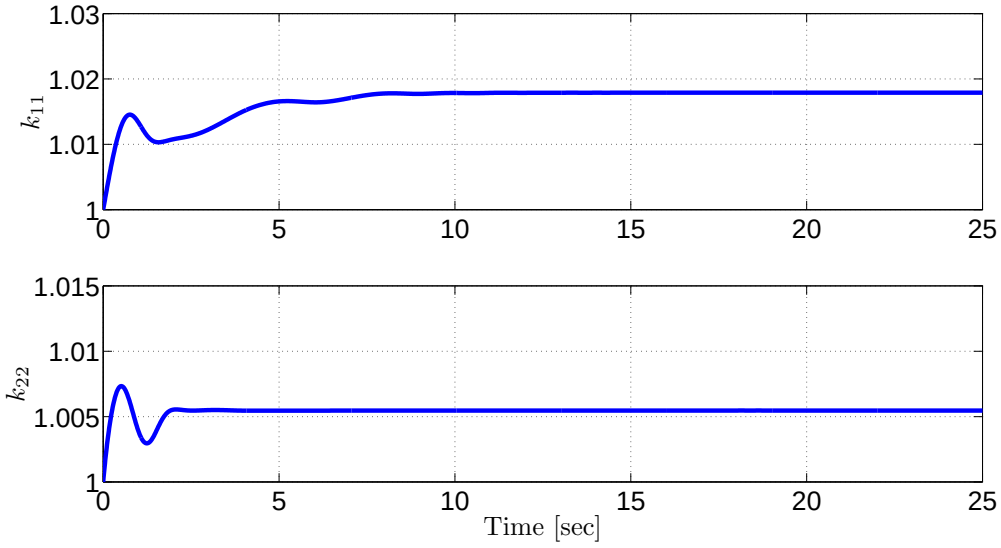

Figure 5.5. Entries of the time–varying gain matrix $K(t)$ for $\omega_r = 0.1$ rad/sec and for $\beta_2 = k_c = 10^{-6} I_2$

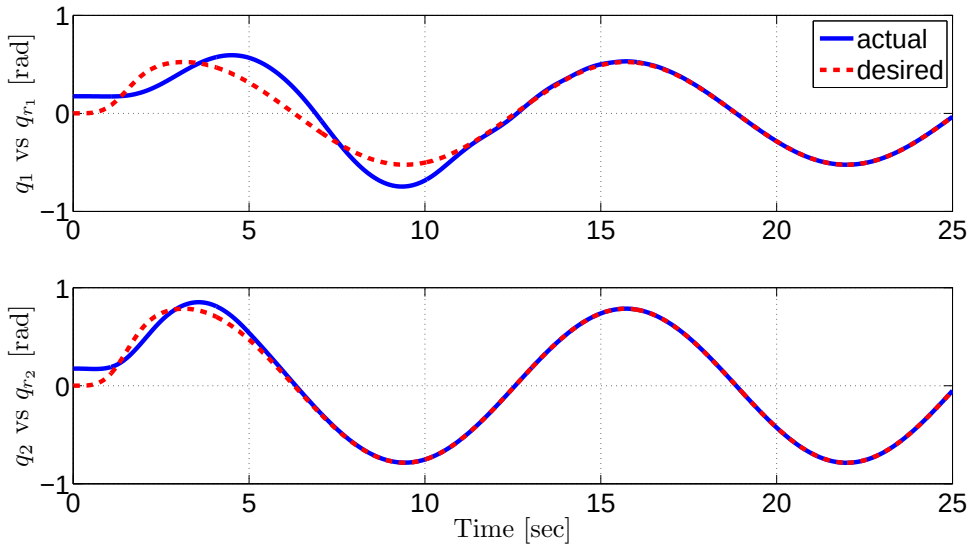

Figure 5.6. Positions for $\omega_r = 0.5$ rad/sec and for $\beta_2 = k_c = 10^{-3} I_2$

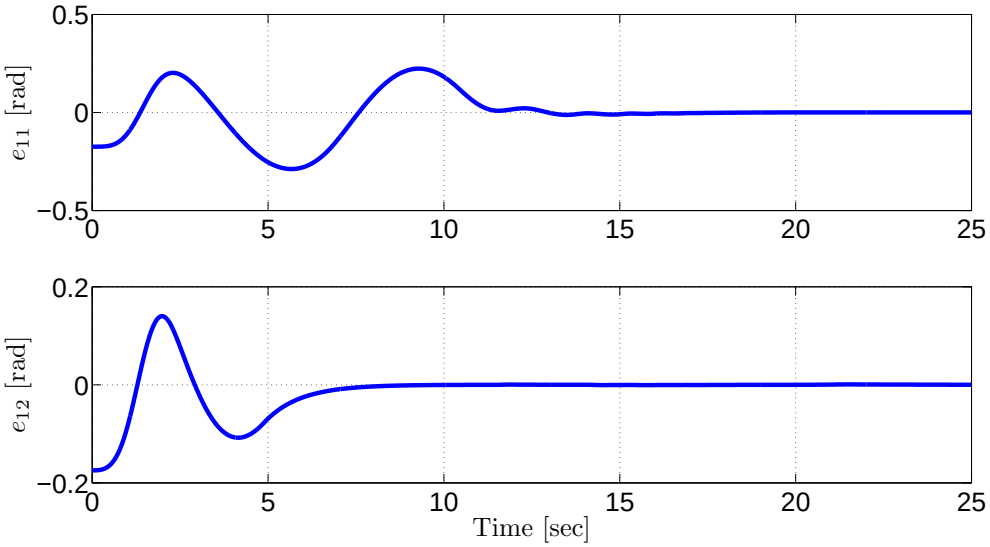

Figure 5.7. Tracking errors for $\omega_r = 0.5$ rad/sec and for $\beta_2 = k_c = 10^{-3} I_2$

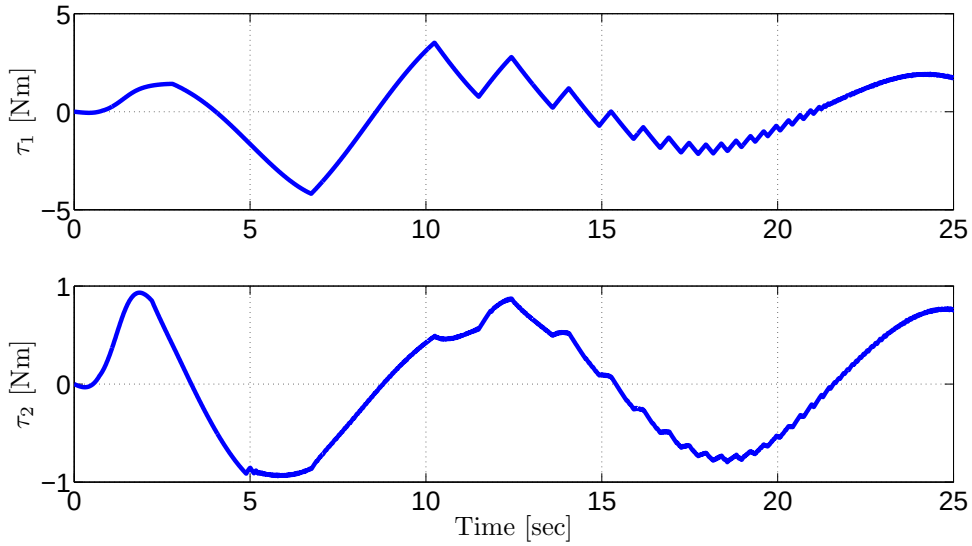

Figure 5.8. Control inputs for $\omega_r = 0.5$ rad/sec and for $\beta_2 = k_c = 10^{-3} I_2$

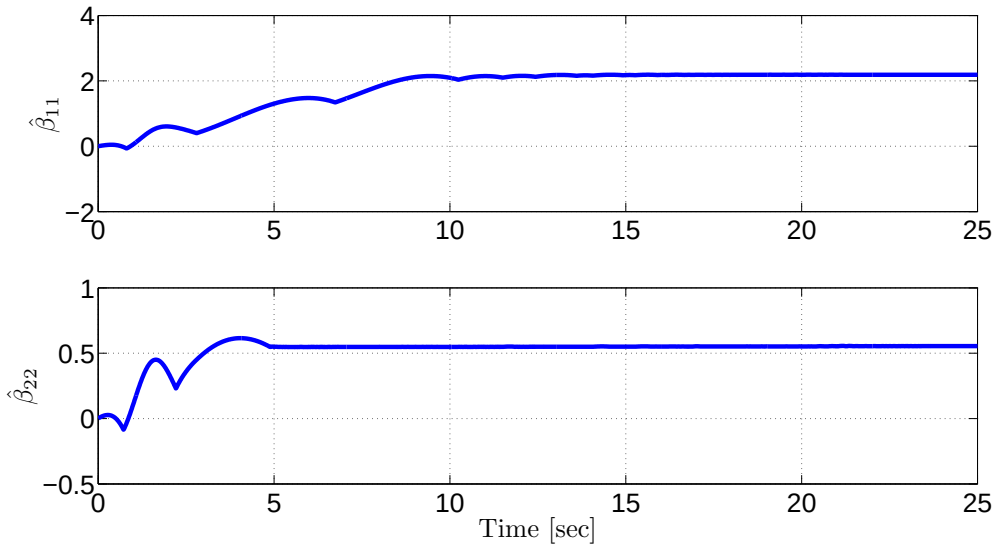

Figure 5.9. Entries of the Time–varying gain matrix $\hat{\beta}(t)$ for $\omega_r = 0.5$ rad/sec and for $\beta_2 = k_c = 10^{-3} I_2$

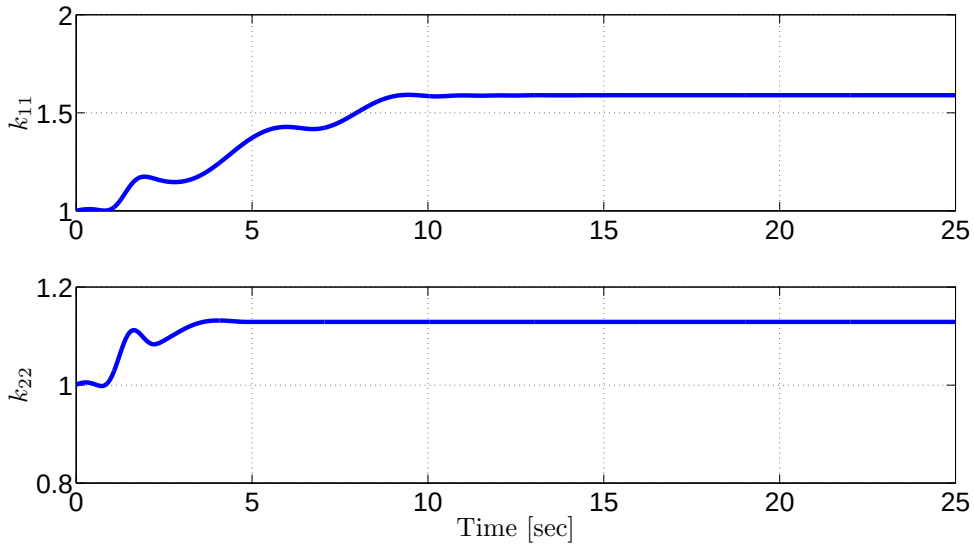

Figure 5.10. Entries of the time–varying gain matrix $K(t)$ for $\omega_r = 0.5$ rad/sec and for $\beta_2 = k_c = 10^{-3} I_2$

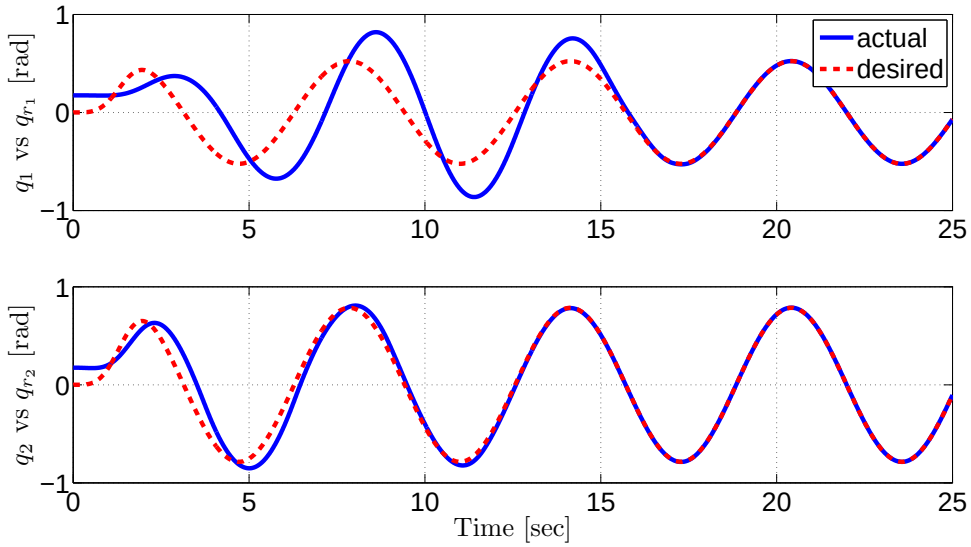

Figure 5.11. Positions for $\omega_r = 1$ rad/sec and for $\beta_2 = k_c = 0.1I_2$

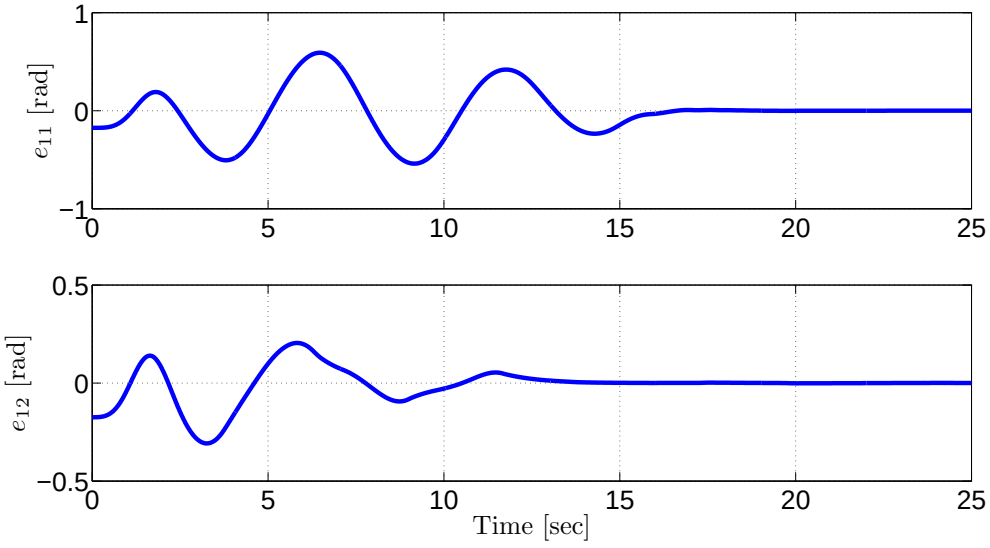

Figure 5.12. Tracking errors for $\omega_r = 1$ rad/sec and for $\beta_2 = k_c = 0.1I_2$

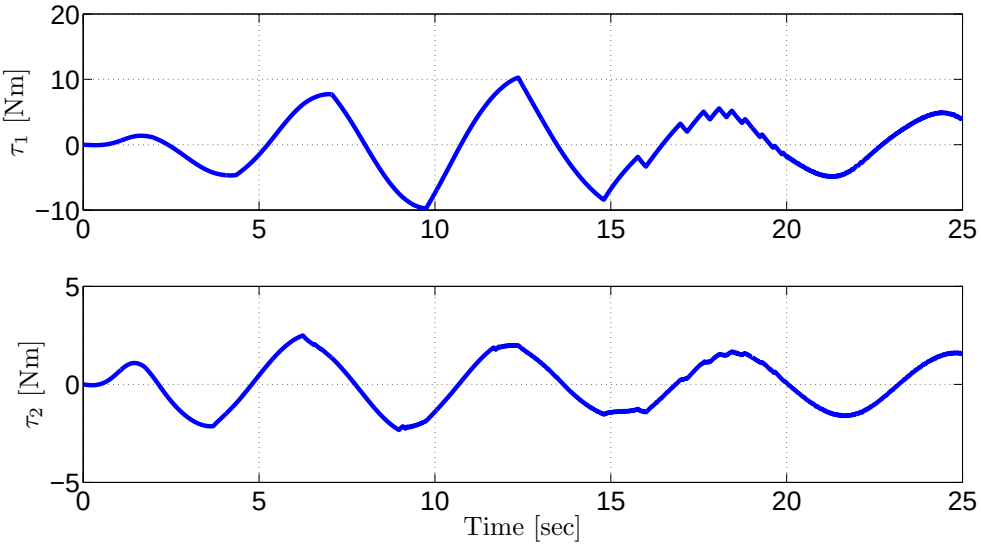

Figure 5.13. Control inputs for $\omega_r = 1$ rad/sec and for $\beta_2 = k_c = 0.1I_2$

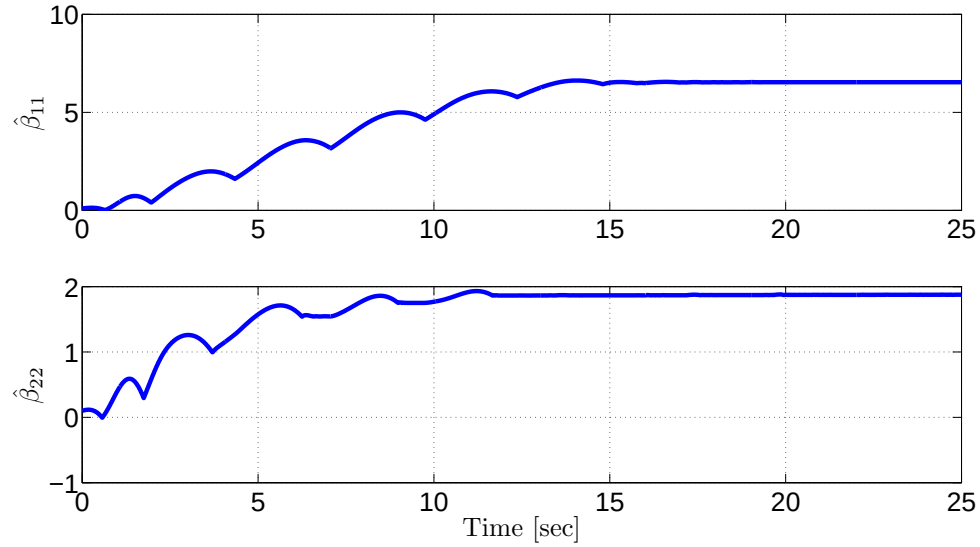

Figure 5.14. Entries of the time–varying gain matrix $\hat{\beta}(t)$ for $\omega_r = 1$ rad/sec and for $\beta_2 = k_c = 0.1I_2$

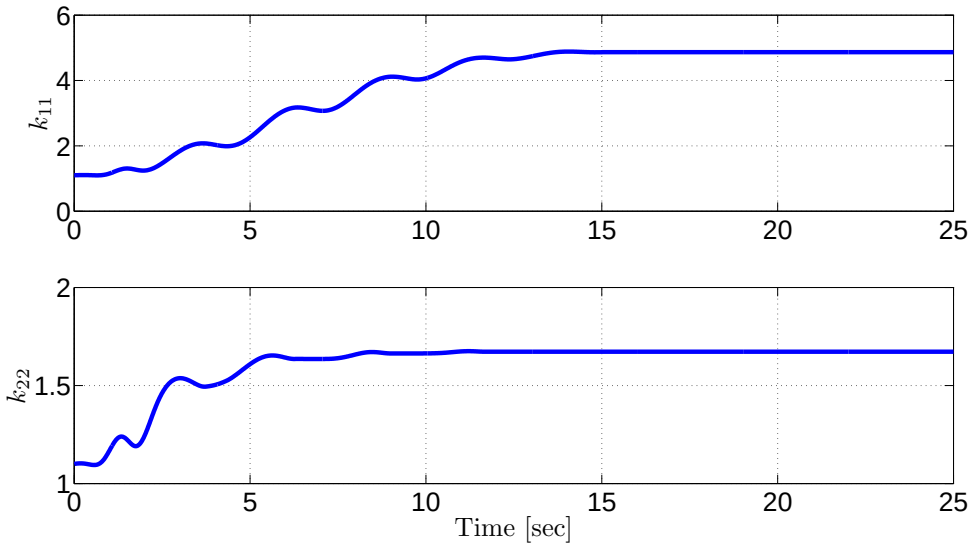

Figure 5.15. Entries of the time–varying gain matrix $K(t)$ for $\omega_r = 1$ rad/sec and for $\beta_2 = k_c = 0.1 I_2$

5.1.1.2. Tracking Results for Sinusoidal Desired Trajectories with Frequency Values Higher Than 5 rad/sec

For this part of the simulation studies, frequency values of the desired trajectory ω_r were selected higher than 5 rad/sec. During these simulations studies, it was observed that sinusoidal desired trajectories with frequency values higher than 5 rad/sec are harder–to–track. Demonstrating the performance of the controller in Chapter 2 for more challenging tasks (*i.e.*, fast varying desired trajectories) is the main purpose of this selection.

As theoretically proven in Chapter 2, tracking errors converge to zero. However, higher control efforts are required for harder–to–track desired trajectories and these control efforts can be provided by selecting higher control gains. Results are examined for different frequency values. Before presenting these results, another observation about these simulation studies is mentioned. During the simulation studies it was observed that given simulation system needs high positive constant parts of the time–varying control gains to meet the tracking control objective in the case of using the proposed self–tuning method. Otherwise, control gains reach to mentioned higher values in a long time and as a natural result of this tracking errors converge to zero in a long duration. This situation is a useless aspect for the control process. However, when the positive constant parts of the time–varying control gains are adjusted to high values, the tracking control objective is met in a very short time and little deviations are observed in the time–varying control gains. Thus self–tuning method does not provide much advantage to the overall control process. As a result of this observation, control gains were selected as constant control gains (*i.e.*, without using the proposed self–tuning method) for this part of the simulation studies. It should be stated that, this situation is about the structure of the selected simulation system.

For $\omega_r = 5$ rad/sec, the tracking control objective was met by selecting constant control gains as $K = 500I_2$ and $\beta = 400I_2$ (*i.e.*, without using self–tuning method). Obtained results are shown in Figures 5.16–5.18. Actual and desired positions are shown in Figure 5.16, while the tracking errors are given in Figures 5.17. From these figures, it is seen that the tracking control objective was met. Control inputs are shown in Figure 5.18.

Simulations were also performed for higher frequency values (*i.e.*, 5, 10, 50, 100,

500, 1000 rad/sec) and the results are presented in Tables 5.10 and 5.11. In the second and third columns of Table 5.10, control gains for different frequency values of desired trajectory are given. Integral of the square of the norm of tracking error and control input are shown in Table 5.11.

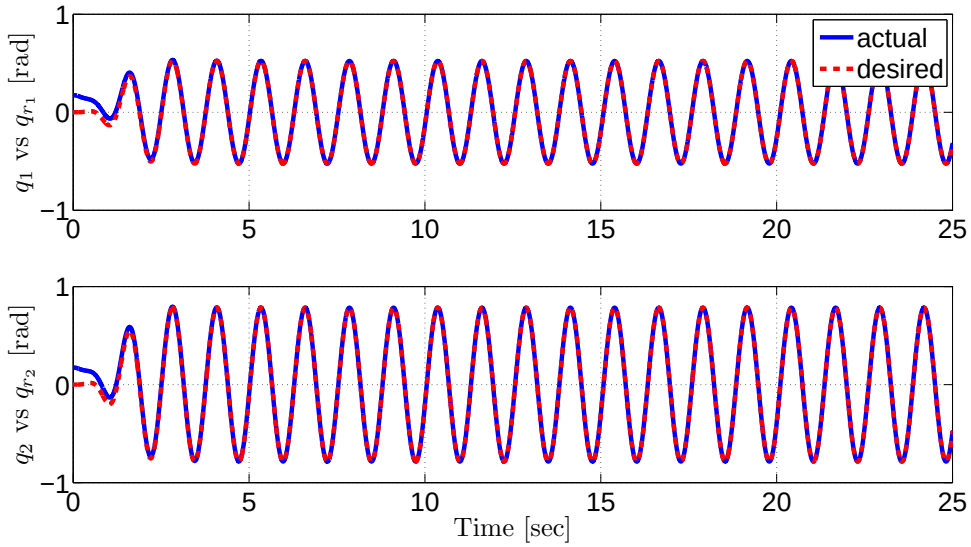

Figure 5.16. Positions for $\omega_r = 5$ rad/sec and for constant control gains $\beta = 400I_2$ and $K = 500I_2$

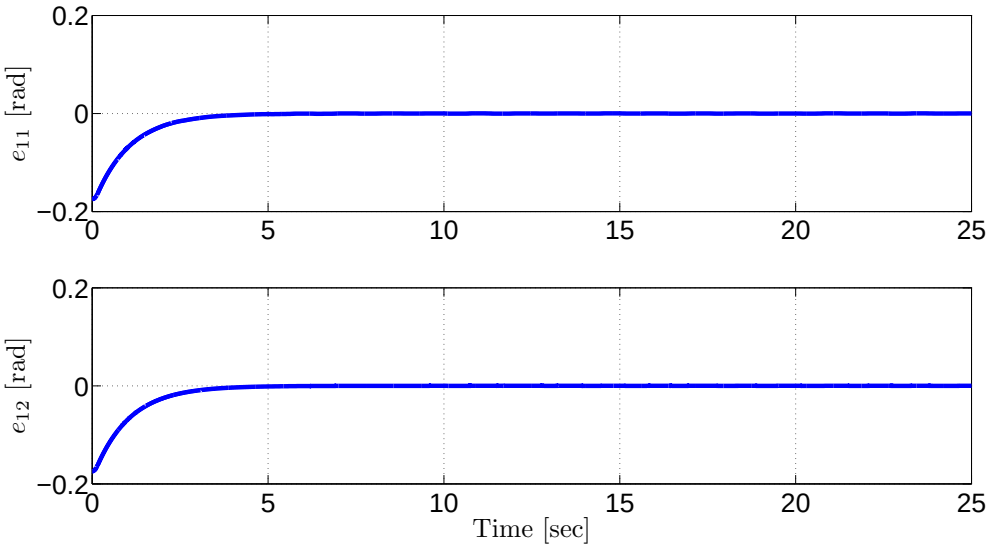

Figure 5.17. Tracking errors for $\omega_r = 5$ rad/sec and for constant control gains $\beta = 400I_2$ and $K = 500I_2$

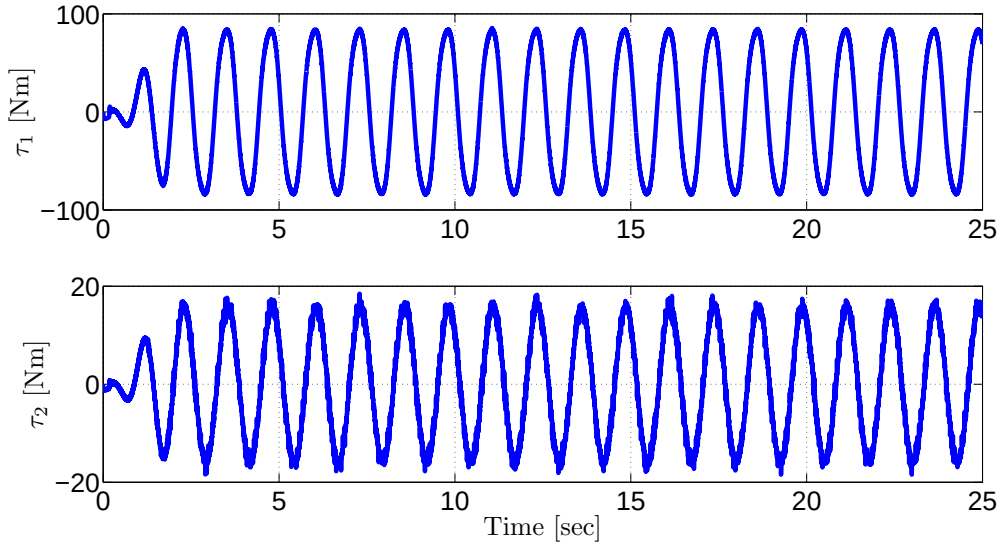

Figure 5.18. Control inputs for $\omega_r = 5$ rad/sec and for constant control gains $\beta = 400I_2$ and $K = 500I_2$

Table 5.10. Constant control gains for different frequencies

ω_r	K	β
5 rad/sec	$10^2 \times \text{diag}\{5,5\}$	$10^2 \times \text{diag}\{4,4\}$
10 rad/sec	$10^3 \times \text{diag}\{5,5\}$	$10^3 \times \text{diag}\{5,5\}$
50 rad/sec	$10^4 \times \text{diag}\{3,3\}$	$10^4 \times \text{diag}\{4,3\}$
100 rad/sec	$10^5 \times \text{diag}\{1,2\}$	$10^5 \times \text{diag}\{1,1\}$
500 rad/sec	$10^6 \times \text{diag}\{1,1\}$	$10^5 \times \text{diag}\{5,8\}$
1000 rad/sec	$10^6 \times \text{diag}\{1,1\}$	$10^6 \times \text{diag}\{2,1\}$

Table 5.11. Performance measures for different frequencies

ω_r	$\int_{t_0}^{t} \|e_1(\sigma)\|^2 d\sigma$	$\int_{t_0}^{t} \|tau(\sigma)\|^2 d\sigma$
5 rad/sec	0.456	9.3×10^4
10 rad/sec	0.372	1.4×10^6
50 rad/sec	0.453	9.1×10^8
100 rad/sec	0.479	9.7×10^9
500 rad/sec	0.210	3.9×10^{11}
1000 rad/sec	0.140	9.3×10^{12}

Results can be summarized as:

- From the obtained results, it can be seen that higher control efforts are required to meet the tracking control objective for frequency values $\omega_r \geq 5$, and higher control efforts can be provided by selecting higher control gains.
- To reach these control gains in a shorter duration, positive constant parts of the control gains have to be selected as high values. In the case of this selection, little deviations are observed in the time–varying control gains and this situation makes the proposed self–tuning method useless.
- The tracking control objective was met for these desired trajectories. However, in applications, high control gains will cause high control efforts that may not be provided by the system.

5.1.1.3. Adaptation Performance of the Proposed Self–Tuning Method

Two different desired trajectories are utilized to observe the adaptation performance of the proposed self–tuning method. One of them is a sinusoidal desired trajectory that contains different frequency components of the following form

$$q_r(t) = (1 - \exp(-0.3t^3)) \begin{cases} \left[\begin{array}{cc} \frac{\pi}{6}\sin(0.1t) & \frac{\pi}{4}\sin(0.1t) \end{array} \right]^T \text{(rad)}, & 0 \leq t < 20 \\ \left[\begin{array}{cc} \frac{\pi}{6}\sin(0.5t) & \frac{\pi}{4}\sin(0.5t) \end{array} \right]^T \text{(rad)}, & 20 \leq t < 40 \\ \left[\begin{array}{cc} \frac{\pi}{6}\sin(t) & \frac{\pi}{4}\sin(t) \end{array} \right]^T \text{(rad)}, & 40 \leq t < 60 \end{cases} . \tag{5.7}$$

For these results, the constant parts of the control gains were selected as $\beta_2 = k_c = I_2$ and simulations were performed after an additive sinusoidal disturbance with the amplitude value of 0.025 and the frequency value of 10 rad/sec had been applied to the output. Simulation results can be seen in Figures 5.19–5.23. Actual and desired positions are shown in Figure 5.19, while the tracking errors are given in Figure 5.20. From these figures, it is seen that the tracking control objective was met. Control inputs are shown in Figure 5.21. In addition to these, entries of the time–varying gain matrices $\hat{\beta}(t)$ and $K(t)$ are shown in Figures 5.22 and 5.23, respectively. During these simulations, time–varying control gains converged to constant final values obtained as $K_\infty = \text{diag}\{3.577, 2.169\}$ and $\hat{\beta}_\infty = \text{diag}\{5.730, 1.332\}$ and simulations were also performed by using these values as constant control gains (*i.e.*, without using self–tuning method). These results are summarized in Tables 5.12 and 5.13.

Table 5.12. Performance measures for the desired trajectory in (5.7) with time–varying control gains

k_c	β_2	$\int_{t_0}^{t} \|e_1(\sigma)\|^2 d\sigma$	$\int_{t_0}^{t} \|\tau(\sigma)\|^2 d\sigma$
I_2	I_2	2.072	298.7

Table 5.13. Performance measures for the desired trajectory in (5.7) with constant control gains (*i.e.*, without using self–tuning method)

K	β	$\int_{t_0}^{t} \|e_1(\sigma)\|^2 d\sigma$	$\int_{t_0}^{t} \|\tau(\sigma)\|^2 d\sigma$
$\text{diag}\{3.577, 2.169\}$	$\text{diag}\{5.730, 1.332\}$	1.91	321

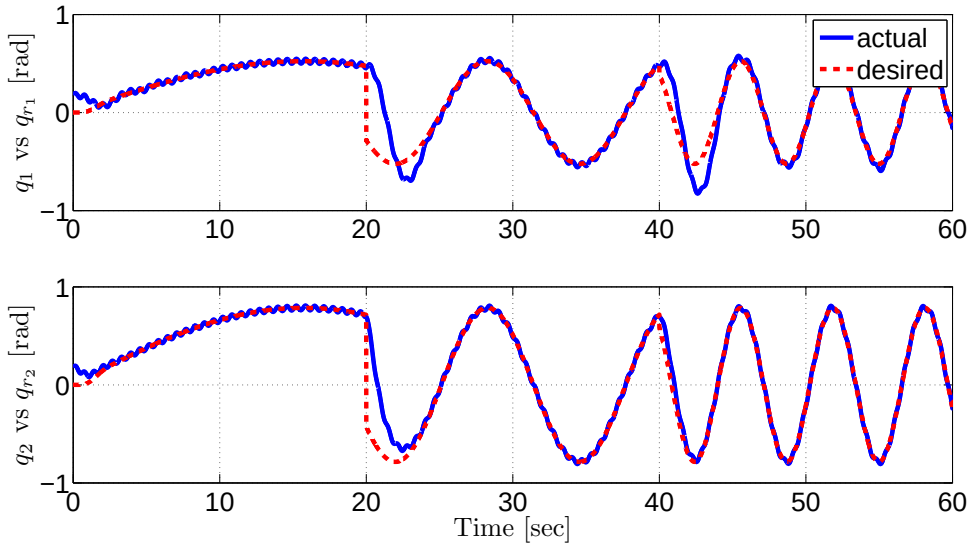

Figure 5.19. Positions for desired trajectory in (5.7) and for $\beta_2 = k_c = I_2$

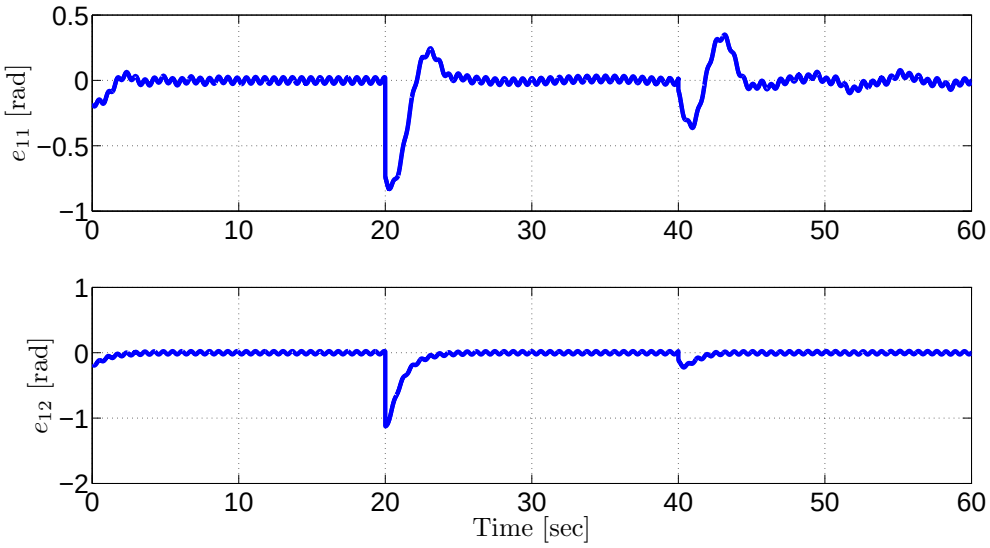

Figure 5.20. Tracking errors for desired trajectory in (5.7) and for $\beta_2 = k_c = I_2$

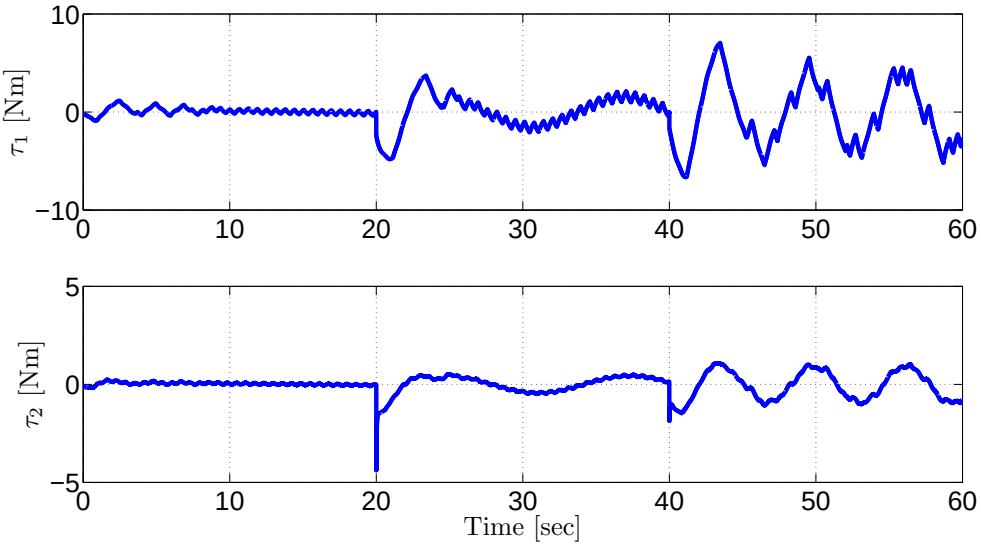

Figure 5.21. Control inputs for desired trajectory in (5.7) and for $\beta_2 = k_c = I_2$

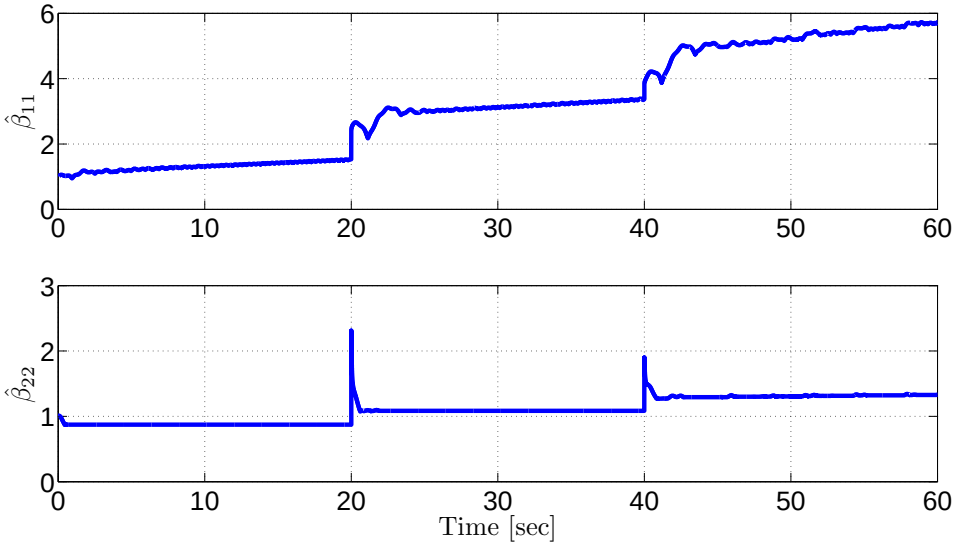

Figure 5.22. Entries of the time–varying gain matrix $\hat{\beta}(t)$ for desired trajectory in (5.7) and for $\beta_2 = k_c = I_2$

Other desired trajectory is a combination of sinusoidal and step desired trajectories and selected as

$$q_r(t) = \begin{cases} (1-\exp(-0.3t^3)) \begin{bmatrix} \frac{\pi}{6}\sin(t) & \frac{\pi}{4}\sin(t) \end{bmatrix}^T \text{(rad)}, & 0 \leq t < 30 \\ \begin{bmatrix} \frac{\pi}{6} & \frac{\pi}{4} \end{bmatrix}^T \text{(rad)}, & 30 \leq t < 60 \end{cases} . \quad (5.8)$$

For these simulations, the constant parts of the control gains were selected as $\beta_2 = k_c = I_2$ and simulations were performed after an additive sinusoidal disturbance with the amplitude value of 0.025 and the frequency value of 10 rad/sec had been applied to the output. Simulation results can be seen in Figures 5.24–5.28. Actual and desired positions are shown in Figure 5.24, while the tracking errors are given in Figure 5.25. From these figures, it is seen that the tracking control objective was met. Control inputs are shown in Figure 5.26. In addition to these, entries of the time–varying gain matrices $\hat{\beta}(t)$ and $K(t)$ are shown in Figures 5.27 and 5.28, respectively. During these simulations, time–varying control gains converged to constant values obtained as $K_\infty = \text{diag}\{4.048, 2.031\}$ and $\hat{\beta}_\infty = \text{diag}\{6.711, 1.271\}$ and simulations were also performed by using these values as constant control gains (*i.e.*, without using self–tuning method). These results are summarized in Tables 5.14 and 5.15, respectively.

Table 5.14. Performance measures for the desired trajectory in (5.8) with time–varying control gains

k_c	β_2	$\int_{t_0}^{t} \|e_1(\sigma)\|^2 d\sigma$	$\int_{t_0}^{t} \|\tau(\sigma)\|^2 d\sigma$
I_2	I_2	1.275	313.3

Table 5.15. Performance measures for the desired trajectory in (5.8) with constant control gains (*i.e.*, without using self–tuning method)

K	β	$\int_{t_0}^{t} \|e_1(\sigma)\|^2 d\sigma$	$\int_{t_0}^{t} \|\tau(\sigma)\|^2 d\sigma$
$\text{diag}\{4.048, 2.031\}$	$\text{diag}\{6.711, 1.271\}$	1.215	324.2

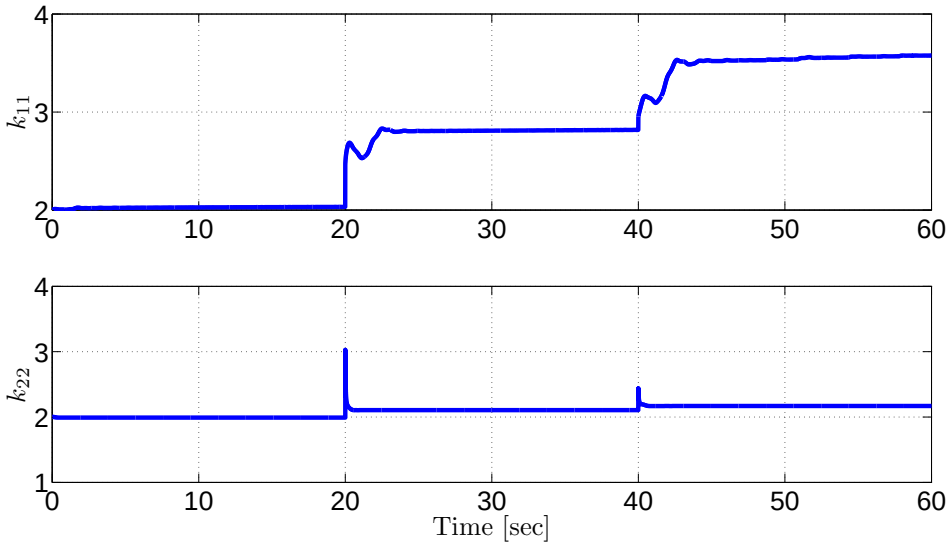

Figure 5.23. Entries of the time–varying gain matrix $K(t)$ for desired trajectory (5.7) and for $\beta_2 = k_c = I_2$

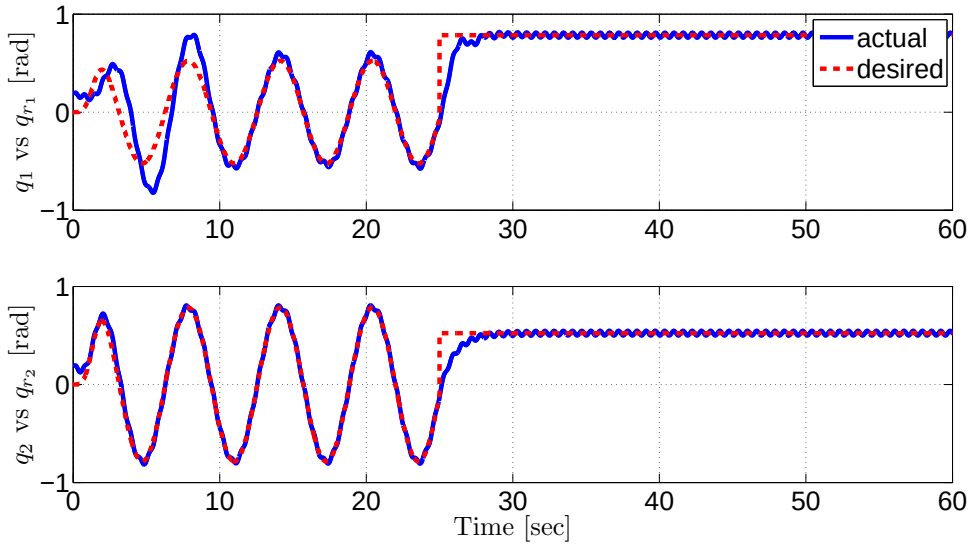

Figure 5.24. Positions for desired trajectory in (5.8) and for $\beta_2 = k_c = I_2$

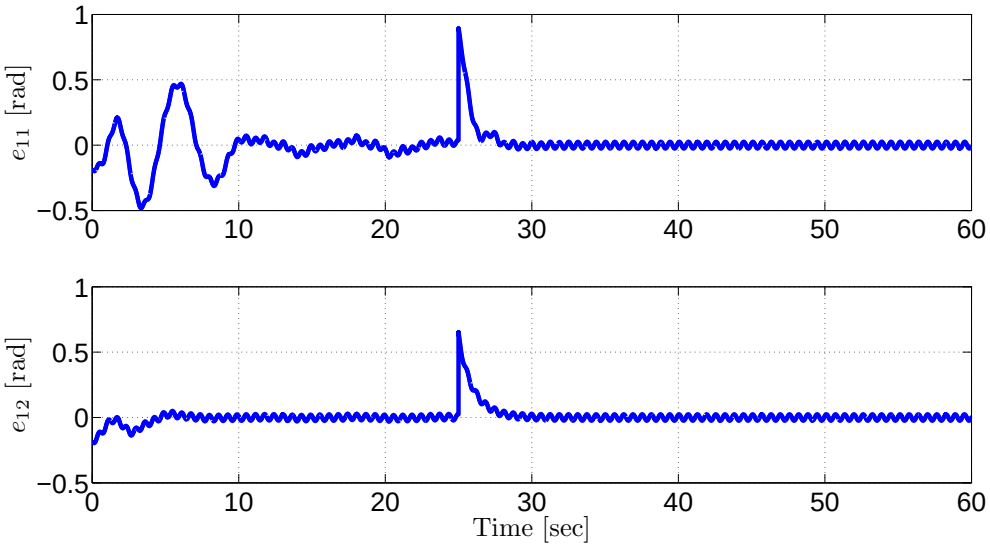

Figure 5.25. Tracking errors for desired trajectory in (5.8) and for $\beta_2 = k_c = I_2$

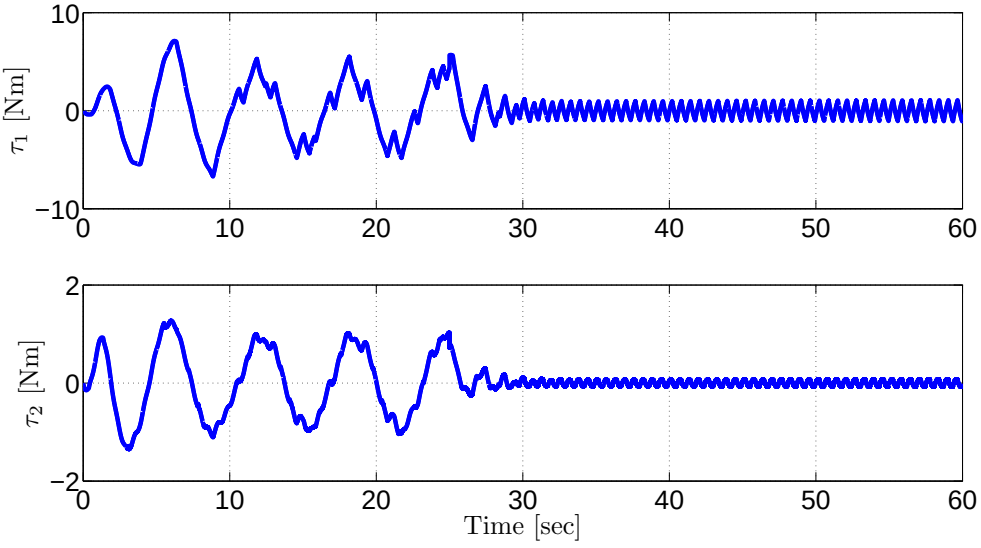

Figure 5.26. Control Inputs for desired trajectory in (5.8) and for $\beta_2 = k_c = I_2$

Results can be summarized as:

- Since the tracking gets harder for desired trajectories with higher frequency values, time varying control gains converge to higher constant values.
- Designed controller can preserve its robust behavior against an additive disturbance and can be used for meeting the tracking control objective in the presence of an additive disturbance.
- Proposed self–tuning method can easily adapt to variations in desired trajectories.

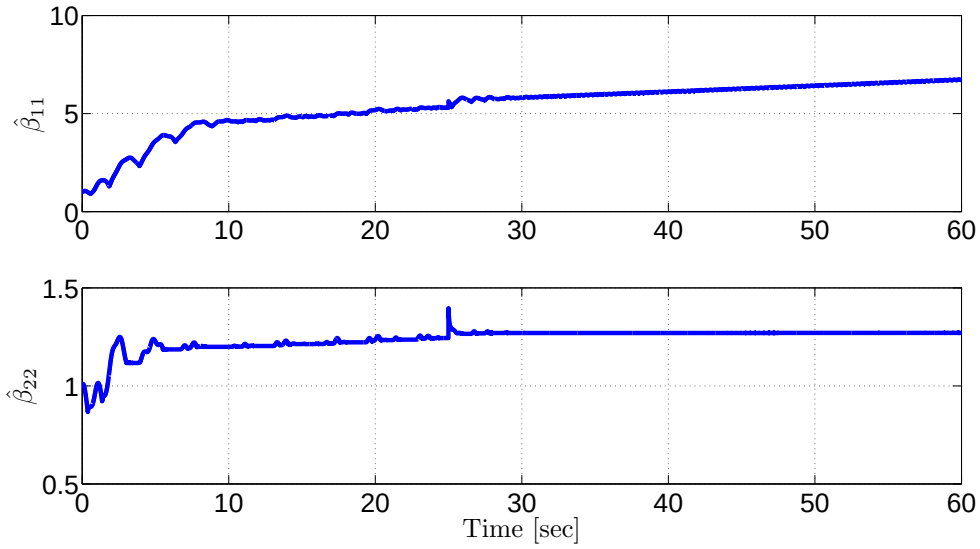

Figure 5.27. Entries of the time–varying gain matrix $\hat{\beta}(t)$ for desired trajectory in (5.8) and for $\beta_2 = k_c = I_2$

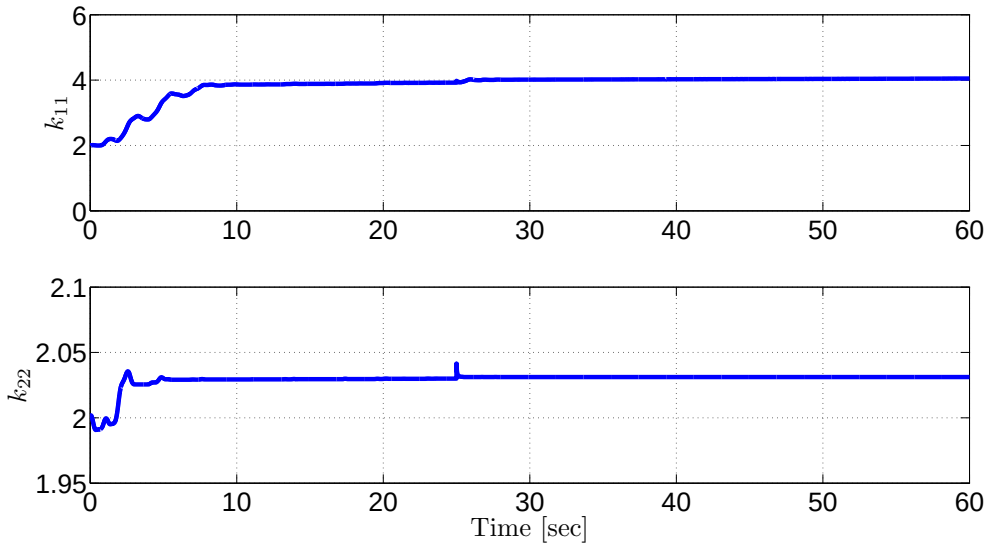

Figure 5.28. Entries of the time–varying gain matrix $K(t)$ for desired trajectory in (5.8) and for $\beta_2 = k_c = I_2$

5.1.2. Experimental Studies

During experimental studies, Phantom Omni haptic device which can be seen in Figure 5.29 was used as the experimental setup. The motion of the first link of the haptic device, labeled by θ_1 in the given figure, was mechanically stopped and the joint space control was realized for the remaining links, labeled by θ_2 and θ_3. Since, the haptic device does not have a non–symmetric behavior in its dynamics, the control input was applied to the device after multiplying it with a unity upper triangular matrix that has the following form

$$M_P = \begin{bmatrix} 1 & \gamma_p \sin(t) \\ 0 & 1 \end{bmatrix} \tag{5.9}$$

where γ_p is a positive constant. As a result of this modification, structure of the experimental setup became similar to (5.1). At this point, it should be stated that neither the structure of the model nor the matrix in (5.9) are known and they were not used during the experimental studies. The control objective is to make $\theta_2(t)$ and $\theta_3(t)$ follow a sinusoidal desired trajectory chosen as

$$\theta_r(t) = \begin{bmatrix} 0.5 + 0.1\sin(0.1t) \\ \cos(0.1t) \end{bmatrix} (\text{rad}). \tag{5.10}$$

The self–tuning method was utilized to adjust the control gains. For all experimental studies, constant parts of time–varying control gains were selected as $\beta_2 = k_c = 10^{-6} I_2$ while the other control gain was selected as $\alpha = I_2$.

Table 5.16. Final values of control gains via self–tuning strategy for different values of γ_p

γ_p	K_∞	$\hat{\beta}_\infty$
0.1	diag$\{0.1629, 0.0906\}$	diag$\{0.0013, 0.0091\}$
0.5	diag$\{0.1914, 0.0485\}$	diag$\{0.0060, 0.0011\}$
1	diag$\{0.0844, 0.0916\}$	diag$\{0.0079, 0.0096\}$
2	diag$\{0.1311, 0.0036\}$	diag$\{0.0085, 0.0093\}$

Experimental results for different values of γ_p can be seen in Figures 5.30–5.48. From these figures, it is clear that the tracking control objective was met while the time–

varying gains converged to constant final values. The constant final values of the control gains are presented in Table 5.16. Performance measures of these experimental studies are summarized in Table 5.17.

Table 5.17. Performance measures for experimental studies

γ_p	$\int_{t_0}^{t} \|e_1(\sigma)\|^2 d\sigma$	$\int_{t_0}^{t} \|\tau(\sigma)\|^2 d\sigma$
0.1	0.822	2.404
0.5	0.686	4.416
1	1.189	5.737
2	1.398	5.906

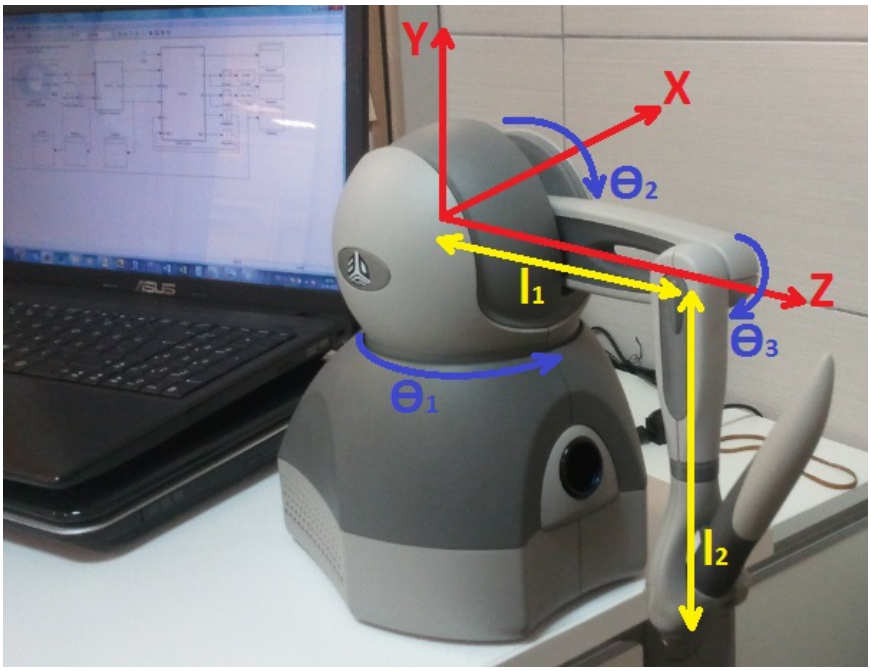

Figure 5.29. Phantom Omni haptic device

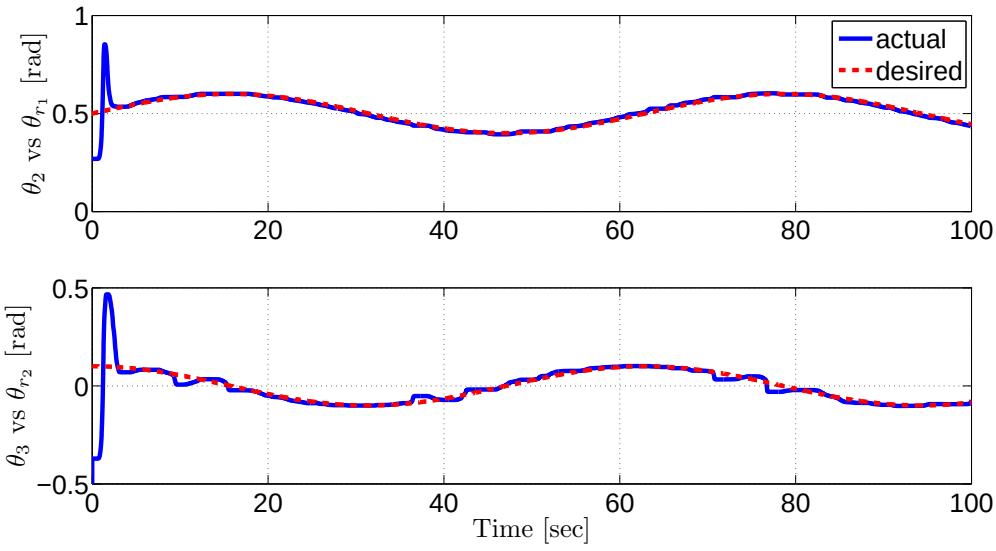

Figure 5.30. Link positions for $\gamma_p = 0.1$

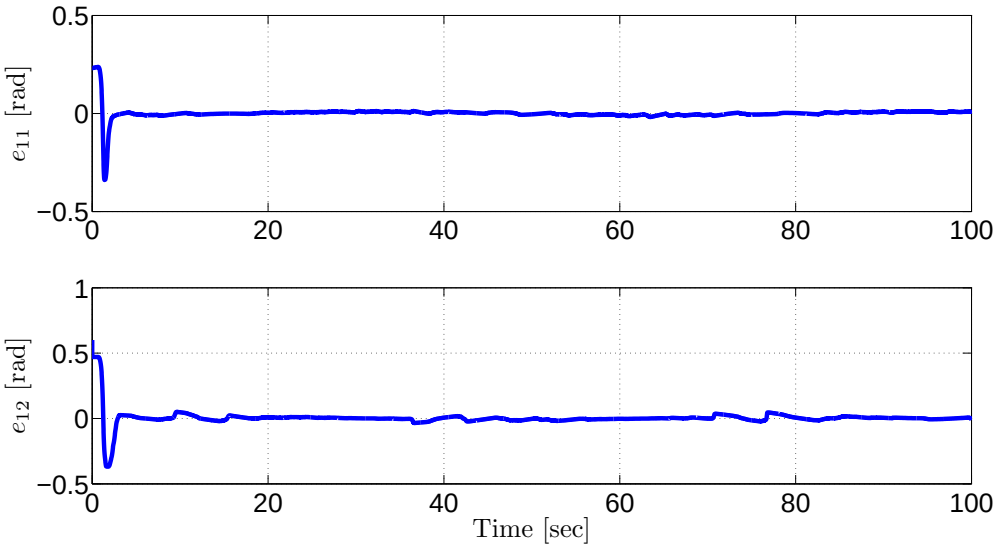

Figure 5.31. Link tracking errors for $\gamma_p = 0.1$

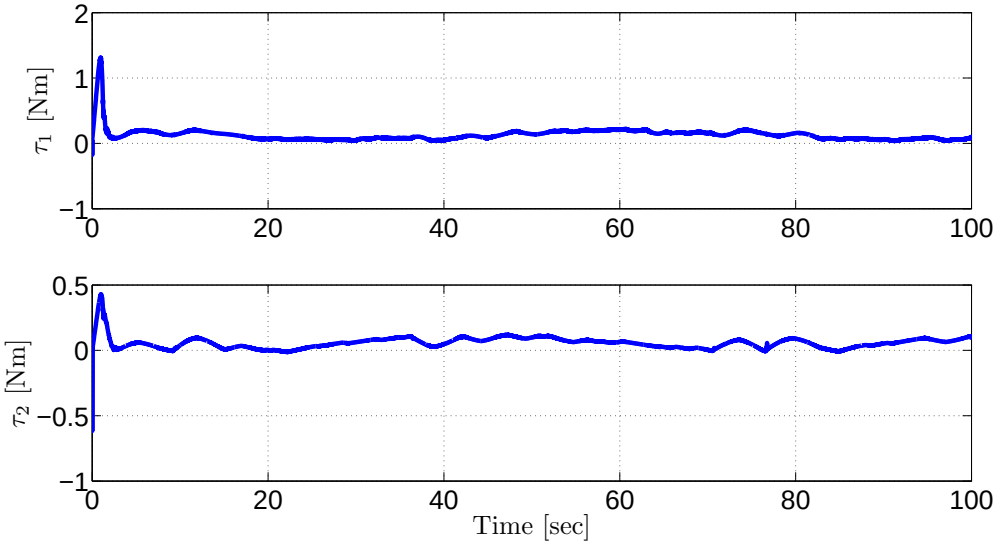

Figure 5.32. Control inputs for $\gamma_p = 0.1$

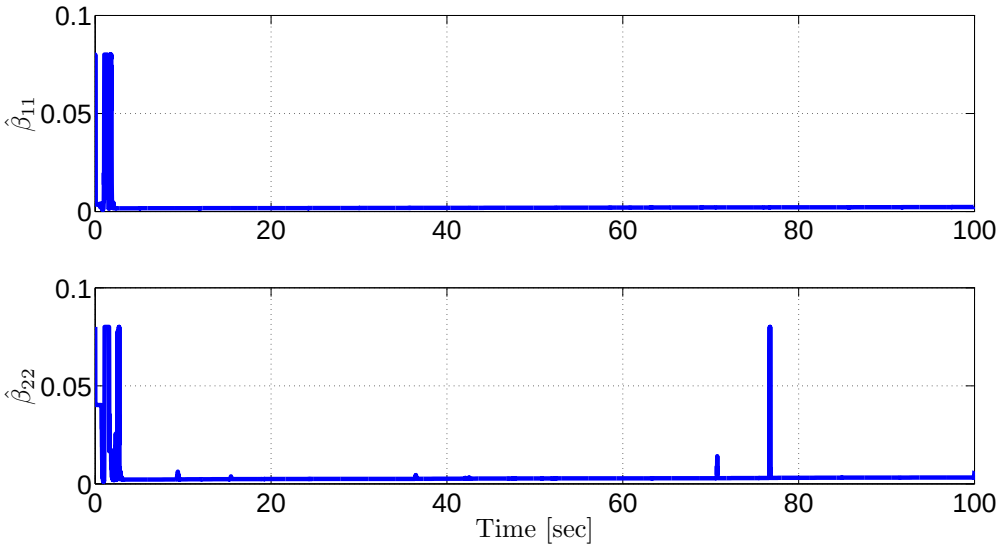

Figure 5.33. Entries of the time–varying gain matrix $\hat{\beta}(t)$ for $\gamma_p = 0.1$

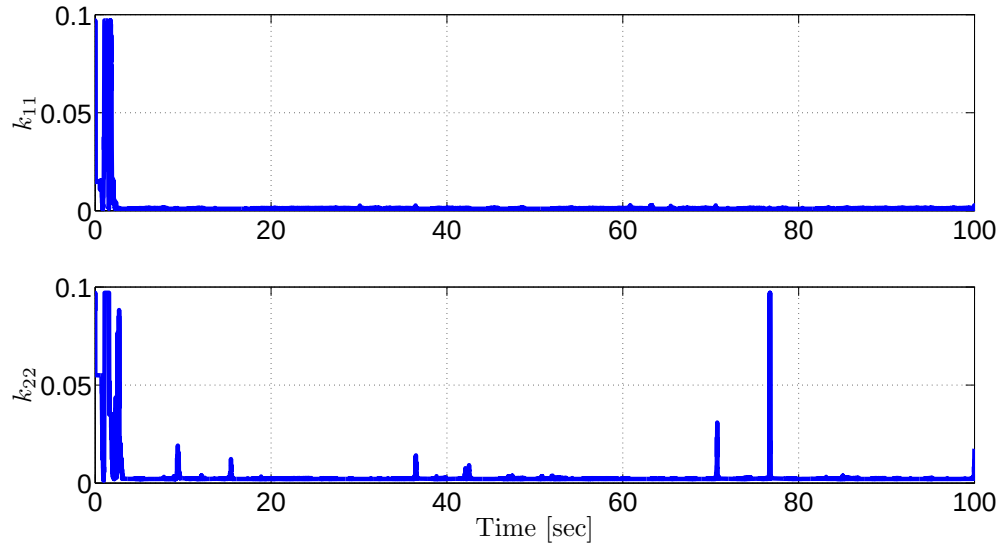

Figure 5.34. Entries of the time–varying gain matrix $K(t)$ for $\gamma_p = 0.1$

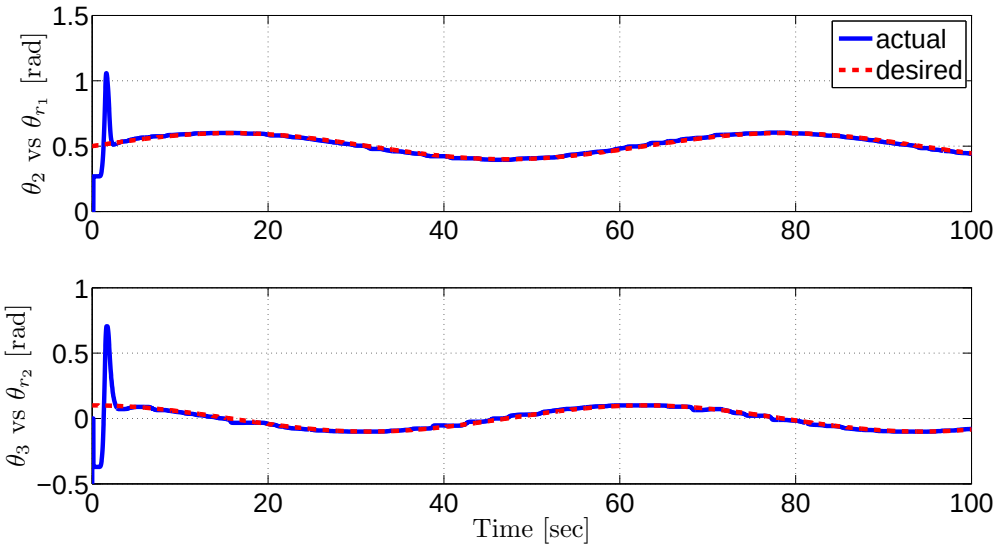

Figure 5.35. Link positions for $\gamma_p = 0.5$

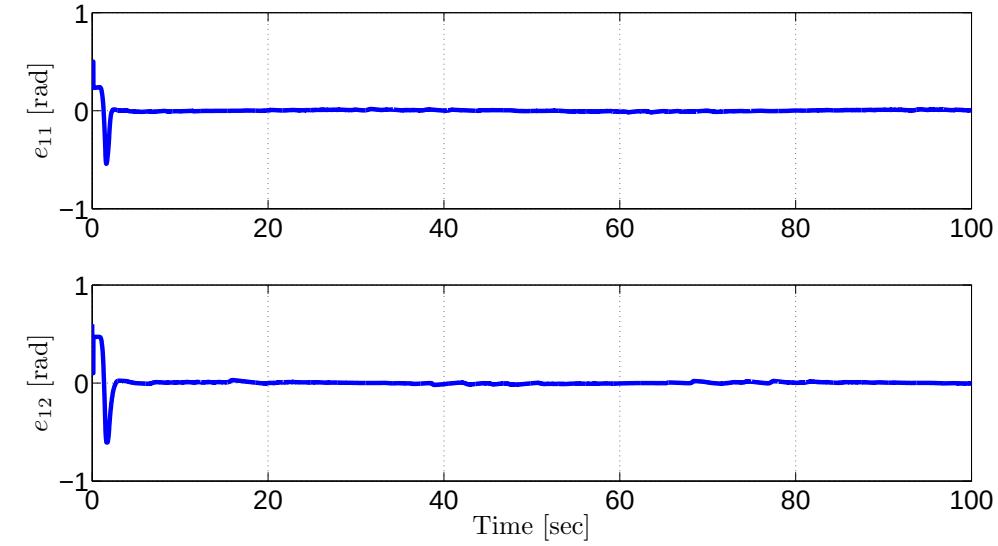

Figure 5.36. Link tracking errors for $\gamma_p = 0.5$

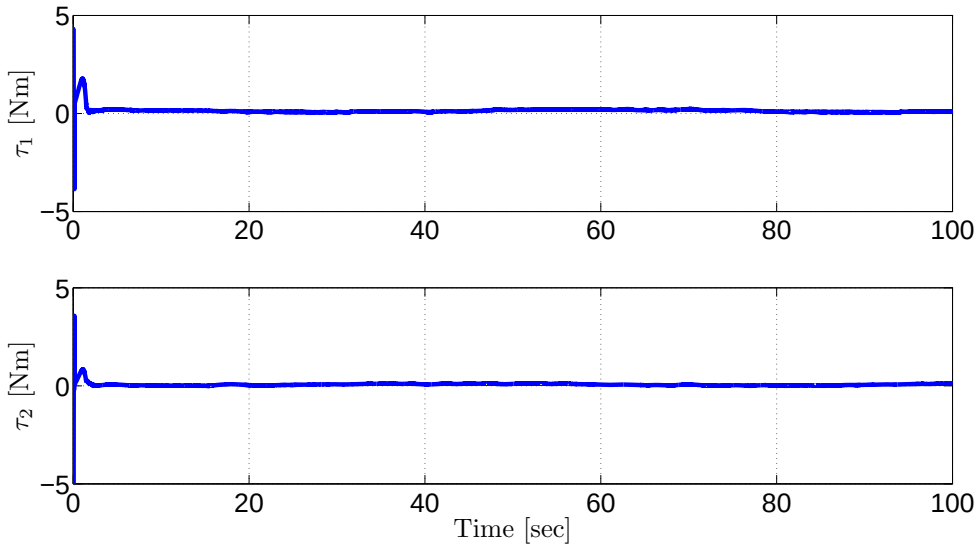

Figure 5.37. Control inputs for $\gamma_p = 0.5$

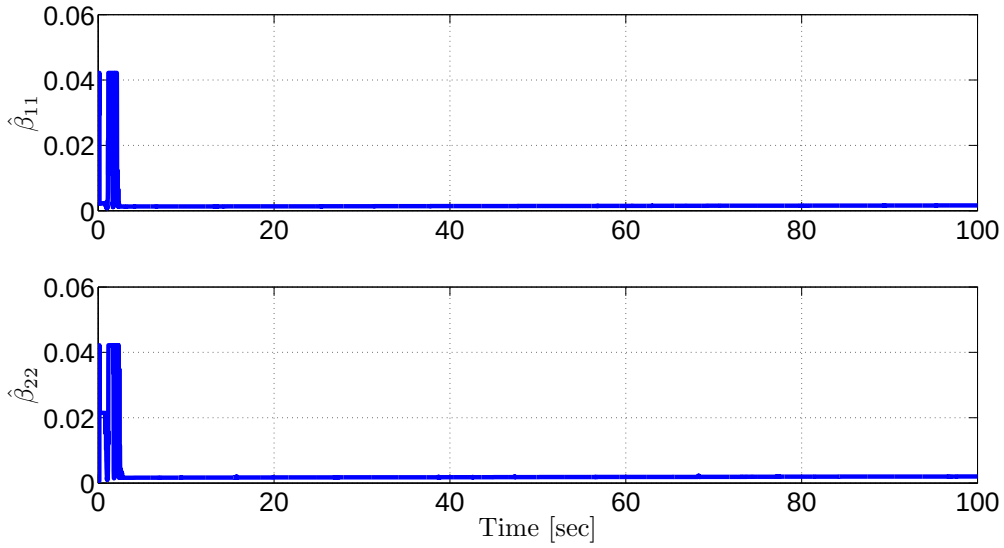

Figure 5.38. Entries of the time–varying gain matrix $\hat{\beta}(t)$ for $\gamma_p = 0.5$

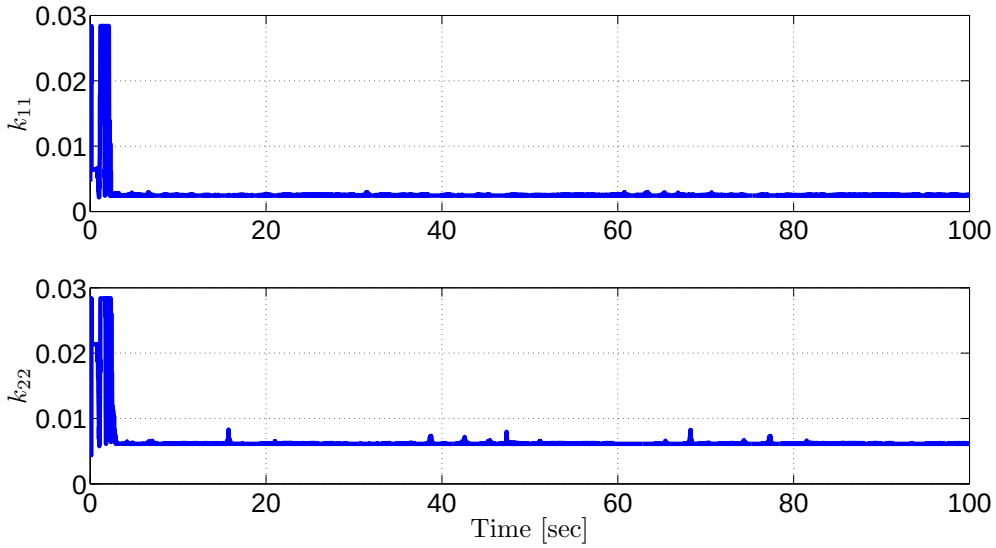

Figure 5.39. Entries of the time–varying gain matrix $K\left(t\right)$ for $\gamma_p = 0.5$

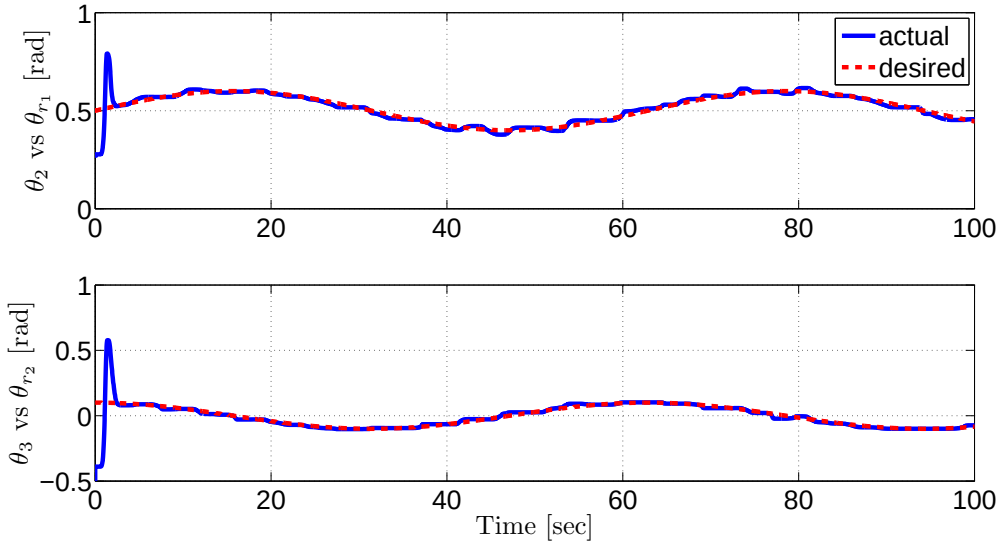

Figure 5.40. Link positions for $\gamma_p = 1$

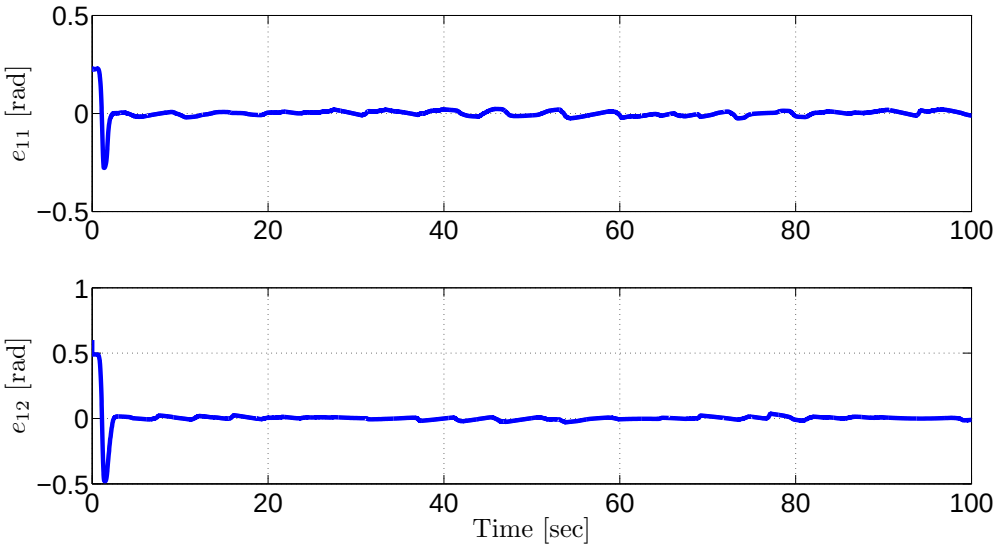

Figure 5.41. Link tracking errors for $\gamma_p = 1$

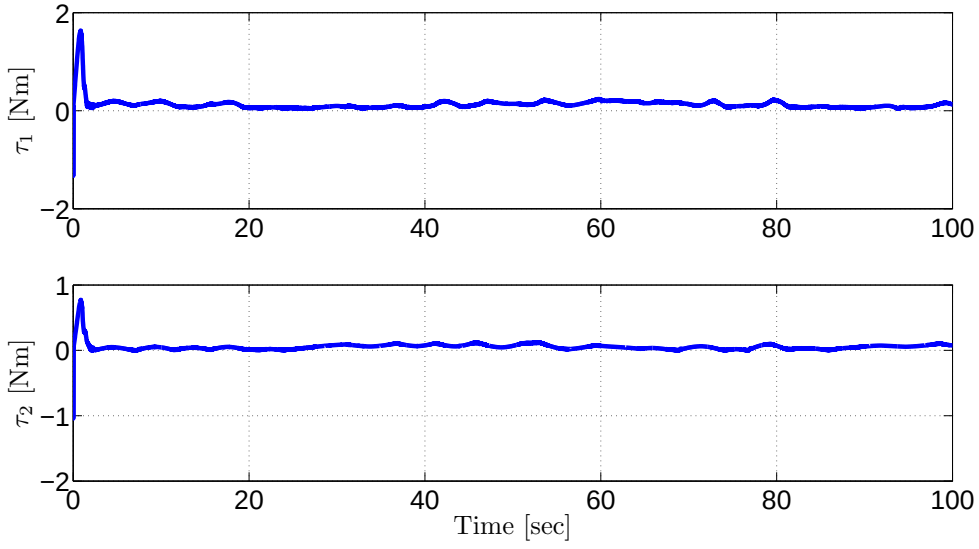

Figure 5.42. Control inputs for $\gamma_p = 1$

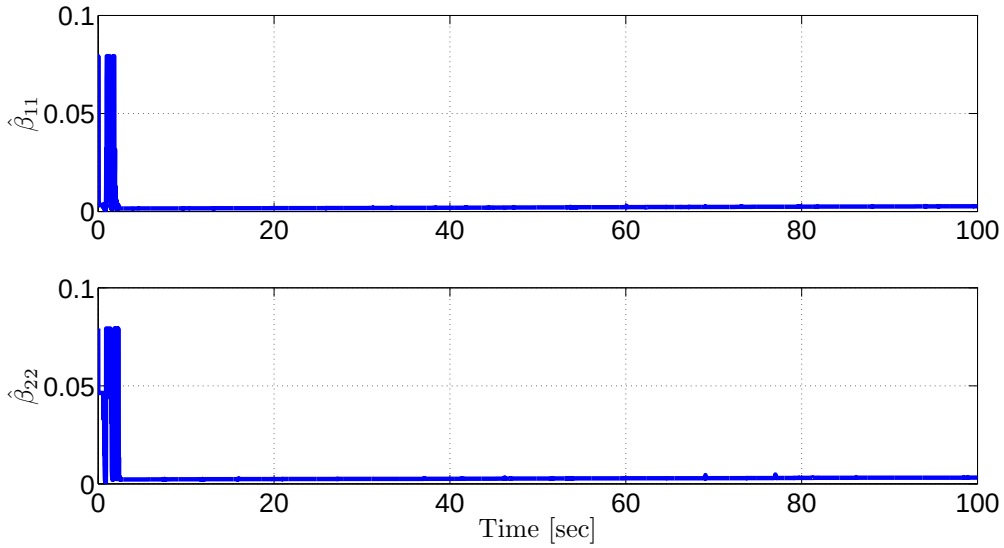

Figure 5.43. Entries of the time–varying gain matrix $\hat{\beta}(t)$ for $\gamma_p = 1$

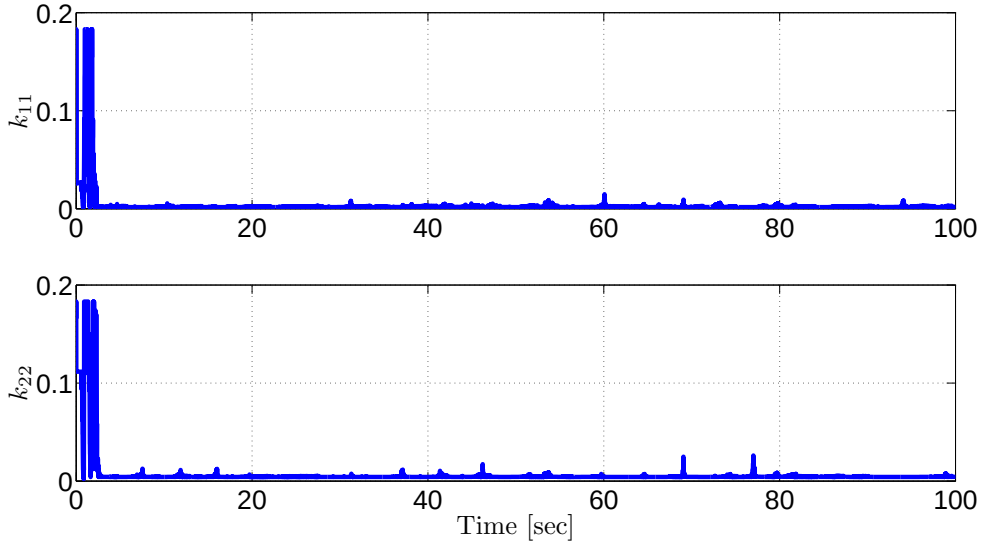

Figure 5.44. Entries of the time–varying gain matrix $K(t)$ for $\gamma_p = 1$

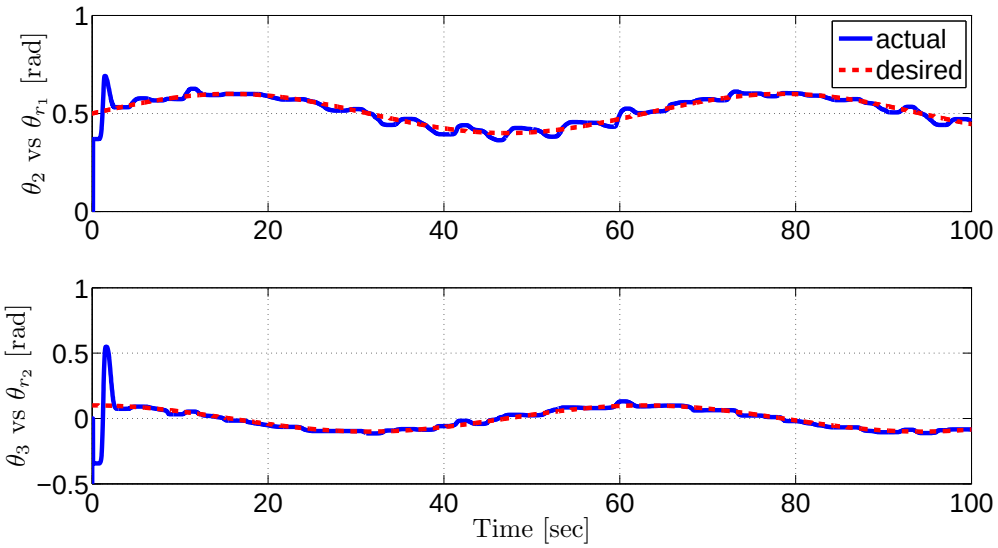

Figure 5.45. Link positions for $\gamma_p = 2$

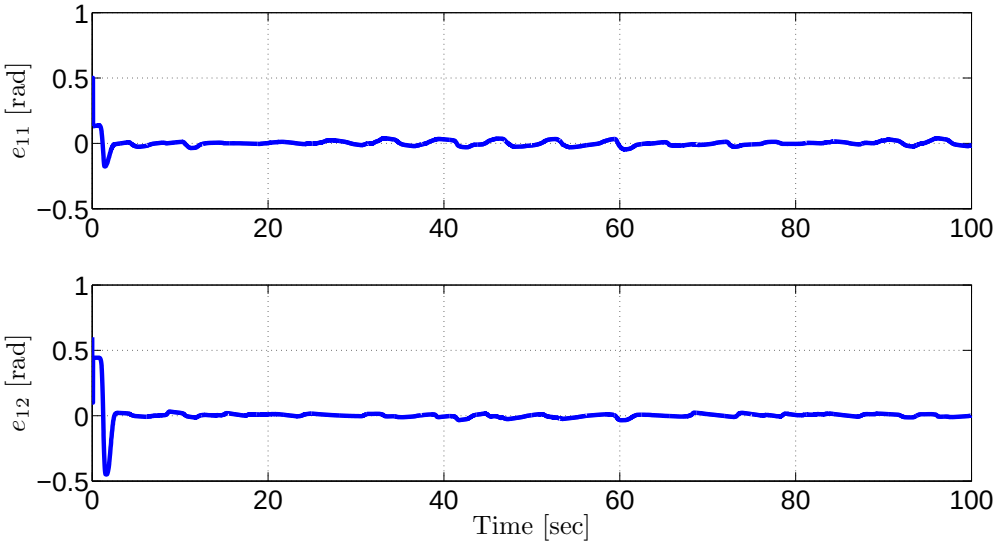

Figure 5.46. Link tracking errors for $\gamma_p = 2$

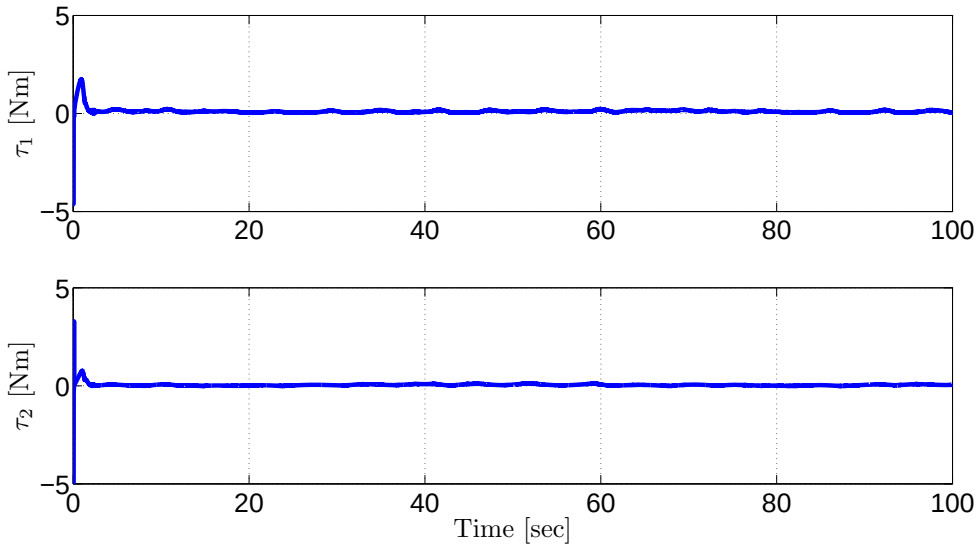

Figure 5.47. Control inputs for $\gamma_p = 2$

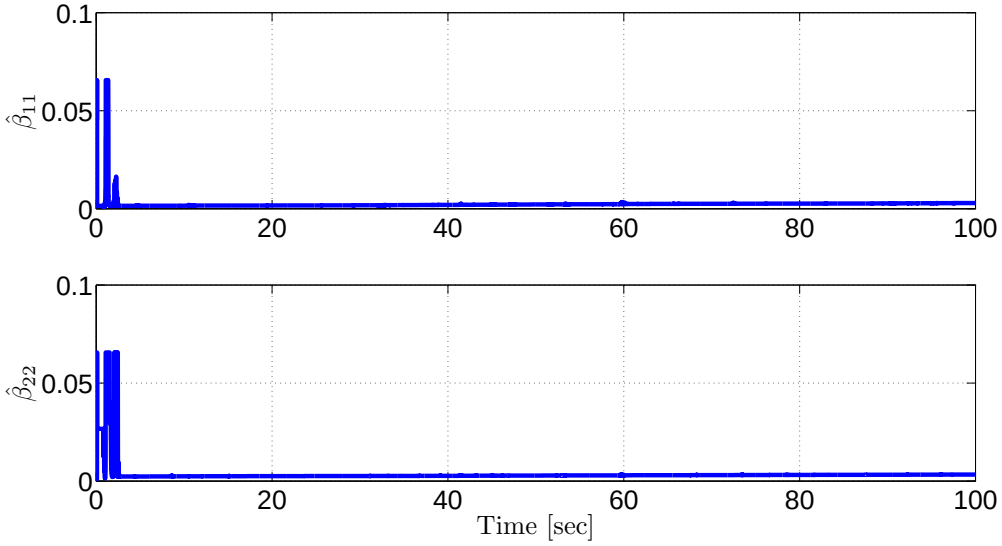

Figure 5.48. Entries of the time–varying gain matrix $\hat{\beta}\,(t)$ for $\gamma_p = 2$

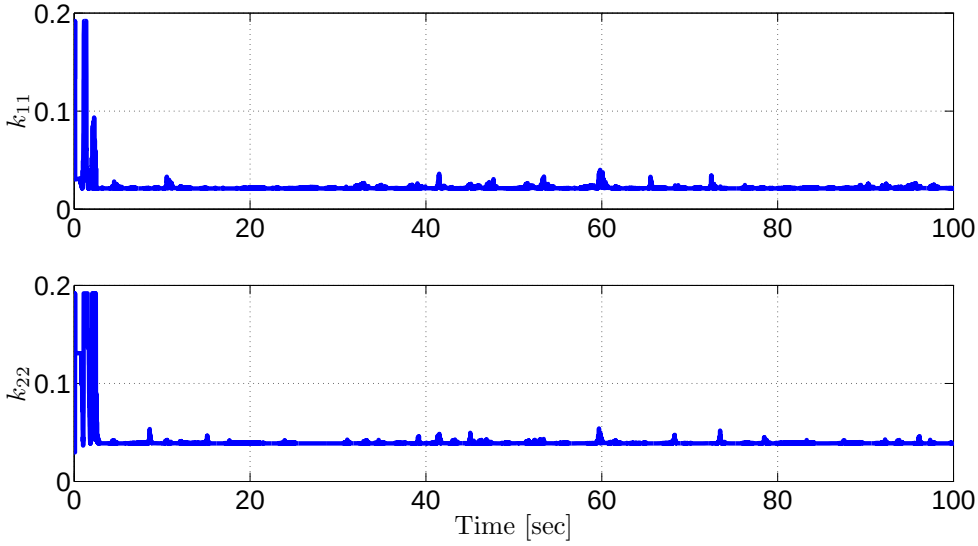

Figure 5.49. Entries of the time–varying gain matrix $K\left(t\right)$ for $\gamma_p = 2$

5.2. Dynamically Positioned Surface Vessel

The mathematical model of the surface vessel in (4.1) was utilized with the inertia matrix that have following rigid body and added mass parts

$$M_{RB} = \begin{bmatrix} m & 0 & 0 \\ 0 & m & mX_g \\ 0 & mX_g & I_z \end{bmatrix}, M_A = \begin{bmatrix} \dot{X}_u & 0 & 0 \\ 0 & -\dot{Y}_v & -\dot{Y}_r \\ 0 & -\dot{N}_v & \dot{N}_r \end{bmatrix}. \tag{5.11}$$

In the above inertia matrix, constant terms $Y_{\dot{r}}$ and $N_{\dot{v}}$ are selected as $Y_{\dot{r}} = 0$, $N_{\dot{v}} = -1$ that yielded a non–symmetric inertia matrix. Detailed explanations about these parameters and numerical values of dynamical model can be found in Skjetne et al. (2004). The centripetal and Coriolis forces matrix has the following form

$$C_s = \begin{bmatrix} 0 & 0 & c_2 \\ 0 & 0 & -c_1 \\ -c_2 & c_1 & 0 \end{bmatrix} \tag{5.12}$$

where its entries are given as

$$\begin{aligned} c_1 &= mu + (-X_{\dot{u}} u_r) \\ c_2 &= -m(x_g \dot{\psi}_s + v) + Y_{\dot{v}} v_r + 0.5(Y_{\dot{r}} + N_{\dot{v}})\dot{\psi}_s. \end{aligned} \tag{5.13}$$

The hydrodynamic damping matrix has the following form

$$D_s = \begin{bmatrix} d_{11} & 0 & 0 \\ 0 & d_{22} & d_{23} \\ 0 & d_{32} & d_{33} \end{bmatrix} \tag{5.14}$$

with its entries defined as

$$\begin{aligned} d_{11} &= -X_u - X_{|u|u} |u_r| - X_{uuu} u_r^2 \\ d_{22} &= -Y_v - Y_{|v|v} |u_r| - Y_{rv} \left|\dot{\psi}_s\right| \\ d_{33} &= -N_r - Y_{|v|v} |u_r| - Y_{|r|v} \left|\dot{\psi}_s\right| \\ d_{23} &= -Y_r - Y_{|v|r} |u_r| - Y_{|r|v} \left|\dot{\psi}_s\right| \\ d_{32} &= -N_v - N_{|v|v} |v_r| - N_{rv} \left|\dot{\psi}_s\right| \end{aligned} \tag{5.15}$$

where $v_r = [3, 0, 0]^T$. All the other system parameters are obtained from the experimental results in Skjetne et al. (2004). It would like to be highlighted that that these model

parameters were used only for simulation purposes and they were not utilized as part of the control input. The surface vessel was considered to be initially at rest at $x(0) = [0.1,\ 1,\ -\frac{\pi}{8}]^T$. The desired position of the surface vessel was given as

$$x_d(t) = \begin{bmatrix} 10\sin(0.1t)\ \text{(m)} \\ 10\cos(0.1t)\ \text{(m)} \\ -0.1t\ \text{(rad)} \end{bmatrix}.$$

The constant parts of time–varying control gains were selected as $k_c = \beta_2 = I_3$ and control gains K and β were obtained via the self–tuning strategy in Chapter 3. During the simulations they converged to following constant final values

$$K_\infty = \text{diag}\{2.9221, 3.153, 2.1997\},\ \hat{\beta}_\infty = \text{diag}\{2.0389, 3.0075, 1.3873\} \tag{5.16}$$

and the other control gain α was selected as $\alpha = I_3$.

The actual and desired positions are shown in Figure 5.50, while the position tracking errors and the control inputs are shown in Figures 5.51 and 5.52, respectively. In addition to these, entries of the time–varying gain matrices $\hat{\beta}(t)$ and $K(t)$ are shown in Figures 5.53 and 5.54, respectively. Simulation results confirm that the proposed controller achieved the tracking objective.

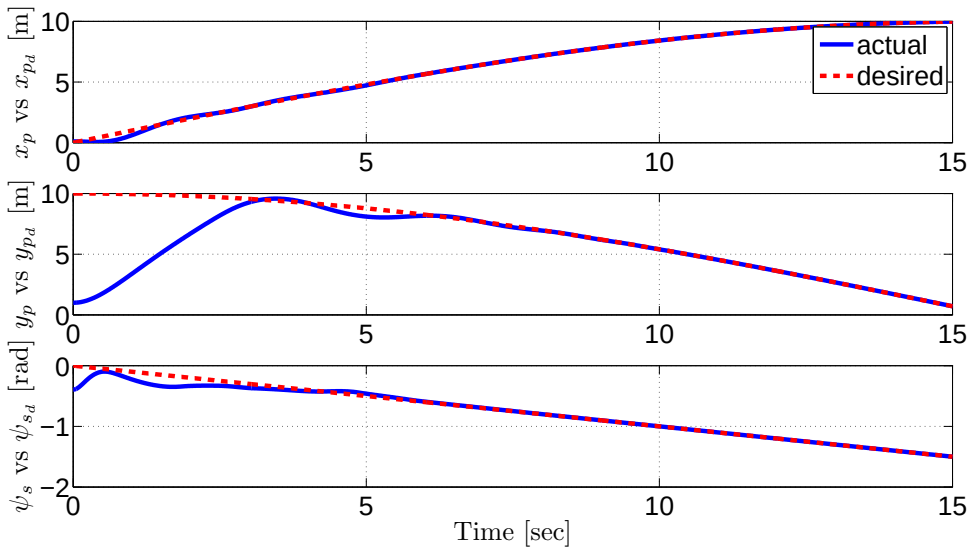

Figure 5.50. Tracking results for dynamically positioned surface vessel

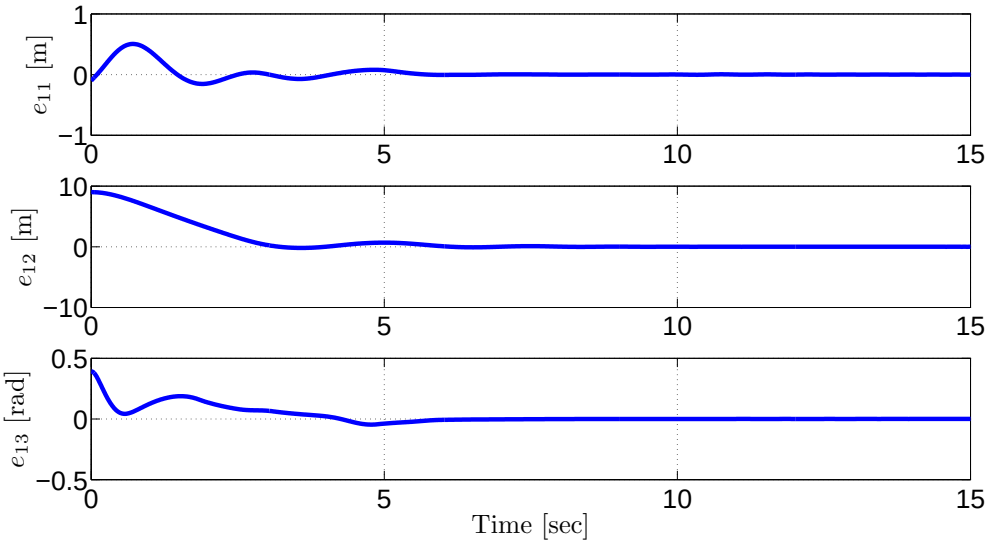

Figure 5.51. Tracking error $e_1\,(t)$ for dynamically positioned surface vessel

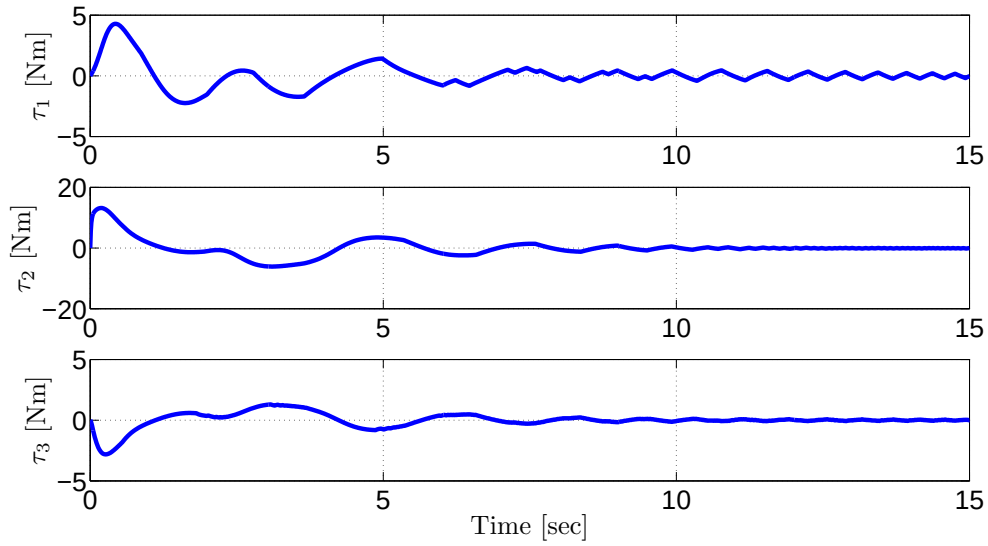

Figure 5.52. Control input torque $\tau\,(t)$ for dynamically positioned surface vessel

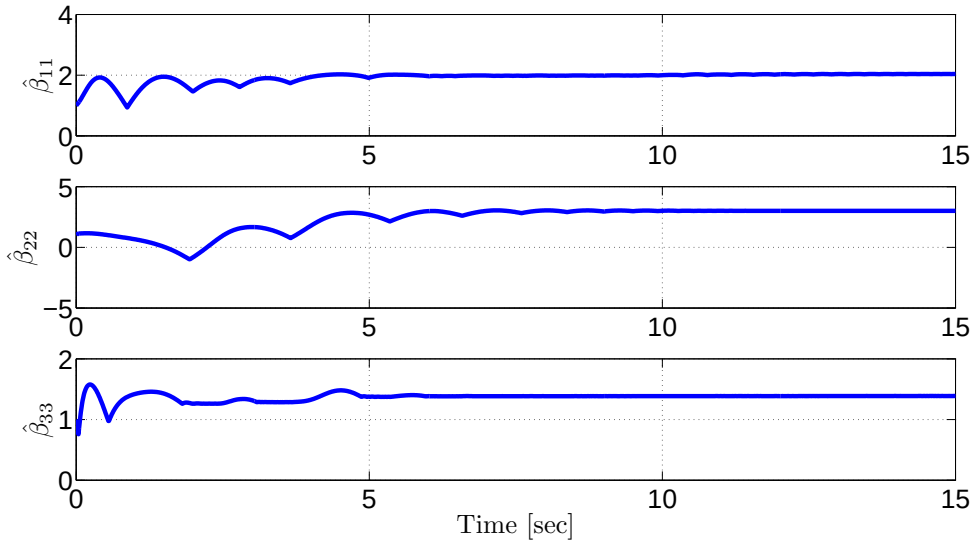

Figure 5.53. Entries of the time–varying gain matrix $\hat{\beta}(t)$ for dynamically positioned surface vessel

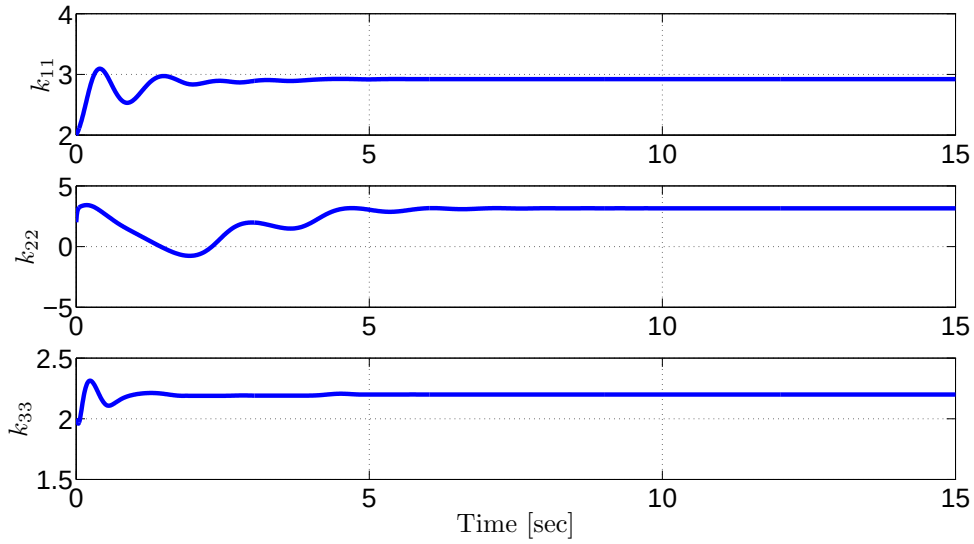

Figure 5.54. Entries of the time–varying gain matrix $K(t)$ for dynamically positioned surface vessel

5.3. Small–Scaled Unmanned Helicopter

The mathematical model of the helicopter in (4.12) was utilized with the inertia matrix that has the following form

$$M_h = \begin{bmatrix} c_0 & 0 & 0 \\ 0 & c_1 + c_2 \cos(c_3\psi) & c_4 \\ 0 & c_4 & c_5 \end{bmatrix}. \tag{5.17}$$

The centripetal and Coriolis forces matrix has the following form

$$C_h = \begin{bmatrix} 0 & 0 & 0 \\ 0 & c_6 \sin(2c_3\psi)\,\dot{\psi} & c_6 \sin(2c_3\psi)\,\dot{\theta} \\ 0 & -c_6 \sin(2c_3\psi)\,\dot{\theta} & 0 \end{bmatrix}. \tag{5.18}$$

The vector of conservative forces is given as

$$G_h = \begin{bmatrix} c_7 \cos(\phi) & 0 & 0 \end{bmatrix}^T. \tag{5.19}$$

The constant model parameters obtained from Fantoni and Lozano (2002), Mettler (2003) and Cai et al. (2011) are given as

$$\begin{aligned} c_0 &= 7.5kg,\, c_1 = 0.4305kgm^2,\, c_2 = 3 \times 10^{-4}kgm^2,\, c_3 = -4.143, \\ c_4 &= 0.108kgm^2,\, c_5 = 0.499kgm^2,\, c_6 = 6.2 \times 10^{-4}kgm^2,\, c_7 = -73.58N. \end{aligned} \tag{5.20}$$

The simplified rotor dynamics given in (4.16) has the form

$$A = \begin{bmatrix} c_8\dot{\psi}^2 & 0 & 0 \\ 0 & c_{11}\dot{\psi}^2 & 0 \\ c_{12}\dot{\psi} + c_{13} & 0 & c_{15}\dot{\psi}^2 \end{bmatrix},\; B = \begin{bmatrix} c_9\dot{\psi} + c_{10} \\ 0 \\ c_{14}\dot{\psi}^2 + c_{15} \end{bmatrix} \tag{5.21}$$

with the constant parameters that are given as

$$\begin{aligned} c_8 &= 3.411kg,\, c_9 = 0.6004kgm/s,\, c_{10} = 3.679N,\, c_{11} = -0.1525kgm, \\ c_{12} &= 12.01kgm/s,\, c_{13} = 10^5N,\, c_{14} = 1.2 \times 10^{-4}kgm^2,\, c_{15} = -2.64N. \end{aligned} \tag{5.22}$$

Constant values denoted by c_i for $i = 0, \cdots, 15$ are physical parameters of the dynamic model of the 3 dof helicopter. Their detailed descriptions can be found in Table 13.3 of

Fantoni and Lozano (2002). Following values were used as coefficients that are related with the simplified rotor dynamics

$$\begin{aligned} A_{lon} &= -0.1\ ,\ A_{lat} = 0.0313\ ,\ A_b = -0.189 \\ B_{lon} &= 0.0138\ ,\ B_{lat} = 0.14\ ,\ B_a = 0.368 \\ K_{ped} &= 2.16. \end{aligned} \tag{5.23}$$

The desired position of the helicopter was given as

$$\eta_r(t) = \begin{bmatrix} 10\sin(0.1t)\ (\text{deg}) \\ 15\sin(0.1t)\ (\text{deg}) \\ 20\sin(0.1t)\ (\text{deg}) \end{bmatrix}. \tag{5.24}$$

The constant parts of time–varying control gains were selected as $k_c = \beta_2 = I_3$ and control gains K and β were obtained via the self–tuning strategy in Chapter 3. During the simulations they converged to following constant final values

$$K_\infty = \text{diag}\{2, 1.999, 2\},\ \hat{\beta}_\infty = \text{diag}\{0.994, 0.983, 0.987\} \tag{5.25}$$

and the other control gain α was selected as $\alpha = I_3$.

The actual and desired positions are shown in Figure 5.55, while the position tracking errors and the control inputs are shown in Figures 5.56 and 5.57, respectively. In addition to these, entries of the time–varying gain matrices $\hat{\beta}(t)$ and $K(t)$ are shown in Figures 5.58 and 5.59, respectively. Simulation results confirm that the proposed controller meets the tracking objective.

The limitations of the proposed controller for the given system dynamics is now investigated. According to the identification results given in Mettler (2003), for the hover flight conditions maximum values of control inputs δ_{lon}, δ_{lat} and δ_{ped} are given as 20, 20 and 8 Nm, respectively. Simulation studies were performed by increasing the frequency of the desired trajectory in (5.24). For all of these simulations, a self–tuning method was utilized to adjust K and β while the other control gain α was selected as $\alpha = I_3$. Control gains and performance measures of these simulations are given in Tables 5.18 and 5.19. As a result, control objectives were met until $\omega_r = 5$ rad/sec without exceeding the given limits of the control inputs.

For $\omega_r = 10$ rad/sec, control limits were exceeded to meet the tracking control objective. Tracking results for this situation are given in Figure 5.60 while the control

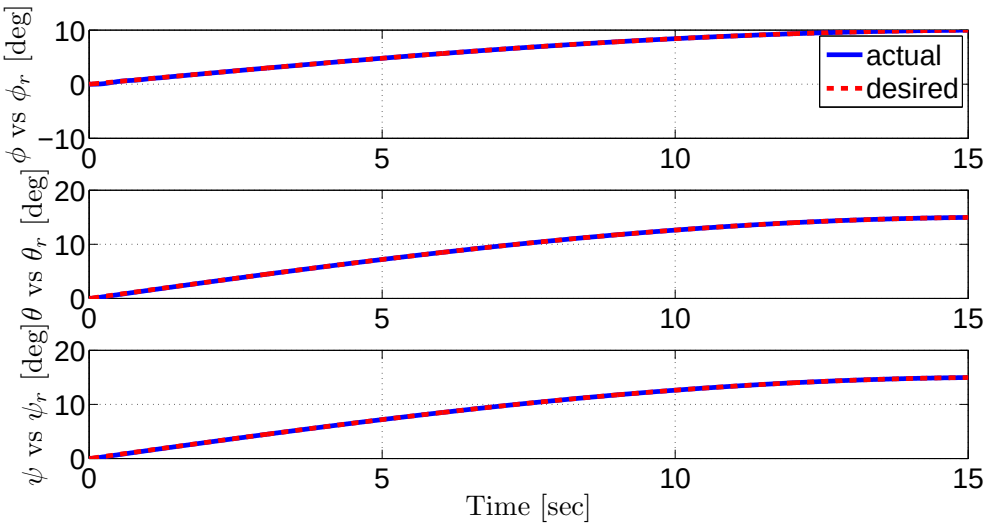

Figure 5.55. Tracking results for small–scaled unmanned helicopter

Table 5.18. Control gains for different frequencies

ω_r	K_∞	β_∞
0.5 rad/sec	diag $\{2, 1.994, 2.003\}$	diag $\{0.978, 0.899, 0.98\}$
1 rad/sec	diag $\{2.005, 1.98, 2.04\} \times 10^3$	diag $\{1.002, 0.822, 1.102\} \times 10^3$
5 rad/sec	diag $\{9.234, 3.28, 3.625\} \times 10^4$	diag $\{22.67, 6.906, 7.156\} \times 10^4$

inputs are given in Figure 5.61. Since it is not physically possible, simulations were reperformed by considering the limits of control inputs. Tracking results for this situation are given in Figure 5.62 and the control inputs are shown in Figure 5.63. From these figures, it is clear that the tracking control objective could not be met. As a result, it can be considered that it is not possible to meet the tracking control objective unless the necessary control effort cannot be provided by the system.

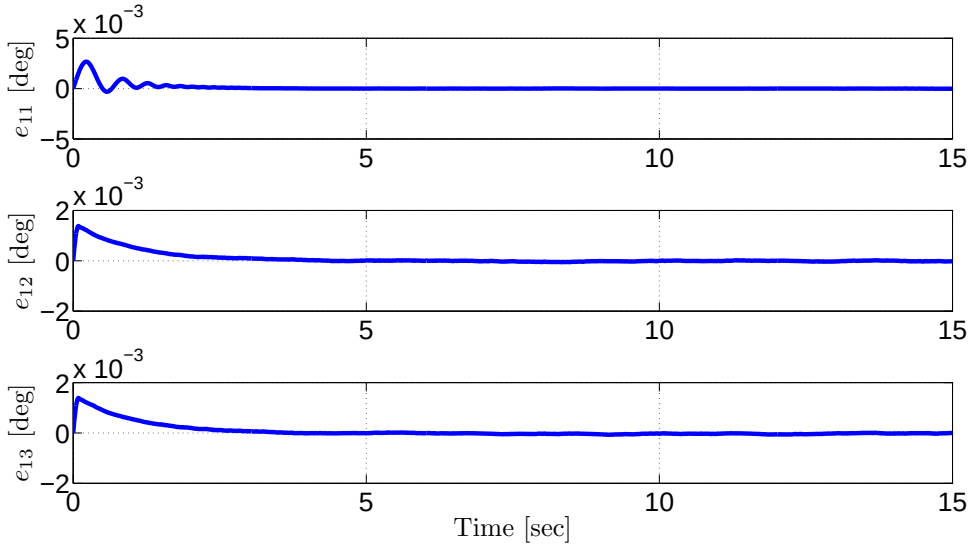

Figure 5.56. Tracking error $e_1\,(t)$ for small–scaled unmanned helicopter

Table 5.19. Performance measures for different frequencies

ω_r	$\int_{t_0}^{t} \|e_1\,(\sigma)\|^2\,d\sigma$	$\int_{t_0}^{t} \|\tau\,(\sigma)\|^2\,d\sigma$
0.5 rad/sec	6.6×10^{-4}	0.63
1 rad/sec	0.134	3.379
5 rad/sec	1.687	18.773

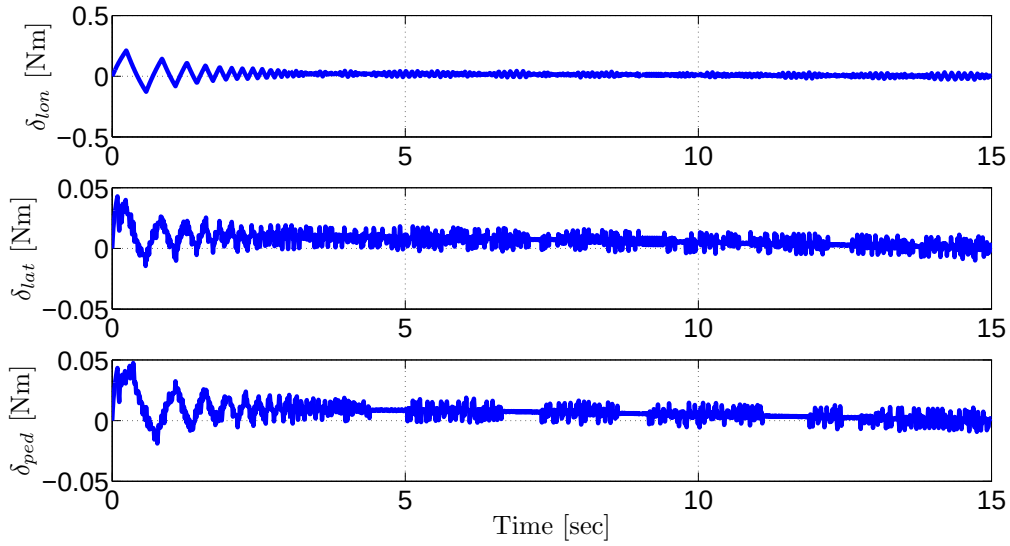

Figure 5.57. Control input torque $\tau\,(t)$ for small–scaled unmanned helicopter

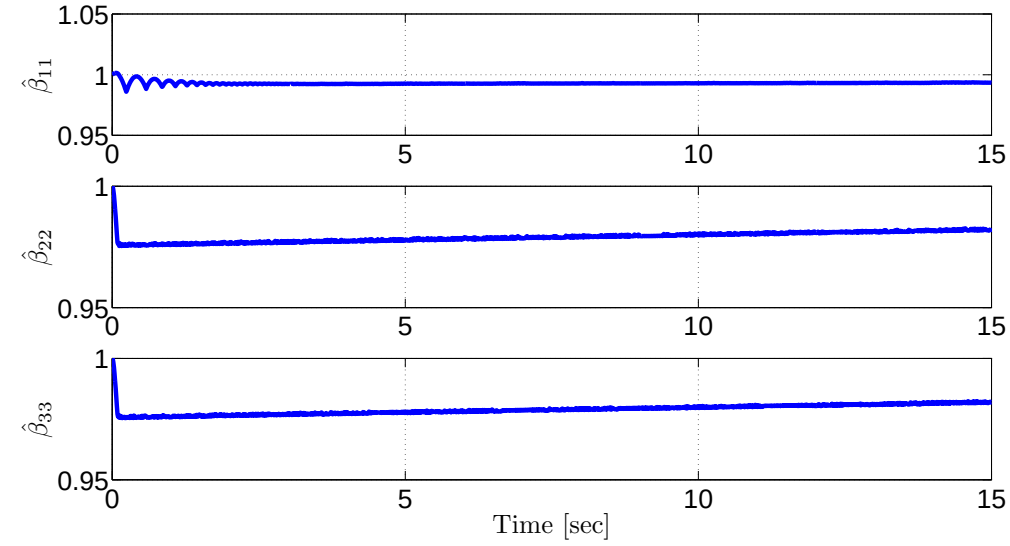

Figure 5.58. Entries of the time–varying gain matrix $\hat{\beta}\,(t)$ for small–scaled unmanned helicopter

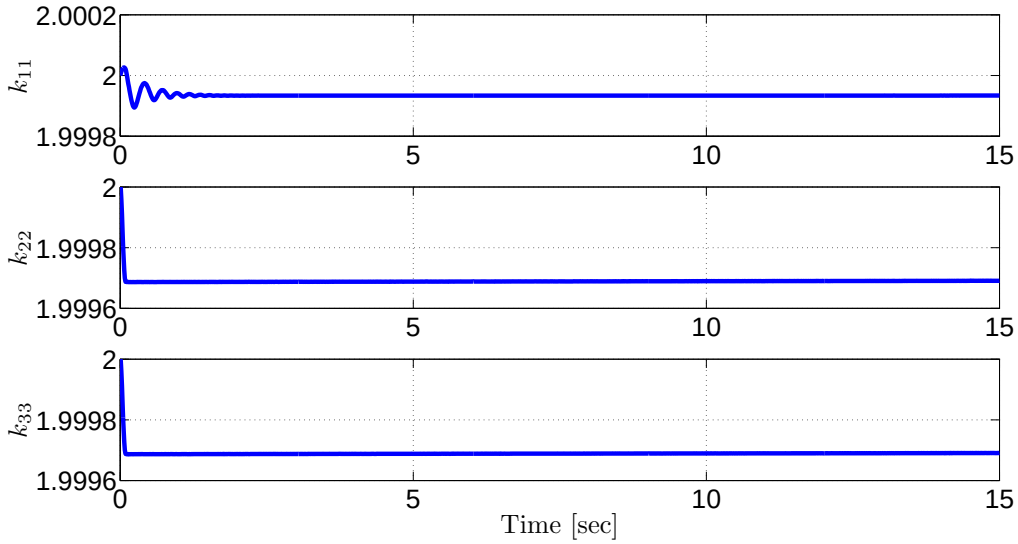

Figure 5.59. Entries of the time–varying gain matrix $K(t)$ for small–scaled unmanned helicopter

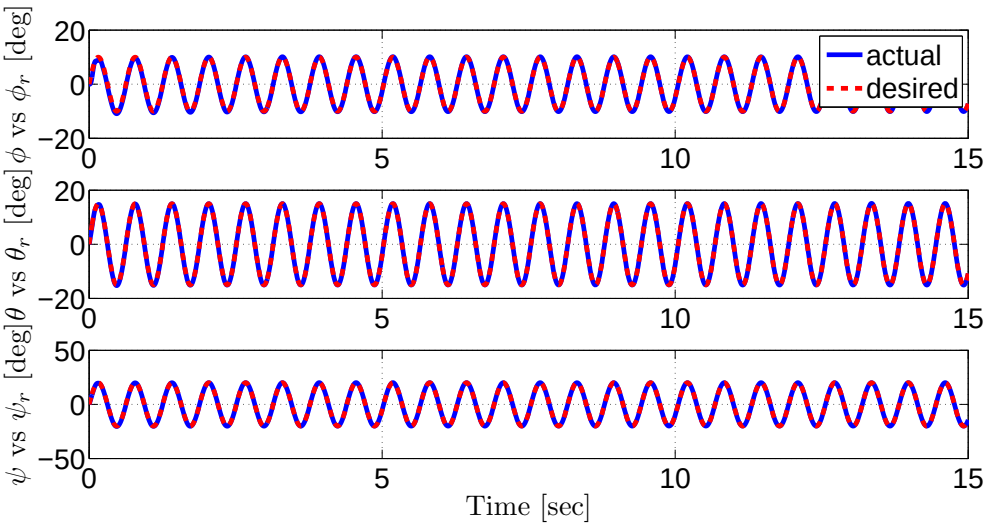

Figure 5.60. Tracking results for $\omega_r = 10$ rad/sec and without limiting the control inputs for small–scaled unmanned helicopter

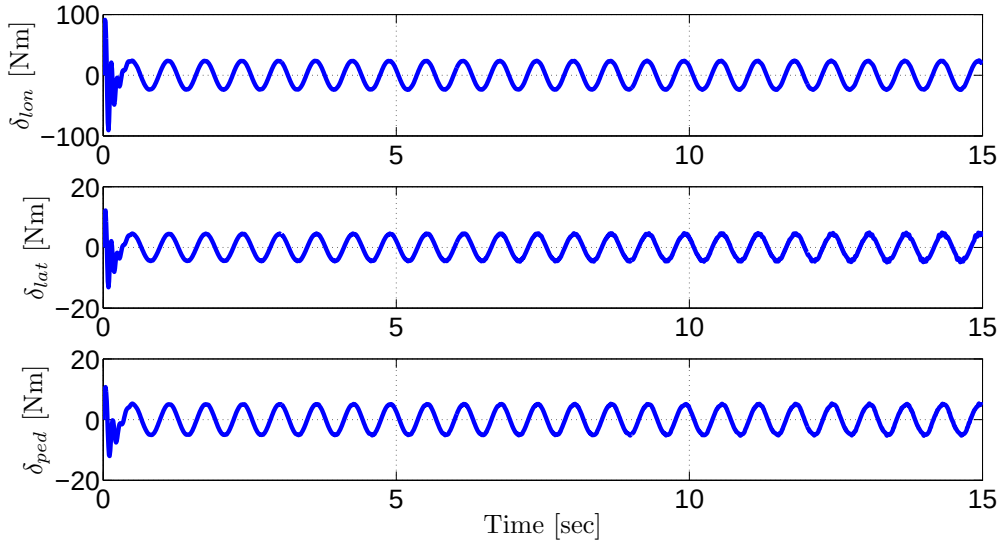

Figure 5.61. Control inputs for $\omega_r = 10$ rad/sec and without limiting the control inputs for small–scaled unmanned helicopter

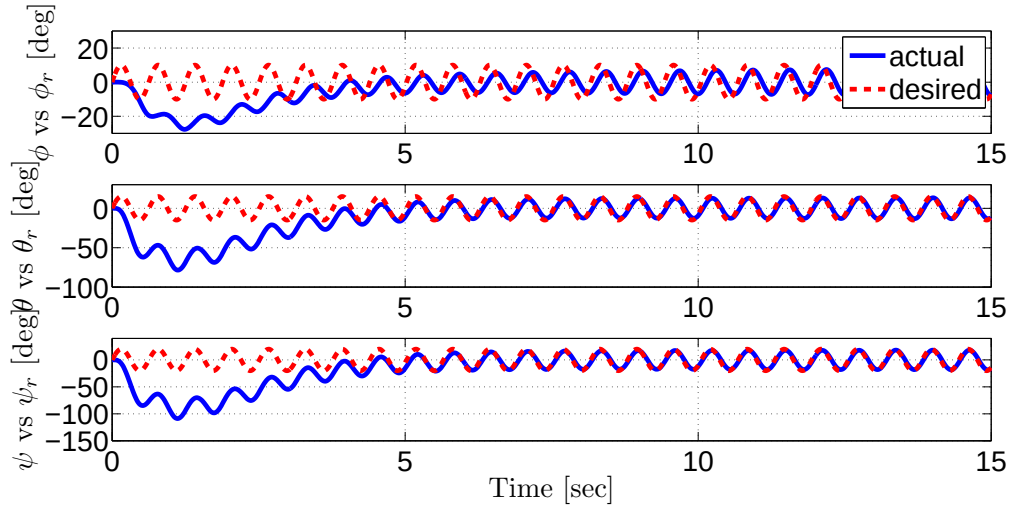

Figure 5.62. Tracking results for $\omega_r = 10$ rad/sec after limiting the control inputs for small–scaled unmanned helicopter

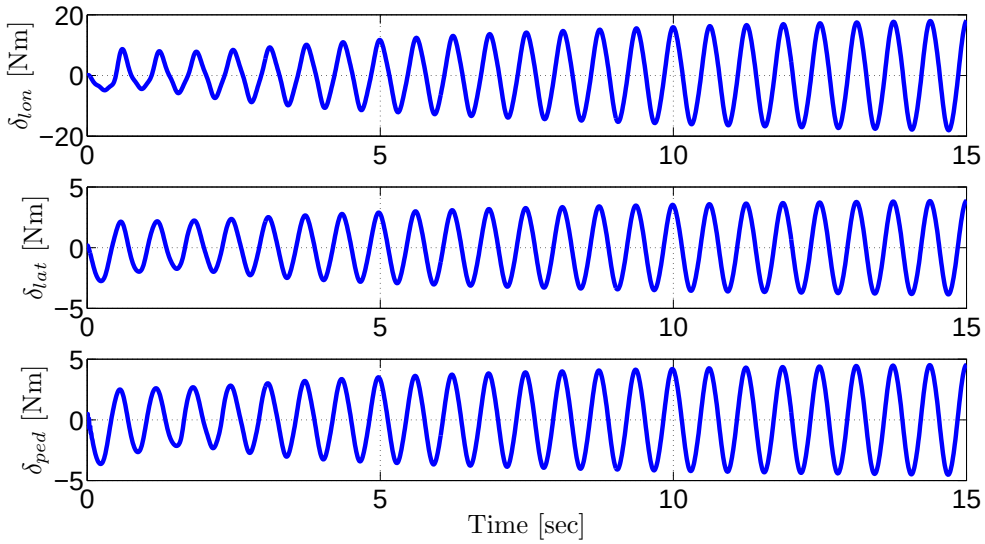

Figure 5.63. Control inputs for $\omega_r = 10$ rad/sec after limiting the control inputs for small–scaled unmanned helicopter

5.4. Unactuated Surface Vessel

The ship model in (4.20) was utilized with the following inertia matrix Fossen (2002)

$$M_t\left(x\right) = \begin{bmatrix} m + X_{\dot{u}} & 0 & 0 \\ 0 & n_a & n_d \\ 0 & n_c & n_b \end{bmatrix} \tag{5.26}$$

where the auxiliary terms n_a, n_b, n_c and n_d are defined as

$$n_a = m - Y_{\dot{v}}, \quad n_b = I_z - N_{\dot{r}}, \quad n_c = mx_g - N_{\dot{v}}, \quad n_d = mx_g - Y_{\dot{r}}. \tag{5.27}$$

In the above inertia matrix, constant terms $Y_{\dot{r}}$ and $N_{\dot{v}}$ are selected as $Y_{\dot{r}} = 0$, $N_{\dot{v}} = -1$ to reflect the effects of added mass which result in a non–symmetric inertia matrix. In the other control approaches about this subject available in the literature, especially in Braganza et al. (2007), the inertia matrix was selected as a symmetric matrix. The hydrodynamic damping matrix has the following form

$$D_t(\nu) = \begin{bmatrix} d_{11} & 0 & 0 \\ 0 & d_{22} & d_{23} \\ 0 & d_{32} & d_{33} \end{bmatrix} \tag{5.28}$$

with its entries defined as

$$d_{11} = -X_u + (-X_{|u|u}\left|u_r\right| - X_{uuu}u_r^2) \tag{5.29}$$

$$d_{22} = -Y_v + (-Y_{|v|v}\left|u_r\right| - Y_{rv}\left|\dot{\psi}\right|) \tag{5.30}$$

$$d_{33} = -N_r + (-Y_{|v|v}\left|u_r\right| - Y_{|r|v}\left|\dot{\psi}\right|) \tag{5.31}$$

$$d_{23} = -Y_r + (-Y_{|v|r}\left|u_r\right| - Y_{|r|v}\left|\dot{\psi}\right|) \tag{5.32}$$

$$d_{32} = -N_v + (-N_{|v|v}\left|v_r\right| - N_{rv}\left|\dot{\psi}\right|). \tag{5.33}$$

The desired vessel position was given as

$$x_d(t) = \begin{bmatrix} 10\sin(0.1t) \text{ [m]} \\ 10\cos(0.1t) \text{ [m]} \\ -0.1t \text{ [rad]} \end{bmatrix}. \tag{5.34}$$

The initial positions were set $x(0) = [0.1,\ 1,\ -\frac{\pi}{8}]^T$ and the initial velocities were $v(0) = 0_3$. The constant parts of time–varying control gains were selected as $k_c = \beta_2 =$

I_3 and control gains K and β were obtained via the self–tuning strategy in Chapter 3. During the simulations they converged to following constant final values

$$K_\infty = \text{diag}\{13.3, 20.16, 7.09\},\ \hat{\beta}_\infty = \text{diag}\{7.1, 1.96, 5.03\} \tag{5.35}$$

and the other control gains were selected as $\alpha = I_3$, $\epsilon_0 = \sqrt{5}$.

In order to obtain a proper time–dependent nature for the tugboats' positions without losing their contact with the vessel's hull, the tugboats were positioned at the following locations with respect to the center of mass of the vessel

$$\begin{aligned}
L_{1a} &= [-0.5, 0.1\sin(t)]^T \\
L_{1b} &= [0.5, 0.2\sin(0.1t)]^T \\
L_{2a} &= [-0.25 + 0.5\sin(t), -0.145]^T \\
L_{2b} &= [-0.25 + 0.3\sin(0.2t), 0.145]^T \\
L_{3a} &= [0.1\sin(t), 0.145]^T \\
L_{3b} &= [0.2\sin(0.2t), -0.145]^T
\end{aligned} \tag{5.36}$$

while the incident angle of each tugboat with respect to the vessel's hull were selected as follows

$$\begin{aligned}
\alpha_{1a} &= \frac{\pi}{180}\sin(0.1t) \\
\alpha_{1b} &= \pi - \frac{\pi}{120}\sin(t) \\
\alpha_{2a} &= \frac{\pi}{2} + \frac{\pi}{180}\sin(0.2t) \\
\alpha_{2b} &= \alpha_{2a} + \frac{\pi}{240}\sin(t) \\
\alpha_{3a} &= 3\pi/2 + \frac{\pi}{180}\sin(0.1t) \\
\alpha_{3b} &= \alpha_{3a} - \pi + \frac{\pi}{90}\sin(t).
\end{aligned} \tag{5.37}$$

In (5.36) and (5.37), time–varying sinusoidal perturbations are added to demonstrate disturbance effects. In these equations, their suitability to the system can be considered as the main reason of the selection of sinusoidal perturbations. Since these type of surface vessels have slowly varying trajectories due to their relatively high mass, slowly changing and smooth trajectories are considered as the most appropriate movements for them. As a result of this situation, using sinusoidal trajectories that have relatively low frequencies are appropriate for these surface vessels.

The actual and desired positions are shown in Figure 5.64, while the position tracking errors and the control inputs are shown in Figures 5.65 and 5.66, respectively. In addition to these, entries of the time–varying gain matrices $\hat{\beta}(t)$ and $K(t)$ are shown in

Figures 5.67 and 5.68. Simulation results confirm that the proposed controller achieved the tracking control objective.

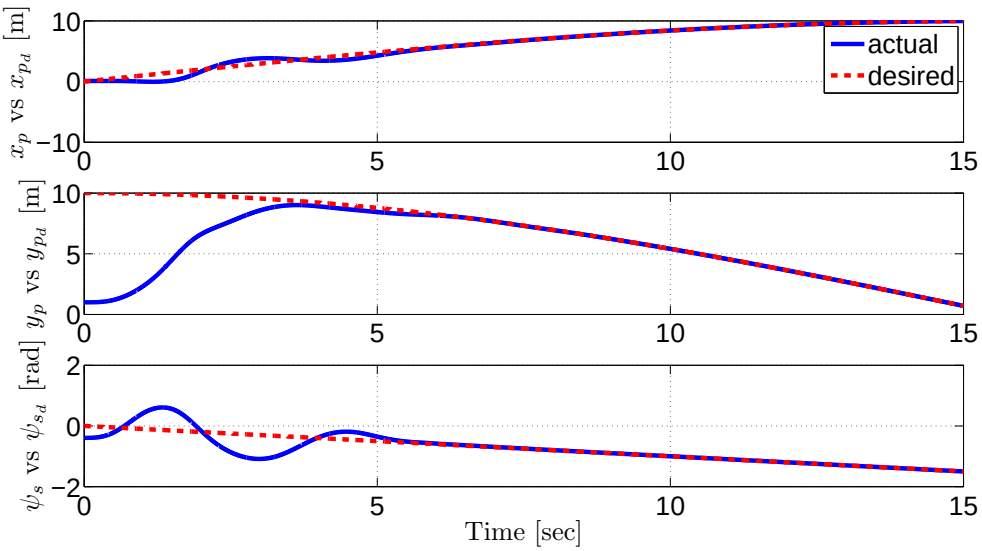

Figure 5.64. Tracking results for unactuated surface vessel

5.5. Conclusions

In the first part of this chapter, the performances of the designed controller in Chapter 2 and proposed self–tuning method in Chapter 3 were tested on modified robotic systems in simulation and experimental studies. In these studies, the performances were examined in a more detailed manner by utilizing different scenarios. Tracking results were shown in the figures while performance measures were demonstrated in the related tables.

Then, simulation studies were performed for mechatronic systems. Results of these simulations were presented in the related figures after the system dynamics of mechatronic systems were introduced.

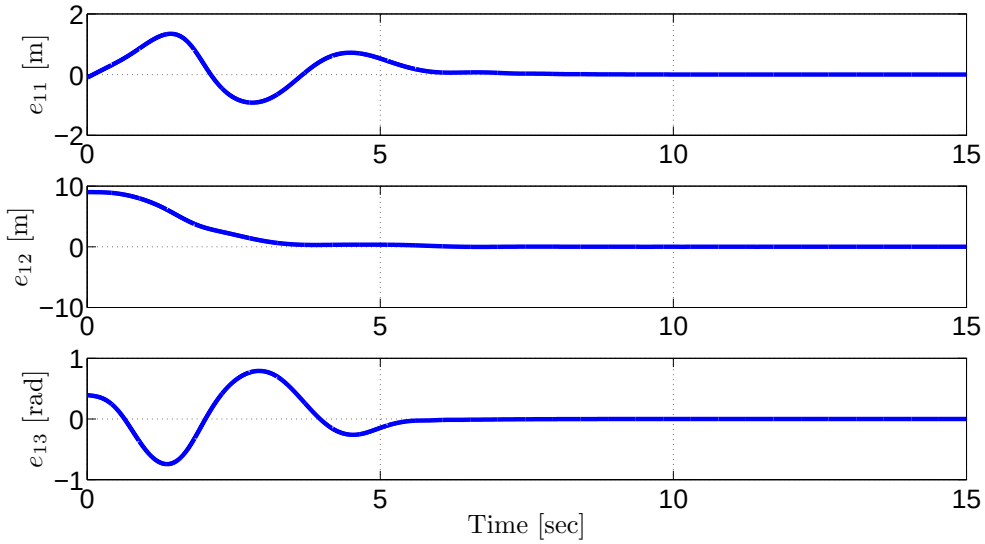

Figure 5.65. Tracking errors $e_1\,(t)$ for unactuated surface vessel

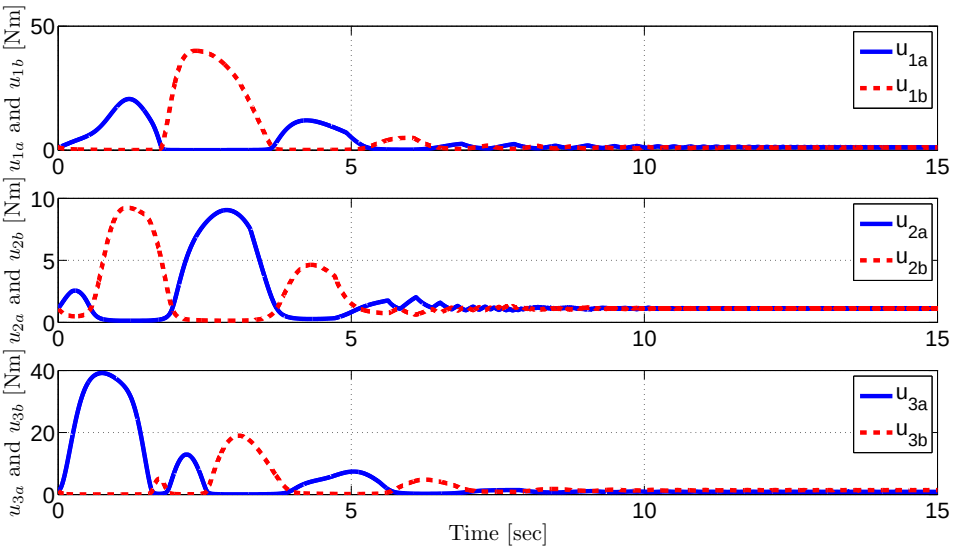

Figure 5.66. Control input torque $\tau\,(t)$ for unactuated surface vessel

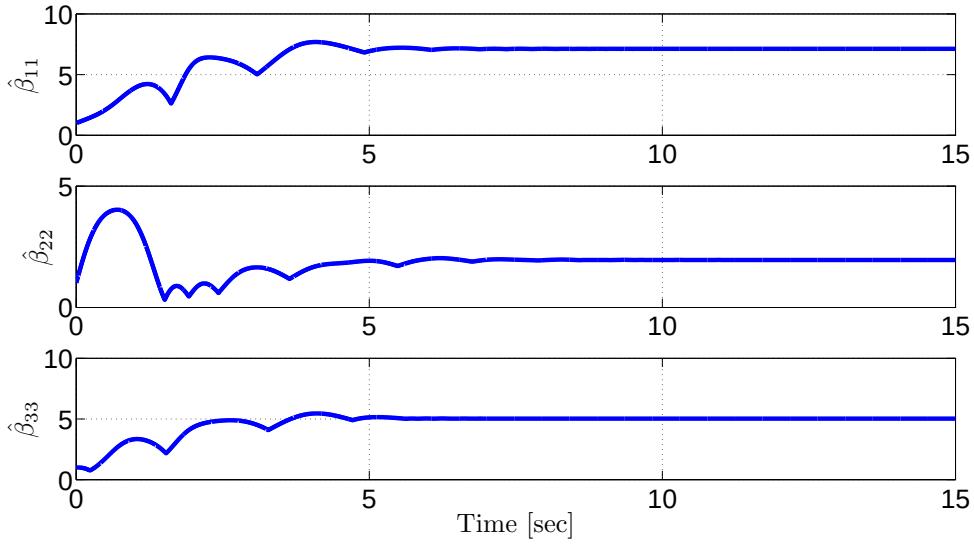

Figure 5.67. Entries of the time–varying gain matrix $\hat{\beta}(t)$ for unactuated surface vessel

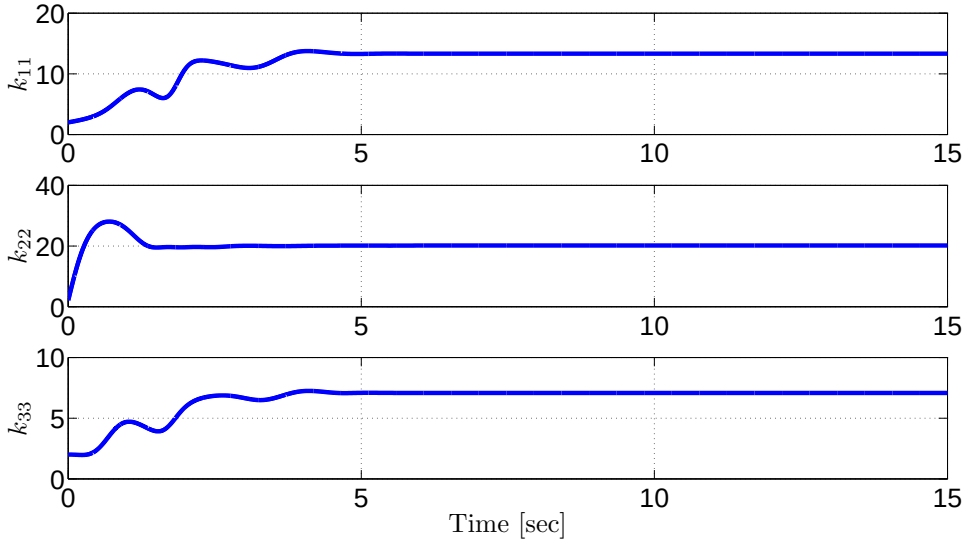

Figure 5.68. Entries of the time–varying gain matrix $K(t)$ for unactuated surface vessel

CHAPTER 6

CONCLUSIONS AND FUTURE WORKS

In this chapter, the conclusions of the research studies realized throughout the doctoral process are discussed. Conclusions of all chapters are examined separately to complete this examination in a more detailed manner. First, these conclusions are presented. Then possible future works that will be important developments to the studies investigated in this dissertation will be presented.

In Chapter 2, a continuous nonlinear robust controller was designed for a class of uncertain MIMO nonlinear systems having non–zero leading principal minors in their input gain matrices. The stability of the closed–loop system was investigated via the use of Lyapunov–based arguments. Specifically, a four step analysis to prove asymptotic stability of the output tracking error and its time derivatives was developed. The results were also demonstrated via numerical simulations and experimental studies to illustrate the viability and the performance of the proposed controller.

The results obtained in this chapter are compared with some of the closest robust control works in the literature. The main novelties of this study can be summarized as:

- The same system model was considered in Chen et al. (2008). The stability result in Chen et al. (2008) was extended to asymptotic as opposed to their UUB result.

- In Xian et al. (2004), the same system model was considered. The results in Xian et al. (2004) were extended by relaxing the positive definiteness of the input gain matrix requirement in the mentioned study. After this, the results in Xian et al. (2004) can now be considered as a special case of the controller presented in this dissertation (*i.e.*, when $DU\left(X\right)$ in (2.1) is an identity matrix).

For the proposed controller in Chapter 2, high gain conditions were to be satisfied by the control gains. Specifically, entries of the uncertainty compensation gain matrix must satisfy the conditions given in (2.65) and (2.66), and entries of the other control gain matrix must be selected large enough compared to the initial conditions of the system. It is also known that there is not much research in the literature that address the gain tuning

for robust controllers. As a result of these, in Chapter 3, studies were devoted to obtain a proper self–tuning strategy for the control gains. To realize this objective, a self–tuning RISE feedback type controller formulation with a time–varying feedback gain and an adaptive uncertainty compensation gain was presented. The proposed formulation does neither need a tuning methodology nor require prior knowledge of upper bounds of the vector containing the desired system dynamics plus functions containing uncertainties. Via Lyapunov–type analysis semi–global tracking was ensured. The convergence of the time–varying gains to constant final values was also proven.

When compared with the existing versions of the RISE feedback controllers, the results in this study is the only design that addressed the self–tuning of the control gains. The time–varying control gains can easily be applied to other RISE type controllers. One possible way to utilize the self–tuning algorithm is to utilize it and when the convergence to a constant value is observed, then to turn off the adaptation (as proposed in Krstic (1996)) and then continue the simulation/experiment.

In the first part of Chapter 4, the position and orientation control problem of an unmanned dynamically positioned surface vessel subject to added mass effects that may lead to a non–symmetric input gain matrix was solved. This system constituted a good example for the sub–class of general systems considered in this dissertation where non–symmetry appears in the inertia matrix of the system. For this, the mathematical model was rearranged to be compatible with the model that was utilized for the general control design. Then, semi–global asymptotic convergence of the tracking error was ensured.

Next, attitude control of a small–scaled unmanned model helicopter was aimed. When the rotor dynamics and the rigid body dynamics are combined by expressing the input torque as a function of actual control input, vector of input torque is multiplied with a non–symmetric matrix. This mechatronic system constitutes a good example for the other sub–class of the general systems considered in this dissertation where the non–symmetry is due to pre–multiplication of the control input with a non–symmetric gain matrix. To obtain semi–global asymptotic convergence of the tracking error, the mathematical model was rearranged to be compatible with the model that was utilized for the general control design. Then, a lower order version of the general control design was utilized.

Finally, control of an unactuated surface vessel manipulated by 6 autonomous uni–directional tugboats was addressed. Unlike the similar works in the literature, the surface

vessel was considered to be under the influence of added mass effects which resulted in a non–symmetric inertia matrix. The control problem is further complicated by the lack of accurate positions and orientations of tugboats. As a result of these issues, the resulting open–loop error system had an uncertain non–symmetric input gain matrix. As a result of these arrangements, this system constituted a good example for both sub–classes of the general systems considered in this dissertation. The stability of the closed–loop system was investigated via detailed Lyapunov–type tools where asymptotic tracking was proven.

Main highlights of the study presented in Chapter 4 can be summarized as:

- When controlling dynamically positioned surface vessels, it is **the first time** global asymptotic convergence of the tracking error was ensured when the vessel dynamics is under the influence of non–symmetric added mass effects.

- Ensuring asymptotic attitude tracking for a small–scaled unmanned helicopter by considering the non–symmetry of its input gain matrix with a continuous robust controller is an important **novelty**.

- For an unactuated surface vessel, it is **the first time** global asymptotic convergence of the tracking error was provided by considering and compensating non–symmetric effects of added mass. In addition to this, solving the control problem without using the accurate knowledge positions and orientations of tugboats is another **novelty**.

In Chapter 5, the performances of the controller in Chapter 2 and the designed self–tuning method in Chapter 3 were demonstrated via simulations and experiments. In section 5.1.1, a modified version of the model of a two–link robot manipulator with coupling between the two links was used as an example system for simulations. Obtaining a structure that is compatible with the general system model that was utilized for the control design was the main purpose of this modification. Simulation studies were realized for different scenarios to examine the performances of the designed controller and the proposed self–tuning methodology.

Then in Section 5.1.2, the performance of the controller and the self–tuning method were demonstrated via experiments. Phantom Omni haptic device was used as the experimental setup for these studies. Since the experimental setup does not have a non–symmetric behavior in its natural dynamics, control input was applied by premultiplying

with a non–symmetric matrix.

Finally, simulation studies for mechatronic systems were conducted to demonstrate the performances of the controllers in Chapter 4. Results for dynamically positioned surface vessels are given in Section 5.2, while the results for small–scaled unmanned helicopter and unactuated surface vessel manipulated by 6 uni–directional tugboats are given in Sections 5.3 and 5.4, respectively.

There is much to be considered as extensions to the results obtained in this dissertation. Although the designed controller is seen as a feasible solution for tracking control of these type of mechatronic systems, in the simulation studies, it was observed that actuator limitations may become a problem for the control process. Designing an optimal version of the proposed controller to deal with actuator limitations is aimed. In another attempt to deal with controller/actuator limitations, estimating the uncertain model parameters adaptively may be considered. Thus, an adaptive version of the proposed controller may be aimed. In addition to these, to deal with both uncertain model parameters and unstructured uncertainties, a neural network compensation term can be fused with the designed controller.

One of the most important example of sub–class of general systems where non–symmetry appears in the inertia matrix of the system dynamics is also encountered in unmanned aerial vehicles. Air balloons that fly on stratospheric levels and known as airships have inertial non–symmetry in their dynamics. The effect of added mass is encountered during these flights. This effect is caused from the motion of air. During the motion, it is considered that this flow is seen as an additional mass that is effective on the airships at acceleration level. Since the mass of the airships is lighter than air, this situation has a significant effect on these vehicles. Solving the position and orientation control problem of these type of vehicles by utilizing the proposed controller in this dissertation can be considered as a possible future work.

Experimental verification of the designed controller in Chapter 4 and its optimal version on a dynamically positioned surface vessel and small–scaled unmanned helicopter can be considered as possible future works.

REFERENCES

Arrichiello, F., S. Chiaverini, and T. I. Fossen (2006). Formation control of underactuated surface vessels using the null–space–based behavioral control. In *Proc. IEEE Int. Conf. on Robotics and Automation*, Orlando, FL, USA, pp. 5942–5947.

Balchen, J. G., N. A. Jenssen, and S. Sællid (1976). Dynamic positioning of floating vessels based on kalman filtering and optimal control. In *IFAC/IFIP Symp. on Automation in Offshore Oil Field Operation*, Amsterdam, the Netherlands, pp. 183–186.

Braganza, D., M. Feemster, and D. Dawson (2007). Positioning of large surface vessels using multiple tugboats. In *Proc. American Control Conf.*, New York, NY, USA, pp. 912–917.

Bui, V., H. Kawai, Y. Kim, and K. Lee (2010). A ship berting system design with four tug boats. *J. of Mechanical Science and Technology 25*(5), 1257–1264.

Bui, V. and Y. Kim (2011). Development of constrained control allocation for ship berthing by using autonomous tugboats. *J. of Control, Automation and Systems 9*(6), 1203–1208.

Cai, G., B. M. Chen, and T. H. Lee (2011). *Unmanned Rotorcraft Systems*. London, UK: Springer–Verlag London Limited.

Chen, J., A. Behal, and D. M. Dawson (2006). Adaptive output feedback control for a class of MIMO nonlinear systems. In *Proc. American Control Conf.*, Minneapolis, MN, USA, pp. 5300–5305.

Chen, J., A. Behal, and D. M. Dawson (2008). Robust feedback control for a class of uncertain MIMO nonlinear systems. *IEEE Tr. on Automatic Control 53*(2), 591–596.

Costa, R. R., L. Hsu, A. K. Imai, and P. Kokotovic (2003). Lyapunov-based adaptive control of MIMO systems. *Automatica 39*(7), 1251–1257.

de Queiroz, M. S. and D. M. Dawson (1996). Nonlinear control of active magnetic bearings: A backstepping approach. *IEEE Tr. on Control Systems Technology 4*(5), 545–552.

Dierks, T. and S. Jagannathan (2009). Neural network control of mobile robot formations using RISE feedback. *IEEE Tr. on Systems, Man, and Cybernetics, Part B 39*(2), 332–347.

Esposito, J. M., M. Feemster, and E. Smith (2008). Cooperative manipulation on the water using a swarm autonomous tugboats. In *Proc. IEEE Int. Conf. on Robotics and Automation*, Pasadena, CA, USA, pp. 1501–1506.

Fang, Y., E. Zergeroglu, M. S. de Queiroz, and D. M. Dawson (2004). Global output feedback control of dynamically positioned surface vessels: An adaptive control approach. *Mechatronics 14*(4), 341–356.

Fantoni, I. and R. Lozano (2002). *Non–Linear Control for Underactuated Mechanical Systems*. London, UK: Spring–Verlag London Limited.

Feemster, M., J. M. Esposito, and J. Nicholson (2006). Manipulation of large objects by swarms of autonomous marine vehicles: Part i–rotation. In *Proc. Southeastern Symp. on System Theory*, Cooksville, TN, USA, pp. 255–259.

Feemster, M. G. and J. M. Esposito (2011). Comprehensive framework for tracking control and thrust allocation for a highly overactuated autonomous surface vessel. *J. of Field Robotics 28*(1), 80–100.

Fischer, N., S. Bhasin, and W. E. Dixon (2011). Nonlinear control of an autonomous underwater vehicle: A RISE-based approach. In *Proc. American Control Conf.*, San Francisco, CA, USA, pp. 3972–3977.

Fjellstad, O. and T. I. Fossen (1994). Quaternion feedback regulation of underwater vehicles. In *Proc. of IEEE Int. Conf. on Control Applications*, Glasgow, Scotland, pp. 857–862.

Fossen, T. I. (1994). *Guidance and Control of Ocean Vehicles*. New York, NY, USA: John Wiley and Sons.

Fossen, T. I. (2002). *Marine Control Systems: Guidance, Navigation, and Control of Ships, Rigs and Underwater Vehicles*. Trondheim, Norway: Marine Cybernetics AS.

Fossen, T. I. (2011). *Handbook of Marine Craft Hydrodynamics and Motion Control*. Hoboken, NJ, USA: John Wiley and Sons.

Fossen, T. I. and Å. Grøvlen (1998). Nonlinear output feedback control of dynamically positioned ships using vectorial observer backstepping. *IEEE Tr. on Control Systems Technology 6*(1), 121–128.

Fossen, T. I. and J. P. Strand (1999). Passive nonlinear design for ships using Lyapunov methods: Full-scale experiments with a supply vessel. *Automatica 35*(1), 3–16.

Gadewadikar, J., F. L. Lewis, K. Subbarao, and B. M. Chen (2008). Structured H_∞ command and control loop design for unmanned helicopters. *J. of Guidance, Control, and Dynamics 31*(4), 1093–1102.

Gee, S. S. and C. Wang (2004). Adaptive neural control of uncertain MIMO nonlinear systems. *IEEE Tr. on Neural Networks 15*(3), 674–692.

Grimble, M. J., R. J. Patton, and D. A. Wise (1980). The design of dynamic positioning control systems using stochastic optimal control theory. *Optimal Control Applications & Methods 1*(1), 167–202.

Ihle, I. A. F., J. Jouffroy, and T. I. Fossen (2006). Formation control of marine surface craft: A Lagrangian approach. *J. of Oceanic Engineering 31*(4), 922–934.

Ji, S. W., V. P. Bui, B. Balachandran, and Y. B. Kim (2013). Robust control allocation design for marine vessel. *Ocean Engineering 63*, 105–111.

Kadmiry, B. and D. Driankov (2004). A fuzzy gain–scheduler for the attitude control of

an unmanned helicopter. *IEEE Tr. on Fuzzy Systems 12*(4), 502–515.

Kagawa, M., H. Katayama, and A. Ichikawa (2005). Attitude control of a helicopter model by feedback linearization. In *SICE Annual Conf.*, Okayana, Japan, pp. 1870–1875.

Kato, A., H. Katayama, and A. Ichikawa (2003). Attitude control of a helicopter model by nonlinear sampled–Data H_∞ control. In *SICE Annual Conf.*, Fukui, Japan, pp. 138–143.

Khalil, H. K. (2002). *Nonlinear Systems, 3rd Edition*. New York, NY, USA: Prentice Hall.

Kosmatopoulos, E. B. and P. A. Ioannou (2002). Robust switching adaptive control of multi-input nonlinear systems. *IEEE Tr. on Automatic Control 47*(4), 610–624.

Krstic, M. (1996). Invariant manifolds and asymptotic properties of adaptive nonlinear stabilizers. *IEEE Tr. on Automatic Control 41*(6), 817–829.

Krstic, M. (2009). *Delay Compensation for Nonlinear, Adaptive, and PDE Systems*. Boston, MA, USA: Birkhauser.

Krstic, M., I. Kanellakopoulos, and P. Kokotovic (1995). *Nonlinear and Adaptive Control Design*. New York, NY, USA: John Wiley & Sons.

Lee, D., E. Tatlicioglu, T. C. Burg, and D. M. Dawson (2008a). Adaptive output tracking control of a surface vessel. In *Proc. IEEE Int. Conf. Decision and Control*, Cancun, Mexico, pp. 1352–1357.

Lee, D., E. Tatlicioglu, T. C. Burg, and D. M. Dawson (2008b). Robust output tracking control of a surface vessel. In *Proc. American Control Conf.*, Seattle, WA, USA, pp. 544–549.

Lewis, E. V. (1989). *Principles of Naval Architecture Volume 3 Motions in Waves and Controllability*. Jersey City, NJ, USA: The Society of Naval Architects and Marine

Engineers.

Liu, H., G. Lu, and Y. Zhong (2013). Robust LQR attitude control of a 3–dof laboratory helicopter for aggressive maneuvers. *IEEE Tr. on Industrial Electronics 60*(10), 4627–4636.

Liu, X., B. Xian, Y. Zhang, and X. Zang (2014). Nonlinear asymptotic attitude tracking control for an unmanned helicopter with input constraints. In *Proc. American Control Conf.*, Portland, OR, USA, pp. 1402–1407.

MacKunis, W., P. M. Patre, K. Kaiser, and W. E. Dixon (2010). Asymptotic tracking for aircraft via robust and adaptive dynamic inversion methods. *IEEE Tr. on Control Systems Technology 18*(6), 1448–1456.

Mettler, B. (2003). *Identification Modeling and Characteristics of Miniature Rotorcraft*. Norwell, MA, USA: Kluwer Academic Publishers.

Morse, A. S. (1993). A gain matrix decomposition and some of its applications. *Systems & Control Letters 21*(1), 1–10.

Nao, T., H. Katayama, and A. Ichikawa (2003). Output regulation of a helicopter model. In *SICE Annual Conf.*, Fukui, Japan, pp. 126–131.

Newman, J. N. (1977). *Marine Hydrodynamics*. Cambridge, MA, USA: MIT Press.

Patre, P., W. E. Dixon, K. Kaiser, and W. MacKunis (2007). Asymptotic tracking for uncertain dynamic systems via a multilayer NN feedforward and RISE feedback control structure. In *Proc. American Control Conf.*, New York, NY, USA, pp. 5989–5994.

Patre, P. M., W. MacKunis, C. Makkar, and W. E. Dixon (2008). Asymptotic tracking for systems with structured and unstructured uncertainties. *IEEE Tr. on Control Systems Technology 16*(2), 373–379.

Qu, Z. and J.-X. Xu (2002). Model-based learning controls and their comparisons using

Lyapunov direct method. *Asian J. Control 4*(1), 99–110.

Sakamato, T., H. Katayama, and A. Ichikawa (2006). Attitude control of a helicopter model by robust PID controllers. In *Proc. of Int. Symp. on Intelligent Control*, Munich, Germany, pp. 1971–1976.

Sharma, N., S. Bhasin, Q. Wang, and W. E. Dixon (2010). RISE-based adaptive control of an uncertain nonlinear system with unknown state delays. In *Proc. IEEE Int. Conf. Decision and Control*, Atlanta, GA, USA, pp. 1773–1778.

Shin, J., H. J. Kim, Y. Kim, and W. E. Dixon (2010). Asymptotic attitude tracking of the rotorcraft-based UAV via RISE feedback and NN feedforward. In *Proc. IEEE Int. Conf. Decision and Control*, Atlanta, GA, USA, pp. 3694–3699.

Shin, J., H. J. Kim, Y. Kim, and W. E. Dixon (2012a). Autonomous flight of the rotorcraft–based UAV using RISE feedback and NN feedforward terms. *IEEE Tr. on Control Systems Technology 20*(5), 1392–1399.

Shin, J., H. J. Kim, Y. Kim, and W. E. Dixon (2012b). Autonomous flight of the rotorcraft-based UAV using RISE feedback and NN feedforward terms. *IEEE Tr. on Control Systems Technology 20*(5), 1392–1399.

Skjetne, R., O. N. Smogeli, and T. I. Fossen (2004). A nonlinear ship manoeuvering model: Identification and adaptive control with experiments for a model ship. *Modeling, Identification and Control 25*(1), 3–27.

Slotine, J. J. E. and W. Li (1991). *Applied Nonlinear Control*. Englewood Cliffs, NJ, USA: Prentice Hall.

Smith, E., M. Feemster, and J. M. Esposito (2007). Swarm manipulation of an unactuated surface vessel. In *Proc. Southeastern Symp. on System Theory*, Macon, GA, USA, pp. 16–20.

Sørensen, A. J., S. I. Sagatun, and T. I. Fossen (1996). Design of a dynamic positioning

system using model–based control. *Control Engineering Practice 4*(3), 359–368.

Stepanyan, V. and A. Kurdila (2009). Asymptotic tracking of uncertain systems with continuous control using adaptive bounding. *IEEE Tr. on Neural Networks 20*(8), 1320–1329.

Suzuki, S., D. Nakazawa, K. Nonami, and M. Tawara (2011). Attitude control of small electric helicopter by using quaternion feedback. *J. of System, Design, and Dynamics 5*(2), 231–247.

Techet, A. H. (2015). 2.016 Hydrodynamics (13.012). Massachusetts Institute of Technology Lecture Notes.

Tee, K. P., S. S. Ge, and F. E. H. Tay (2008). Adaptive neural network control for helicopters in vertical flight. *IEEE Tr. on Control Systems Technology 16*(4), 753–762.

Topp, J. and M. Feemster (2010). An adaptive control design for a system with unknown control direction: Experimental results. In *Proc. Southeastern Symp. on System Theory*, Tyler, TX, USA, pp. 81–84.

Tran, V. L. and N. Im (2012). A study on ship automatic berthing with assistance of auxiliary devices. *Int. J. of Naval Architecture and Ocean Engineering 4*, 199–210.

Vlachos, K. and E. Papadopoulos (2013). Modeling and control of a novel over-actuated marine floating platform. *Ocean Engineering 63*, 10–22.

Wang, Z. and A. Behal (2011). Continuous robust control for a class of uncertain MIMO nonlinear systems. In *Proc. IEEE Int. Conf. Decision and Control*, Orlando, FL, USA, pp. 7561–7566.

Wang, Z., A. Behal, B. Xian, and J. Chen (2011). Lyapunov–based adaptive control design for a class of uncertain MIMO nonlinear systems. In *Proc. of Int. Symp. on Intelligent Control Part of IEEE Multi–Conf. on Systems and Control*, Denver, CO, USA, pp. 1510–1515.

Wang, Z., J. Chen, and A. Behal (2010). Robust adaptive control design for a class of MIMO nonlinear systems. In *Proc. of Int. Symp. on Intelligent Control Part of IEEE Multi–Conf. on Systems and Control*, Yokohama, Japan, pp. 2284–2289.

Wit, C. C. D., E. Olguin, D. Perrier, and M. Perrier (1998). Robust nonlinear control of an underwater vehicle/manipulator system with composite dynamics. In *Proc. IEEE Int. Conf. on Robotics and Automation*, Leuven, Belgium, pp. 452–457.

Wondergem, M., E. Lefeber, K. Y. Pettersen, and H. Nijmeijer (2011). Output feedback tracking of ships. *IEEE Tr. on Control Systems Technology 19*(2), 442–448.

Xian, B., D. M. Dawson, M. S. de Queiroz, and J. Chen (2004). A continuous asymptotic tracking control strategy for uncertain nonlinear systems. *IEEE Tr. on Automatic Control 49*(7), 1206–1211.

Xian, B., M. S. de Queiroz, and D. M. Dawson (2003). A continuous control mechanism for uncertain nonlinear systems. In *Control, Stabilization, and Nonsmooth Analysis, Lecture Notes in Control and Information Sciences*, pp. 251–262. Heidelberg, Germany: Springer-Verlag.

Xian, B., G. Jianchuan, Z. Yao, and Z. Bo (2015). Sliding mode tracking control for miniature unmanned helicopters. *Chinese J. of Aeronautics 28*(1), 277–284.

Xu, H. and P. A. Ioannou (2003). Robust adaptive control for a class of MIMO nonlinear systems with guaranteed error bounds. *IEEE Tr. on Automatic Control 48*(5), 728–742.

Yang, Q., S. Jagannathan, and Y. Sun (2011). NN/RISE-based asymptotic tracking control of uncertain nonlinear systems. In *Proc. of Int. Symp. on Intelligent Control Part of IEEE Multi–Conf. on Systems and Control*, Denver, CO, USA, pp. 1361–1366.

Zhang, X., A. Behal, D. M. Dawson, and B. Xian (2005). Output feedback control for a class of uncertain MIMO nonlinear systems with non–symmetric input gain matrix. In *Proc. IEEE Int. Conf. Decision and Control*, Seville, Spain, pp. 7762–7767.

Zhang, X. T., D. M. Dawson, M. S. de Queiroz, and B. Xian (2004). Adaptive control for a class of MIMO nonlinear systems with non–symmetric input matrix. In *Proc. American Control Conf.*, Taipei, Taiwan, pp. 1324–1329.

Zhang, Y., B. Xian, B. Zhao, and X. Liu (2014). A continuous robust control design for a class of non-affine nonlinear dynamics with non-varnishing disturbance. In *Proc. American Control Conf.*, Portland, OR, USA, pp. 2330–2335.

VITA

Barış Bıdıklı received the B.Sc. degree in Electrical & Electronics Engineering from Pamukkale University, Denizli, Turkey and the Ms.C. degree in Electrical & Electronics Engineering from İzmir Institute of Technology, İzmir, Turkey in 2011 and 2013 respectively. Since 2013, he has continued his Ph.D. at Department of Electrical & Electronics Engineering at İzmir Institute of Technology, İzmir, Turkey.

His research interests include estimation techniques, observer design, adaptive, robust and optimal control of uncertain nonlinear systems, partial state feedback and output feedback control techniques, nonlinear control techniques for mechatronic systems, dynamic modeling and dynamic simulation of mechatronic systems, swarm robotic applications.